Dissertation zur Erlangung des Doktorgrades

der Fakultät für Chemie und Pharmazie

der Ludwig-Maximilians-Universität München

Aminoethylene-lipopeptides for intracellular delivery of gene modulating tools

Jasmin Kuhn

aus Villingen-Schwenningen, Deutschland

2019

TABLE OF CONTENTS

<u>Erklärung</u>

Diese Dissertation wurde im Sinne von § 7 der Promotionsordnung vom 28. November 2011 von Herrn Prof. Dr. Ernst Wagner betreut.

<u>Eidesstattliche Versicherung</u>

Diese Dissertation wurde eigenständig und ohne unerlaubte Hilfe erarbeitet.

München, 12.12.2019

...........……………………………

Jasmin Kuhn

Dissertation eingereicht am 13.12.2019

1. Gutachter: Prof. Dr. Ernst Wagner

2. Gutachter: Prof. Dr. Wolfgang Frieß

Mündliche Prüfung am 04.02.2020

Meiner Familie, die mich lehrte eigenständig nachzudenken

und Tim, der jetzt mit den Konsequenzen leben muss!

Table of Contents

1   Introduction

This chapter provides a brief introduction into the research field of molecular therapeutics and associated efficient delivery strategies. It is not considered to be a complete review of the whole scientific area.

1.1   Regulation of gene expression

Different mechanisms in cells regulate the synthesis of gene products like RNA and proteins. These modulation programs build the fundament for the proteomic and functional diversity of eukaryotes and the ability of the cell to activate different developmental stages, to respond to extracellular signals and to adapt to environmental conditions.[1]

Since less than two percent of the human genome belongs to the ~25.000- 35.000 protein coding genes, the main part of the genome consists of non-coding DNA.[1] A part of the non-coding DNA is transcribed into transfer, ribosomal or nuclear RNA molecules as well as other transcriptional and translational regulatory elements. Considering that the human proteome consists of over 100.000 proteins, it seems certain that the "one-gene-one-enzyme hypothesis" of Beadle and Tantum from 1941 explaining the relationship between genes and proteins is too simple.[2] Several post-transcriptional modification processes were identified, which play an important role in the generation of the proteome diversity of eukaryotes. One of the most notable contributions to that enormous diversity can be generated by a process called RNA processing.[3-4]

1.1.1   RNA processing

The discovery that every RNA sequence is not representing a simple copy of its coding DNA, as well as the detection of long heterogeneous nuclear RNAs (hnRNAs), investigated the role of RNA regulation as a central point in gene expression.[5-6]

Controlled by transcription factors, *cis*-elements as well as promoter, enhancer and silencer sequences, the nowadays termed pre messenger RNA (pre-mRNA) is transcribed from the DNA template by the RNA-Polymerase II. After transcription, the conversion of pre-mRNA transcripts into smaller mature messenger RNA (mature mRNA) takes place. This process is called RNA processing. The pre-mRNA undergoes three main modifications, the 5´ capping, 3' polyadenylation, and RNA splicing.[7] These nuclear processes determine the fate of the transcript and thereby regulate the cellular machinery.[8]

The first RNA processing event is the 5' capping. Here, the 5' triphosphate terminus (pppN) of a primary transcript is modified by the enzymatic activity of a triphosphatase, a guanyl transferase and a methyl transferase to a 7-methylguanosine-triphosphate (7meGpppN).[9] This modification protects the RNA from exonucleases[10] and facilitates the transport through nuclear pores into the cytosol as well as the recruitment of the mature mRNA to the ribosomes.[7] After the final endonucleolytic cleavage, 10-30 nucleotides downstream of a signal sequence, the resulting 3' end gets polyadenylated by the polyadenylate polymerase using ATP as a precursor.[10] The poly(A) tail also protects the transcript and thereby defines the half-life of the mature mRNA.[11]

The third and most complex part of RNA processing is the removal of noncoding intervening sequences (introns) from the pre-mRNA sequence and the rearrangement of coding sequences (exons). The splicing process is controlled and catalyzed by a large complex called spliceosome. The complex comprises several proteins and small nuclear RNA molecules forming small nuclear ribonucleoproteins (snRNPs) to interact with the intron and to form the different complex compositions needed for the splicing process.[12-13] The intron recognition and removal relies on three certain sequences, including the 5' splice site, the branch point and the 3' splice site (Figure 1). The highly conserved 5' splice site (acceptor site) labels the transition

from an exon to an intron and is composed of two nucleotides (GU). The 3' splice site (donor site) AG is located at the end of an intron and is connected to an upstream polypyrimidine tract followed by an adenosine as branching point.[3, 14] The splicing mechanism consists of two sequential transesterification reactions. First, the 2' OH-group of the branching point builds a phosphodiester bond with the nucleotide of the 5' splice site, forming the lariat intermediate. This is followed by the ligation of the two exons, in which the free 3' OH group of the released 5' exon is attacking the last nucleotide of the intron at the 3' splice site, releasing the intron lariat.[12, 15]
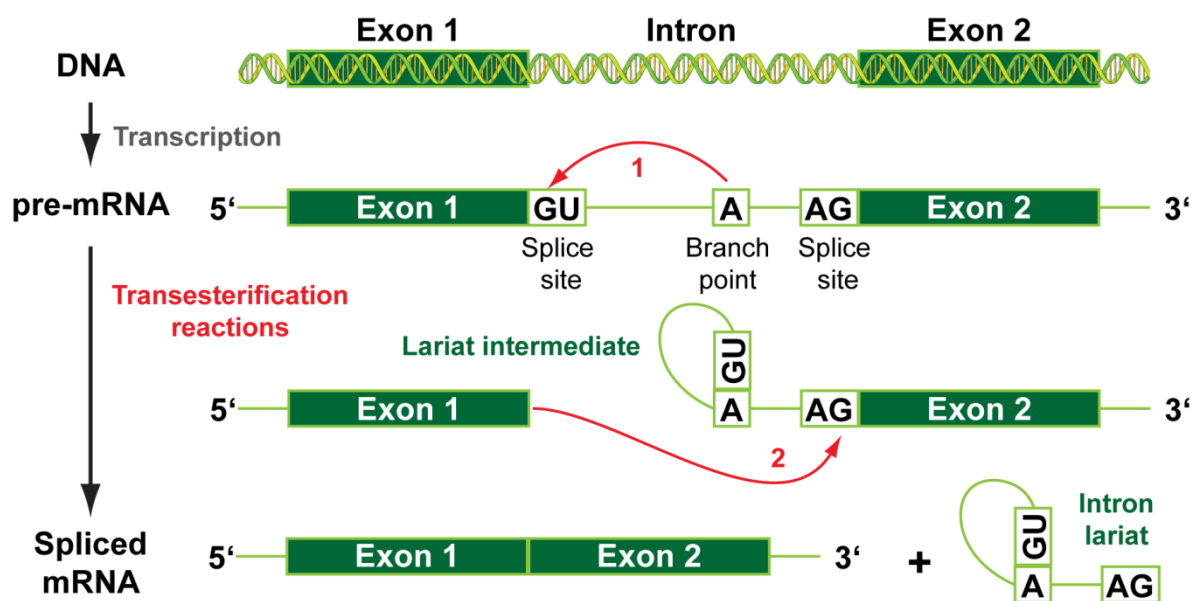
Figure 1. RNA splicing mechanism. After the transcription of the DNA into an exact RNA copy called precursor messenger RNA (pre-mRNA) the noncoding intron sequences have to be removed and the coding exons are joined together. This mechanism is regulated and catalyzed by the spliceosome, a large RNA-protein complex consisting of five small nuclear RNPs and numerous additional proteins. The identification of the noncoding intragenic region is obtained by conserved sequences flanking this sequence: the 5' splice site (GU) and 3' splice site (AG) as well as an adenine nucleotide (A) as branching point in close proximity to the 3' splice site. The biochemical mechanism is based on two sequential transesterification reactions (indicated in red). After the first transesterification of the 5' splice site and the branch point a lariat intermediate is formed. The second transesterification assembles the exon sequences forming the spliced mRNA and releases the intron lariat.

1.1.2   Alternative splicing - Multiple proteins from a single gene

Alternative splicing is one of the key mechanisms of proteomic and functional diversity in eukaryotes.[16] This tightly regulated gene expression process leads to a single gene coding for multiple proteins (Figure 2) in a cell type and developmental stage specific manner. Various alternative splicing forms, regulated by a system of trans-acting proteins (activators and repressors) and their *cis*-acting binding sides (silencer and enhancer), are responsible for the correct integration of the right exons.[17] The process of constitutive splicing aligns all exons of a pre-mRNA transcript. The most common alternative splicing mode in humans is exon skipping. Hereby, an exon is completely spliced out, which results in a shorter mRNA transcript (Figure 2). Alternative splicing thereby directs the synthesis of various protein isoforms with different cellular functions from a single mRNA transcript.
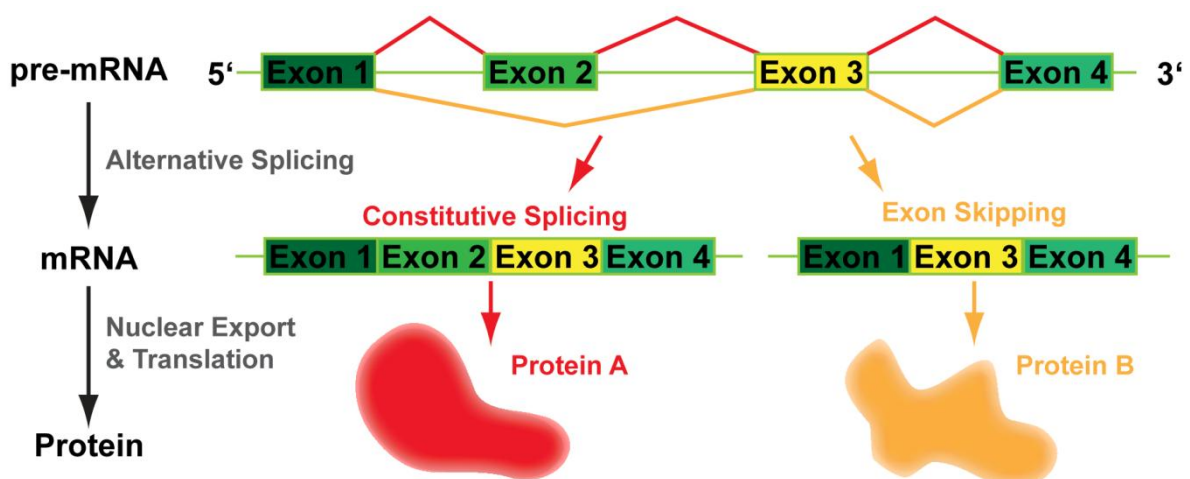
Figure 2. Schematic illustration of the alternative splicing process. This process enables mRNA to direct synthesis of various protein isoforms from a single pre-mRNA transcript. After the transcription of pre-mRNA, the molecule undergoes the splicing procedure as one part of the RNA processing. The constitutive splicing process (red) aligns all exons of the pre-mature transcript and removes the introns. The alternative splicing process is most often conducted by exon skipping (orange) resulting in various forms of mature mRNA coding for different protein isoforms.

It was shown that more than 95% of the human genes containing several exons undergo alternative splicing processes.[16, 18-20] Not only exon-skipping but also intron retention, mutually exclusive exons or the induction of alternative 3' or 5' splice sites are possible alternative splicing events (Figure 3). Since alternative splicing impacts development and physiology, alterations in mRNA splicing caused by genomic mutations can induce numerous human diseases.

1.1.3 Aberrant splicing

Splicing is a tightly regulated gene expression process. Alterations caused by genomic mutations can lead to incorrect splice site recognition. Furthermore, changes and defects in the splicing machinery can occur, both resulting in aberrantly spliced mRNA.[21-22] Mutations in the *cis*-acting elements (splicing sites) have a direct impact on the expression of one gene and can mainly result in skipping of one or more exons as well as intron retention.[23] Single-nucleotide polymorphisms (SNPs) located in coding regions can have a severe influence on splicing, inducing various diseases.[24] This process is driven either by splice site disruption, or activation of cryptic splice sites when a mutation disrupts the original site or create a *de novo* splice site (Figure 3).[25]
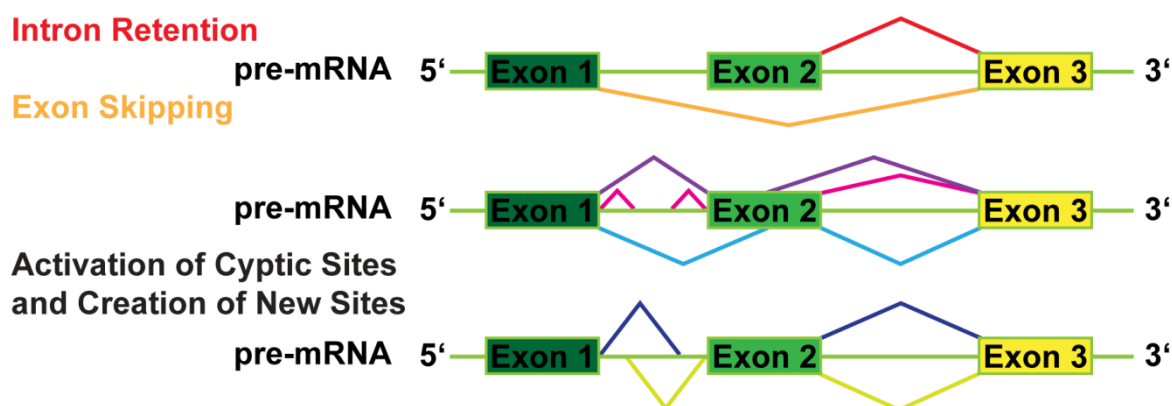
Figure 3. Schematic illustration of alternative or aberrant splicing patterns. A multi-exon pre-mRNA sequence can be spliced in various modes, resulting in different mature mRNAs. In contrast to constitutive splicing, intron retention (inclusion of an intron), exon skipping (exclusion of an exon), or the extension and shortening of sequence parts by the activation and creation of new cryptic sites can take place. Alterations in mRNA splicing caused by genomic mutations can induce defective alternative splicing patterns and severe diseases.

Partly intron retention in β-Thalassemia, a genetic blood disorder, is caused by a point-mutation in intron 2 of the β-globin gene activating aberrant splice sites.[26-27]

Disruption of an alternative splice site in cystic fibrosis caused by a *cis*-acting mutation results in loss of function of the cAMP-dependent transmembrane chloride channel that is expressed in secretory epithelium, which is followed by a severe pulmonary and pancreatic disease.[28]

The congenital neuropathy Familial Dysautonomia (FD) is induced by a splice site mutation of the IKBKAP gene. An intronic T→C substitution disrupts binding of the U1 snRNP to the 5' splice site (donor site), causing exon skipping which results in a frameshift. Dysfunctional IKBKAP generates a demyelinating phenotype affecting the autonomic nervous system and somatic sensory neurones.[29]

Hutchinson–Gilford progeria syndrome (HGPS) is caused by mutations in the lamin gene (*LMNA*), coding for two alternatively spliced proteins. The most common mutation is a C→T point mutation in exon 11, activating a cryptic splice site, resulting in a partly exon exclusion. This genetic disorder leads to premature aging including postnatal growth retardation, atherosclerosis and bone dysplasia.[30]

Tauopathies are an example for diseases of the central nervous system caused by a change in the protein isoforms ratio. Here, the microtubules binding tau protein induces abnormal intracellular filament accumulations, due to an aberrant ratio of the protein isoforms containing three or four microtubule binding regions. Especially mutations effecting the splicing regulation of exon 10 (inclusion or skipping) alter the normal fraction of tau protein isoformes.[31]

Alternative splicing has also been shown to be a main participant in cancer development, including uncontrolled proliferation, migration, methylation changes and resistance to apoptosis and chemotherapy. It contributes to tumorigenesis due to the production of cancer progress stimulating splice isoforms induced by mutations effecting splice sites or the spliceosome.[32-36]

Alteration in the splicing process can directly cause diseases and is also able to modify the severity of the disease phenotype or be linked with disease susceptibility. An enormous amount of diseases are based on mutations exhibiting a primary pathogenic effect on splicing.[28] These numbers reveal the necessity to target mRNA processing directly, to modulate the disease at its roots.

1.2 Molecular therapeutics to modulate the disease at its roots

The completion of the Human Genome Project enabled the identification and biochemical characterization of genes as well as the detection of diseases derived by abnormalities in the genome or gene expression.[1, 37]

The evolving knowledge about genetic disorders accelerated the development of biomedical research and the strongly connected field of molecular therapy. The substitution of deficient genes by transfer of genetic material known as gene therapy, as well as protein transduction and the combination of both, build novel strategies for a causal treatment of diseases.

Up to now approaches to treat human disease are most often focused on the end of the defective signaling cascade like inhibiting enzymes, supplementing metabolites or interfering in signaling pathways. To directly target the genome, which serves as a blueprint of all downstream activities, or the direct transcripts revolutionized the toolbox of molecular therapeutics to modulate the disease at its roots. Furthermore, previous studies have shown that even a small portion of drug reaching the molecular target site is able to provide the therapeutic effect, indicating the strength of molecular therapeutics including gene therapy.[38]

Antisense oligonucleotides (ASOs) targeting the splicing mechanism in mRNA processing hold great promises due to the high amount of aberrant splicing diseases and the involvement of splicing aberrations in cancer development. Furthermore, ASOs can be applied to alter the splicing pattern and thereby restore functional gene expression of several acquired or inherited diseases caused by mutations in the genomic DNA,.[39-41]

Another encouraging approach is to treat the disease just once by direct targeting of the genomic DNA. Purposive treatment of the genomic DNA could have the ability to replace further treatments and cure several hereditary genetic diseases. To realize this concept, an editing tool with the ability to target, cut and alter the genomic DNA in a highly specific manner is needed. The investigation of the CRISPR/Cas9 system comprises these characteristics and thereby constitutes a promising technique to treat genetic disorders on DNA level.

1.3   Splice-switching antisense oligonucleotides as therapeutic drugs

The concept of synthetic ASOs was first reported in 1978.[42] Their identification as an efficient tool to regulate gene expression aroused the interest in this technology in terms of therapeutic applications. However, the successful application of ASOs as therapeutic drugs require a deeper understanding of the molecular mechanisms, as well as the development of efficient and safe delivery vehicle. Classical therapeutic ASOs are 15 to 30 nucleotides long and target a specific complementary mRNA region.

This chapter focuses on ASOs which specifically target and alter the splicing process and are therefore termed splice-switching oligonucleotides (SSOs). To use this technology several limitations needed to be addressed. First, the effective intracellular delivery of sufficient SSO amounts had to be enabled. A favorable pharmacokinetic profile with a high stability and low toxicity of the SSO as well as a high specificity with low off-target effects to keep other cellular functions intact was crucial.[43]

SSOs are synthetic molecules, designed to complementary bind pre-mRNA creating a steric block to alter the recognition by splicing factors resulting in an alternative splicing pattern or the reactivation of the normally used splice site.[41] To perform this task the SSO needs to be chemically modified to avoid cleavage by RNase H[44-45] and to increase serum stability due to resistance against enzymatic degradation. Further characteristics like a strong binding to the pre-mRNA sequence as well as a low immunogenicity are needed for further *in vivo* applications.[36] Several chemical modifications including carbohydrate, backbone and base modifications were investigated to fulfill the requirements needed for successful splicing alteration.

After the improvement of the first ASO chemistry from a phosphodiester to a more stable phosphorothioate moiety, several further synthetic derivatives with a high stability and affinity were developed. Modifications at the 2'-hydrogen of the ribose with different residues like a 2'-O-methyl (OMe) and 2'-O-methoxyethyl (MOE) or a 2'-O-aminopropyl (AP) results in RNase H resistance as well as nuclease resistance in general and higher binding affinities (Figure 4).[46] Therefore, these nucleic acid modifications made them suitable for the usage in SSOs. Many phosphorothioates are currently being developed as potential therapeutic for several diseases including

the Alzheimer disease,[47] spinal muscular atrophy,[48] DMD,[49-50] Huntington disease,[51] hypercholesterolemia[52] as well as in different cancer treatments.[36, 53]

Another promising ASO group are the locked nucleic acid (LNA) oligomers. In LNAs, the 2' oxygen and 4' carbon of the ribose are linked via a methylene bridge resulting in a locked 3'-endoconformation, which reduces the conformational flexibility of the ribose. This leads to remarkably high binding affinities with an increased melting temperature of around 5 °C per base and nuclease resistance.[54]

Besides carbohydrate modifications, alteration of the entire backbone revealed a high potential for further SSO therapeutic development (Figure 4). Peptide nucleic acids (PNAs) with a polyamide backbone[55] and especially phosphorodiamidate morpholinos (PMOs) with bases bound to morpholine rings linked through uncharged phosphorodiamidate groups have demonstrated efficacy in the treatments of genetic disorders.[44, 56] PMOs combine all key properties required for effective antisense splice-switching activity like sequence specificity, resistance to degradation, a lack of off-target effects as well as no significant effects on the on the innate immune system, good water solubility and well as no required assistance from other cell factors.[44, 56-57] However, a safe and efficient *in vivo* delivery technology resulting in sufficient intracellular PMO amounts still constitutes the major obstacle.
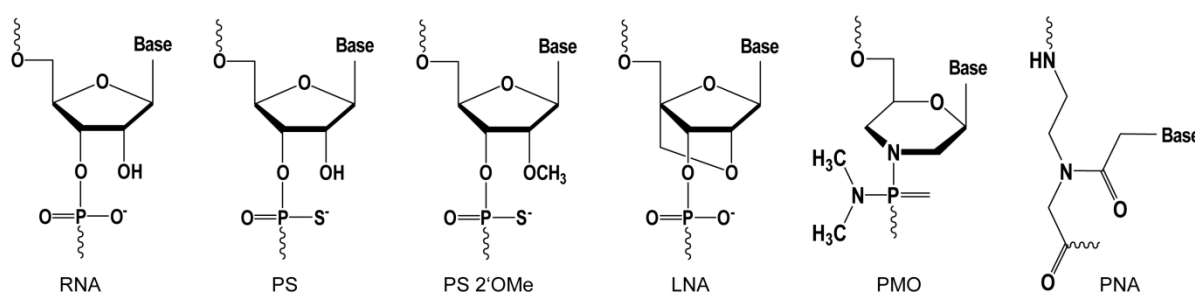
Figure 4: Chemical structure of different oligonucleotide analogs. RNA: Ribonucleic acid; PS: Phosphorothioate RNA; PS 2'OMe: Phosphorothioate 2'-O-methyl; LNA: Locked-nucleic acid; PMO: Phosphorodiamidate morpholino oligomer; PNA: Peptide nucleic acid

Nusinersen and eteplirsen are the first successful examples of FDA approved SSOs.[48, 58] Nusinersen (Spinraza™, Ionis Pharmaceuticals) is a phosphorothioate SSO, with a methoxyethyl modification on the 2′ position of the ribose sugar, against spinal muscular atrophy (SMA). This autosomal recessive disease is caused by mutations in the SMN1 gene resulting in a loss of SMN1 protein function and thereby

the degradation of motor neurons. A nearly identical gene from the same family called SMN2 just differs in a single nucleotide that result in the exclusion of exon 7 and a fast degradation of the nonfunctional RNA transcript. Nusinersen is targeting the intronic splicing silencer N1 resulting in the inclusion of exon 7 in SMN2 restoring a fully functional SMN protein.[48]

Eteplirsen (Exondys 51™, Sarepta Therapeutics Inc.) is a PMO for the treatment of DMD, a X-linked recessive neuromuscular disorder.[58] DMD is caused by mutations in the DMD gene coding for a membrane associated protein linking cytoskeletal actin with the extracellular matrix. Several different possible mutations in the DMD gene are known to either result in the disruption of the reading frame or to introduce a stop codon. Exon 51 is part of the mutation hotspot region in this gene, approximately 13 % of DMD patients suffer from inclusion of a defective exon 51 transcript. Eteplirsen binds specifically to a binding site in exon 51 resulting in exon skipping and restoration of the reading frame producing a shorter but functional dystrophin-like protein.[59-61]

1.4   The CRISPR/Cas9 system as genome editing tool

The investigation of the CRISPR/Cas9 system as an easily programmable RNA guided nuclease revolutionized the field of genome engineering. The technology, derived from the bacterial adaptive immune system, enables fast and accurate altering of genomic information with a simple two-component system.[62-63]

The molecular mechanism of the Cas9 protein complexed to a single guide RNA (sgRNA) relies on the generation of DNA double-strand breaks (DSBs, Figure 5). The sgRNA is composed of a crRNA sequence, a 20 nucleotides long sequence at the 5' end matching the target gene sequence fused to the hairpin building *trans* activating crRNA (tracrRNA) sequence at the 3' end that binds to the Cas9 protein. This enables the sgRNA to bind, stabilize and guide the Cas9 endonuclease to the DNA target site.[62] Watson-Crick base-pairing between the sgRNA and the target DNA as well as the presence of the protospacer adjacent motive (PAM-sequence, consisting of a NGG)[64] activate the two catalytic nuclease domains of the Cas9 protein.[65] After inducing a double-strand-break the DNA damage is repaired by cellular DNA repair mechanisms, either via the non-homologous end joining DNA repair pathway (NHEJ) or the homology directed repair (HDR) pathway. The repair of the DNA is error prone. Thereby the insertions and deletions, which might be introduced, can disrupt the gene function and cause a knockout of the target gene due to the induction of frameshift mutations (Figure 5).[63, 66] By providing a donor DNA with homologous regions the HDR pathway can be utilized for the introduction of precise genetic modifications creating transgenic DNA.[67-69]

RNA guided DNA recognition of the CRISPR/Cas9 system offers several advantages over other genome editing systems such as the Zinc Finger Nucleases (ZFNs) or Transcription Activator-like Effector Nucleases (TALENs). It provides high specificity and efficiency regardless of the methylation status of the target gene. Usage of more than one sgRNA sequence enables editing of multiple genes simultaneously, so-called multiplexing.[70] Furthermore, it has a high simplicity in target design and no need to reengineer the nuclease for each new target.[71]

Not only the therapeutic use of this technology[72-75] will have a high impact on molecular therapeutics, it will also have a big influence on drug discovery.[76-78] By using the CRISPR/Cas9 system to inactivate or accelerate specific genes, the

determination of genes or proteins that affect or cause a disease will provide new targets for potential drugs. Furthermore, engineered cell based or *in vivo* models with precise genetic modifications will help to predict efficacy as well as side effects.[75, 79]
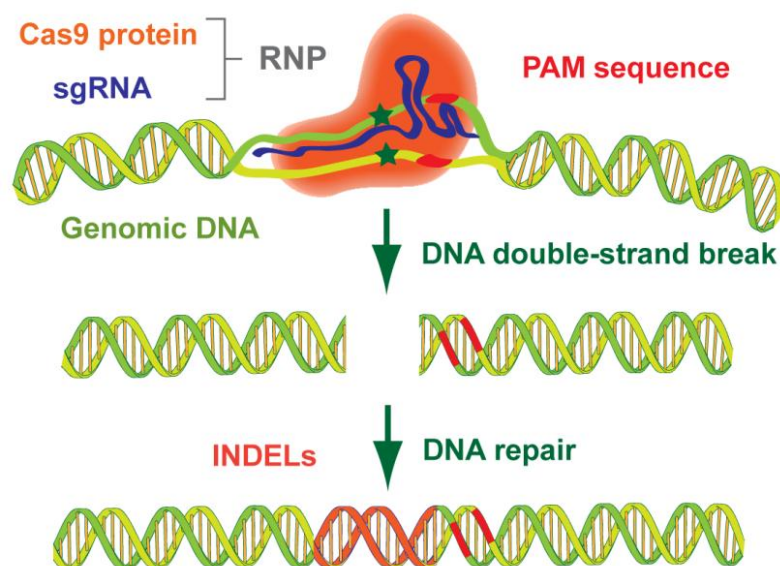
Figure 5. Schematic illustration of the CRISPR/Cas9 genome editing mechanism. To use the CRISPR/Cas9 system as genomic tool a minimal set of two molecules is needed. The Cas9 nuclease and the sgRNA build the ribonucleoprotein complex (RNP). Binding of the sgRNA to the target DNA next to a protospacer adjacent motive (PAM) sequence results in a blunt double-strand break of the DNA. Repair of the double-strand break by cellular DNA repair mechanisms is error prone. Nucleotide insertion and deletions (INDELs) can occur and destroy the gene function.

A clear drawback of this technology are the off-target effects, immunogenicity as well as the size of the Cas9 protein which complicates efficient delivery. Developing better delivery strategies and minimizing off-target effects by limiting the presence of the functional complex, have the ability to further develop the usage of this innovative genomic tool. Previous studies have shown that the direct delivery of the RNP complex instead of the DNA or RNA analogues is able to reduce off-target effects due to the timely degradation. Furthermore, the complex is directly functional without the need of transcription and translation and avoids the risk of spontaneous genome integration. The following chapter of this thesis will focus on most recent delivery strategies of Cas9/sgRNA RNP complexes.

1.5 Delivery strategies for different molecular therapeutics

To use molecular therapeutics for efficient treatment, it is imperative to achieve sufficient intracellular drug concentrations. The cellular uptake and especially endosomal escape of unmodified macromolecular drugs including nucleic acids and their analogs, proteins as well as RNP complexes are very low. Therefore, the success of these molecular therapeutics rises and falls with an efficient delivery vehicle. For the development of a suitable carrier system several circumstances need to be considered, including cargo properties, target tissue, intracellular target site as well as the targeted molecule and the molecular mechanism - all requiring different carrier characteristics.[80-81] In comparison to viral vectors, which are limited to a rather low capacity, non-viral vectors exhibit enormous high flexibility regarding possible cargos including macromolecular structures like proteins.[82] This given fact, as well as several further limitations of viral vectors like the scale-up of virus production, the potential for insertional mutagenesis and possible immune responses,[83] suggest the development of synthetic carrier systems towards higher efficiency as the most promising strategy.[84]

To reach the target site, several hurdles need to be addressed, like rapid molecule degradation in biological fluids, fast clearance after systemic administration, immune system recognition, as well as target cell penetration and intracellular release.[85] Besides the already discussed chemical modifications, also conjugation to a carrier molecule or supramolecular assembly into nanosized formulations can mediate cargo protection and a favorable pharmacokinetic profile. The different delivery stages require biodynamic flexibility of the physicochemical and biological properties of an effective carrier system. The surface charge, size, polydispersity, shape and surface hydrophobicity/hydrophilicity can significantly influence the interaction with serum proteins and thereby the particle stability as well as the particle identity due to the emerging protein corona.[86-87] Depending on the nanoparticulate characteristics interaction with the cell membrane results in the uptake mainly through endocytosis. Depending on the cell type, as well as the carrier and cargo properties different active endocytotic uptake mechanisms are taking place.[88-89] Furthermore, unspecific adsorption of positively charged carrier systems to the negatively charged cell surface can mediate enhanced cellular uptake as well as cytotoxicity, due to increased surface tension and pore formation.[90-92] Another important role is

constituted by hydrophobicity and interfacial force between nanoparticles and the cellular membrane, resulting in an enhanced lipid membrane interaction.[93-94]

The intracellular fate of the internalized cargo, initially results in vesicular or endosomal entrapment.[95] Most of the early endosomes undergo a series of maturation stages driven by acidification and recruitment of lysosomal enzymes. Escape of the cargo from this destructive environment into the cytosol is a crucial step for further cellular trafficking to the final target site.[96] Escape from the endolysosomal compartment requires membrane disturbance, for example through cationic carrier systems initiating the proton sponge mechanism, first described by Jean-Paul Behr.[97-98] The classical hypothesis describes a buffering mechanism induced due to protonation of the amino groups, followed by proton accumulation and chloride influx into the endosomal lumen, which leads to osmotic swelling and finally endosomal membrane rupture.[98-99] Beside cytosolic delivery, intracellular transfer to the site of action, as well as cargo release are required for therapeutic efficiency. Extracellular and intracellular requirements differ tremendously regarding particulate stability, a compromise between a stable extracellular assembly and intracellular disassembly is required for successful cargo release within a desired cellular region. Depending on the cargo and target site, specific localization tags, like the nuclear localization signal (NLS) peptide sequence for nuclear targeting, can influence the intracellular trafficking.[100]

Several approaches for enhancing the intracellular delivery of macromolecules have been investigated, including the use of cationic polymers,[99, 101] peptides,[102-103] proteins,[104] and lipids,[105-106] as well as liposomes,[107-109] and membrane translocating peptides.[110] Especially carrier systems with an amphiphilic character have proven to be successful for macromolecular drug delivery.[88, 99, 106, 111-113] A better understanding of the relationship between physicochemical properties and biological behavior as well as a redesign of the properties based on this knowledge could optimize the activity/toxicity profile of carrier systems tremendously.

1.5.1 Delivery systems for synthetic uncharged antisense oligonucleotides

The use of chemically modified synthetic nucleic acids in the antisense therapy is highly promising and already showing first success in various clinical trials.[114] Nevertheless, efficient and safe delivery of sufficient ASOs amounts to the intracellular target site is still a major obstacle for further clinical development. Due to their favorable characteristics, uncharged ASOs such as PNAs and PMOs hold great promises as antisense therapeutics, especially for treatments based on splicing modification (Chapter 1.3). Although SSOs can be delivered as naked oligonucleotides,[115] after systemic administration the unmodified molecules are cleared rapidly and additionally insufficient amounts are delivered to the intracellular target site due to poor cellular uptake.[116-117] The development of a carrier system could increase tissue specific delivery and efficiency at lower doses, limiting off-target effects and toxicity.

Since uncharged nucleic acids are not prone to form ionic complexes with positively charged carrier systems, covalent modification (conjugation to targeting ligands or carrier systems) or incorporation into a drug delivery system (nanoparticle-based approaches) are needed for a successful intracellular delivery. Previous strategies for improved delivery have been largely based on cell penetrating peptides (CPPs).[118-121] But also guanidine dendrimers,[122] cationic backbone[123] and lipidic[124] modifications, as well as liposomes,[125] were utilized to enhance the transfection efficiency of SSOs. The already discussed, convincing characteristics of PMOs lead to a number of delivery approaches to enhance *in vivo* transfection efficiency. The investigation of CPPs covalently conjugated to PMOs achieved remarkable results in pre-clinical DMD and SMA mouse models.[103, 126-128] The uptake mechanism of CPPs is discussed controversially, from the initial widespread theory of direct translocation across the cell membranes, to interaction of the positively charged CPPs with the negatively charged cell surface followed by endocytic pathways.[129-135] Nevertheless, most CPPs suffer from high toxicity, low cell, and tissue selectivity as well as poor endosomal escape abilities upon endosomal entrapment and instability due to enzymatic degradation in biological fluids.

Various advanced SSOs with highly specific target sites were detected,[41, 136] the combination with improved delivery vehicles would be of great utility and provides insights into potential SSO-based therapeutics.

1.5.2 Cas9/sgRNA delivery

Genome editing technologies like the CRISPR/Cas9 system have the potential to be utilized to cure diseases caused by a genetic disorder. To use this system therapeutically, a safe and efficient delivery into the nucleus of the target cells is needed. Previous strategies are most commonly based on the delivery of the nucleic acid precursors of both needed components. Beside physical delivery methods including microinjection,[137-138] electroporation[139-140] and hydrodynamic delivery[141] with limited *in vivo* applications, several viral vector based delivery methods evolved to use this highly efficient gene editing tool. Especially for *in vivo* applications viral vectors including specifically engineered adeno-associated virus (AAV)[142] and full sized adenovirus[143] as well as lentivirus[144] vehicles are used due to the high knock out efficiencies. However, mutagenesis, immunogenicity and limited loading capacity are major drawbacks for their use as carrier systems for therapeutic approaches.

The direct delivery of the functional Cas9 protein complexed with its sgRNA has several advantages over the delivery of their encoding DNA sequences or mRNA molecules, as described in chapter 1.4. However, the stability of proteins and especially single stranded RNA molecules in biological fluids is rather low due to enzymatic degradation. Therefore, incorporation into a stable carrier system is required to retain functionality for efficient intracellular activity. Furthermore, binding of the slightly positively charged Cas9 protein to the negatively charged sgRNA results in a negatively charged RNP complex exhibiting a poor membrane permeability, but a proper binding affinity to potentially positively charged carrier systems. Based on this characteristic and several further approaches different non-viral delivery technologies evolved for the delivery of Cas9/sgRNA RNP complexes.

Ramakrishna et al. successfully generated the first Cas9 protein and sgRNA co-delivery system by a CPP-conjugated recombinant Cas9 protein and co-delivered CPP-complexed sgRNA in form of positively charged nanoparticles. They demonstrated in several cell lines efficient gene disruption, with reduced off-target effects relative to plasmid transfection.[145]

Another highly promising approach is based on gold nanoparticles with a cationic arginine surface modification complexed to an engineered Cas9/sgRNA RNP resulting in remarkable knock out efficiencies.[146] Lee et al. also reported the use of

gold nanoparticles complexed to RNP complexes and finally coated with a silica layer to increase the negative charge density followed by coating with endosomal disruptive polymer, to treat mice suffering from DMD. They demonstrated that a single injection showed partially recovered dystrophin gene expression and thereby muscle function and reduced levels of fibrosis.[147]

Liposome, as well as cationic lipid based systems, are well-established nonviral vector systems used for a wide range of macromolecules.[148] Lipid nanoparticles demonstrated several advantages including protein and nucleic acid protection due to encapsulation. Furthermore, the lipid moieties are able to interact with the cellular membrane enhancing cellular uptake and endosomal escape. Zuris and colleagues used the commercially available Lipofectamine 2000™ for the packaging of the highly anionic RNP complex and demonstrated gene knock out in the mouse inner ear *in vivo*, demonstrating cationic lipids as a powerful tool for the delivery of Cas9/sgRNA RNPs.[111] Using bioreducible cationic lipids containing a disulfide linkage in the hydrophobic tail, lead to the degradation of the lipid in the reductive intracellular environment, enhancing cargo release and thereby knock out efficiency.[149] In a more recent study, nanoliposomes containing lecithin were used to modulate the function of glucagon-like peptide 1, by delivery of functional Cas9/sgRNA RNP complexes in type 2 diabetes mellitus mice, resulting in normalized blood glucose levels.[150]

Polymeric carriers exhibit ideal characteristics for a reasonable delivery material, due to their biocompatibility, flexibility, and simplicity. In a recent work from Liu et al. boronic acid-rich dendrimers were used for the delivery of several native proteins and Cas9/sgRNA RNPs. The dendrimer efficiently assembled the RNP complexes into nanoparticles and showed GFP knock out efficiencies up to 40%. Furthermore, the system was used to target multiple genome loci of different cell lines, which indicates a promising and broad biomedical applicability.[151]

Several Cas9/sgRNA RNP delivery systems evolved since the discovery of the CRISPR/Cas9 system. But major drawbacks including immunogenicity, low *in vivo* efficiency, and toxicity demonstrate the requirement of better carrier systems for a more favorable activity/toxicity profile and precise genome modification.

1.5.3 Sequence-defined oligo(ethylenamino) amides

Sequence-defined oligo(ethylenamino) amides (OAAs) are a versatile delivery platform for various therapeutic modalities, like nucleic acids,[152-153] proteins[101, 106] and drugs.[154-155] These artificial peptide-like structures consist of different combinations of distinct building blocks, like natural α-amino acids, artificial oligoamino acids as well as hydrophobic fatty acid domains. Different topological subclasses, like 2-arm,[156] 3-arm,[152] 4-arm,[157-158] comb architectures[159] or T-shaped,[152] were developed.

OAAs are assembled via solid phase assisted peptide synthesis, which determines their highly precise nature.[160] They can be tailored specifically to meet the requirements of different cargos and were optimized in several studies towards their specific payload. The oligomers typically contain several repetitions of the artificial oligoamino acid succinyl-tetraethylenpentamine (Stp). This cationizable building block is partially protonated at physiological pH and enables the complexation of negatively charged cargos, like nucleic acids, into nanoparticles. Furthermore, the Stp units facilitate endosomal escape, due to the "proton-sponge effect" and thereby overcome a major obstacle in the delivery pathway.[99, 161] Additionally, the oligomers contain different natural α-amino acids. Terminal cysteines (Cys) have been shown to promote improved nanoparticle stability due to their crosslinking-potential through the formation of disulfide bonds.[161] The introduction of histidines (His) was shown to induce improved endosomal buffering and thus, endosomal escape.[162] Fatty acid domains can on the one hand stabilize the delivery systems via hydrophobic interactions. On the other hand, they enable efficient intracellular delivery by promoting membrane lipid disorders.[163] Structural modifications of the hydrocarbon moieties have been shown to impact the bioactivity of the carrier system.[164-165] Tyrosine tripeptide motifs promote the stable incorporation of the cargo into the nanoparticle via π-stacking effects.[166] T-shape lipo-OAAs, which consist of a linear backbone of natural and artificial amino acids and a branching fatty acid unit, have been successfully used for the delivery of various therapeutic molecules.[154, 166-168]

To reduce the risk for unspecific interactions with biological components upon exposure to physiological media, the surface of the delivery system can be modified by covalent attachment of shielding agents like polyethylene glycol (PEG). The introduction of an active targeting ligand can facilitate the efficient internalization of the nanoparticle into the target cell.[155, 167-168]

1.6   Aim of the thesis

Novel molecular therapeutics like artificial antisense nucleotides and genome editing nucleases revolutionized the field of molecular therapeutics. Efficient intracellular delivery of sufficient drug amounts is imperative to achieve a therapeutic effect. Combining save and efficient delivery system with these technologies could lead to a new era of individualized molecular medicine to treat diseases at their origin.

The aim of this thesis was the development of delivery strategies for two highly promising molecular therapeutics, with substantially different physicochemical characteristics: phosphorodiamidate morpholino oligomers (PMOs) and Cas9/sgRNA ribonucleoprotein (RNP) complexes. In both cases, the nucleus is the ambitious target site to achieve intended therapeutic actions. For both cargo types, carrier systems based on sequence-defined aminoethylene lipopeptides were to be developed and optimized.

PMOs are a class of artificial ASOs and hold great potential to treat diseases by splicing modification. Since PMOs are uncharged molecules they do not form ionic complexes with positively charged carriers. Modification of PMOs with dibenzocyclooctyne needed to be introduced for the covalent linkage of azide-bearing lipopeptides via strain-promoted azide-alkyne addition for the development of new aminoethylene-based PMO conjugates. Further structural variations, different formulations and mechanistic studies needed to be conducted to determine the impact of the contained fatty acid.

The CRISPR/Cas9 system is a highly precise and programmable endonuclease. The presence of this functional RNP complex inside cells is imperative for intended specific genome modifications. For the development of a favorable carrier system, a human optimized version of the Cas9 protein needed to be expressed, several sgRNAs *in vitro* transcribed and both components purified. Binding of the negatively charged sgRNA by the Cas9 protein results in negatively charged RNPs. Suitable carriers needed to be identified to stably encapsulate both components to protect the enzymatic activity of the protein as well as the highly labile single stranded RNA against enzymatic degradation. Structural variation and complex formation studies needed to be conducted to obtain intranuclear delivery of the functional RNP complex for efficient knock out of an endogenous gene construct.

2 Chapter I:

Supramolecular Assembly of Aminoethylene-Lipopeptide PMO Conjugates into RNA Splice-Switching Nanomicelles

Jasmin Kuhn[1], Philipp M. Klein[1], Nader Al Danaf[2], Joel Z. Nordin[3,5], Sören Reinhard[1], Dominik M. Loy[1], Miriam Höhn[1], Samir El Andaloussi[3], Don C. Lamb[2], Ernst Wagner[1], Yoshitsugu Aoki[5], Taavi Lehto[3,4], and Ulrich Lächelt[1]

[1]Department of Pharmacy and Center for NanoScience (CeNS), LMU Munich, 81377 Munich, Germany

[2]Department of Chemistry and Center for NanoScience (CeNS), LMU Munich, 81377 Munich, Germany

[3]Department of Laboratory Medicine, Karolinska Institutet, 17177 Stockholm, Sweden

[4]Institute of Technology, University of Tartu, 50411 Tartu, Estonia

[5]Department of Molecular Therapy, National Institute of Neuroscience, National Center of Neurology and Psychiatry (NCNP), Kodaira, 187-8502 Tokyo, Japan

The following sections are directly adapted from the original publication, which was finally published as Kuhn et al., Adv. Funct. Mater. 2019, 1906432.

Sections may have been moved for consistency.

Contributions: JK performed the experiments (PMO modifications, lipopeptide formulations for all experiments, HeLa pLuc/705 treatments *in vitro* and *in vivo*, erythrocyte leakage assays and flow cytometry) and wrote the manuscript. PMK synthesized the sequence defined aminoethylene-lipopeptides. NAD and the group of DCL performed the fluorescence correlation spectroscopy. JZN and the group of YA performed the treatment and RT-PCR analysis of H2K-*mdx*52 cells. SR supported the erythrocyte leakage assays. DML captured the transmission electron microscopy pictures. MH captured the confocal laser scanning microscopy pictures. TL and the group of SEA performed RT-PCR experiments and conducted splice-switching and luciferase activity assays in pLuc/705 based human hepatoma (Huh7), murine neuroblastoma (Neuro2A) and murine myoblast (C2C12) cells. EW provided conceptual advice. TL and UL conceived the study and wrote the manuscript. All authors contributed to the manuscript and conclusions of this work.

2.1   Abstract

Phosphorodiamidate morpholino oligomers (PMOs) are oligonucleotide analogs that can be used for therapeutic modulation of pre-mRNA splicing. Similar to other classes of nucleic acid-based therapeutics, PMOs require delivery systems for efficient transport to the intracellular target sites. Here, we present artificial peptides based on the oligo(ethylenamino) acid succinyl-tetraethylenpentamine (Stp), hydrophobic modifications and an azide-group, which we use for strain-promoted azide-alkyne cycloaddition conjugation with splice-switching PMOs. By systematically varying the lead structure and formulation, we determined that the type of contained fatty acid and supramolecular assembly have a critical impact on the delivery efficacy. A compound containing linolenic acid with three *cis* double bonds exhibited highest splice-switching activity and significantly increased functional protein expression in pLuc/705 reporter cells *in vitro* and after local administration *in vivo*. Structural and mechanistic studies revealed that the lipopeptide-PMO conjugates form nanoparticles which accelerates cellular uptake and that the content of unsaturated fatty acids enhances endosomal escape. In an *in vitro* DMD exon skipping model using H2K-*mdx*52 dystrophic skeletal myotubes, the highly potent PMO conjugates mediated significant splice-switching at very low nanomolar concentrations. The presented aminoethylene-lipopeptides are thus a promising platform for the generation of PMO-therapeutics with favorable activity/toxicity profile.
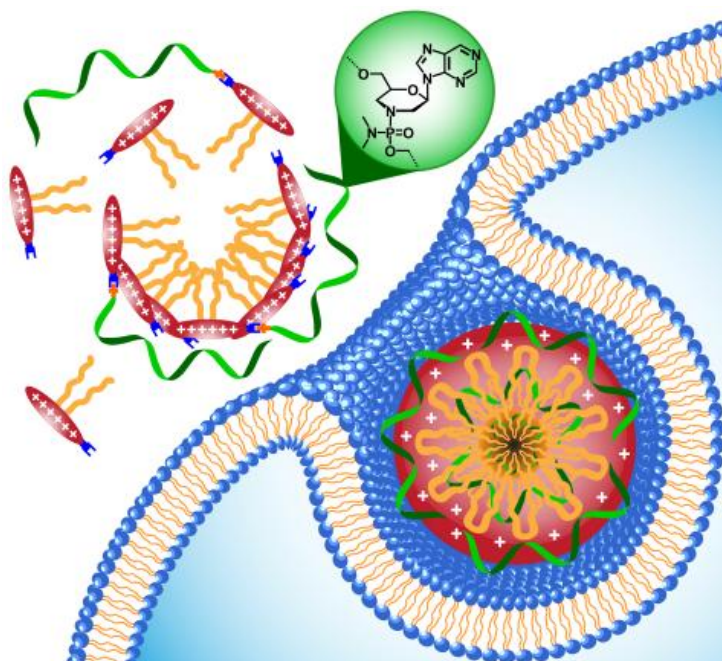
2.2 Introduction

Antisense oligonucleotides (ASOs) are a versatile molecular tool to modulate cellular processes by interacting with endogenous nucleic acids. Phosphorodiamidate morpholino oligomers (PMOs) are a class of artificial, uncharged ASOs with favorable stability, nuclease-resistance, low immunogenicity and toxicity.[56] A promising therapeutic approach based on ASOs is the modulation of gene expression by interfering with pre-mRNA splicing.[136, 169] Such splice-switching oligonucleotides (SSOs) represent innovative therapeutics and could be applied for a diverse range of acquired or inherited diseases,[41] including neuromuscular disorders,[112, 170-173] thalassemia,[174-175] inflammation,[176] retinopathies[177-178] and cancer.[179-180]

Eteplirsen, a PMO for treatment of Duchenne muscular dystrophy (DMD) and nusinersen, a phosphorothioate oligonucleotide against spinal muscular atrophy (SMA), are first examples of approved SSO therapeutics.[48, 58] Similar to other therapeutic nucleic acid approaches, SSOs require delivery systems for efficient transport to their target tissues and intracellular target sites.[181-182] Previous strategies for improved delivery of PMOs have been based on cell-penetrating peptides (CPPs),[118-120, 183-186] guanidine dendrimers[122] or cationic backbone modifications.[123] Wood and Gait have developed highly potent and well-studied PMO conjugates based on arginine-rich CPPs termed Pips that display remarkable efficacy in DMD and SMA mouse models.[103, 126-128, 187] Although not yet conclusively resolved, for the efficient cellular uptake of guanidinium-containing scaffolds, such as arginine-rich CPPs or dendrimers, contribution of non-endocyototic translocation mechanisms is discussed.[129-131, 133-134] A well-established alternative chemical motif of intracellular delivery systems is based on repeated aminoethylene units, such as in polyethyleneimine or related polyamines and conjugates.[188-194] Although the exact mechanism also here is still disputed, the high efficiency is generally attributed to a characteristic protonation of the repeating aminoethylene units in the endosomal range between pH 5 and 7.4 after endocytotic internalization.[98, 195-199] Sequence-defined oligo(ethylenamino) amides based on artificial oligoamino acids and solid-phase synthesis have been established as a delivery platform for charged nucleic acids and other therapeutics, which combines the advantages of aminoethylene based polymers with the chemical precision and versatility of peptides.[200-201] Here,

the synthetic strategy was utilized for the specific development of new aminoethylene based PMO conjugates.

2.3 Material and Methods

2.3.1 Materials

Phosphorodiamidate morpholino oligomers (PMOs) with the sequence CCTCTTACCTCAGTTACAATTTATA targeting a T to G point mutation at position 705 in intron 2 of the human β-globin gene (IVS2-705), and 51D with the sequence TTGTTTTATCCATACCTTCTGTTTG targeting the splice donor site of *Dmd* exon 51, were acquired from Gene Tools, LLC (Philomath, OR, USA). All PMOs were modified with a 3'-primary amine (PMO-NH$_2$) for DBCO functionalization. For experiments with fluorescence-based detection, PMO labeling was carried out using an additional 5'-azide modification (PMO-N$_3$).

Deionized water was purified in-house using an Evoqua Ultra Clear® Glass Panel Systems (Günzburg, Germany) and was used for all experiments.

Kaiser test solutions: 80 % (w/v) phenol in EtOH; 5 % (w/v) ninhydrine in EtOH; 20 μM KCN in pyridine (2 mL of 1 mM KCN (aq) in 98 mL of pyridine).[3]

HEPES buffered glucose (HBG, 20 mM HEPES, 5 % w/v glucose, pH 7.4) was prepared by dissolving 2.38 g HEPES (10 mmol) and 27.5 g glucose monohydrate in 490 mL water. The pH was adjusted to 7.4 by the addition of NaOH and water was added to a final volume of 500 mL.

2.3.2   Solid-phase peptide synthesis

Table 1. Summary of synthesized peptide sequences.

ID	Description	Sequence (C->N)
991	LP CholA	Y_3-Stp$_2$-K-ε[G-K-α,ε(CholA)$_2$]αStp$_2$-Y_3
1106	LP CholA	Y_3-Stp$_2$-K-ε[G-K-α,ε(CholA)$_2$]αStp$_2$-Y_3-K-ε(N$_3$)
1169	LP OleA	Y_3-Stp$_2$-K-ε[G-K-α,ε(OleA)$_2$]αStp$_2$-Y_3-K-ε(N$_3$)
1171	LP LinA	Y_3-Stp$_2$-K-ε[G-K-α,ε(LinA)$_2$]αStp$_2$-Y_3-K-ε(N$_3$)
1172	LP SteA	Y_3-Stp$_2$-K-ε[G-K-α,ε(SteA)$_2$]αStp$_2$-Y_3-K-ε(N$_3$)
1195	LP LenA	Y_3-Stp$_2$-K-ε[G-K-α,ε(LenA)$_2$]αStp$_2$-Y_3-K-ε(N$_3$)
1204	LP GonA	Y_3-Stp$_2$-K-ε[G-K-α,ε(GonA)$_2$]αStp$_2$-Y_3-K-ε(N$_3$)
1205	LP AraA	Y_3-Stp$_2$-K-ε[G-K-α,ε(AraA)$_2$]αStp$_2$-Y_3-K-ε(N$_3$)
1206	LP EPA	Y_3-Stp$_2$-K-ε[G-K-α,ε(EPA)$_2$]αStp$_2$-Y_3-K-ε(N$_3$)
1207	LP DHA	Y_3-Stp$_2$-K-ε[G-K-α,ε(DocA)$_2$]αStp$_2$-Y_3-K-ε(N$_3$)
1228	Pip6a-azide	H$_2$N-K-ε(N$_3$-Hx)-KBRXRBRXRILFQYRXRRBRRXR-Ac
1239	LP (RRRR) CholA	Y_3-R$_4$-K-ε[G-K-α,ε(CholA)$_2$]-R$_4$-Y_3-K-ε(N$_3$)
1240	LP (RRXRR) CholA	Y_3-R$_2$XR$_2$-K-ε[G-K-α,ε(CholA)$_2$]-R$_2$XR$_2$-Y_3-K-ε(N$_3$)
1241	LP (RKRK) CholA	Y_3-RKRK-K-ε[G-K-α,ε(CholA)$_2$]-KRKR-Y_3-K-ε(N$_3$)
1242	LP (RHRH) CholA	Y_3-RHRH-K-ε[G-K-α,ε(CholA)$_2$]-HRHR-Y_3-K-ε(N$_3$)

α-amino acids are indicated in one-letter code. Stp, succinyl-tetraethylenpentamine; K-ε(N$_3$), azidolysine; N$_3$-Hx, 6-azido-hexanoic acid; B, β-alanine; X, 6-aminohexanoic acid; CholA, 5β-cholanic acid; OleA, oleic acid; LinA, linoleic acid; SteA, stearic acid; LenA, linolenic acid; GonA, gondoic acid; AraA, arachidonic acid; EPA, eicosapentaenoic acid; DHA, docosahexaenoic acid; Ac, N-acetyl.

Loading of 2-chlorotrityl chloride resin

2-Chlorotrityl chloride resin (750 mg) was weighed in a syringe microreactor and swollen in water-free DCM (5 mL) with an overhead shaker for approximately 20 min. The C-terminal Fmoc protected amino acid of the sequence (0.35 mmol) and DIPEA (0.7 mmol) were dissolved in water-free DCM (5 mL), added to the resin and shaken for 60 min. The reaction solvent was drained and a mixture of DCM/MeOH/DIPEA (80/15/5 v/v/v) (5 mL) was added twice for 10 min each. After the removal of the reaction mixture, the resin was washed 5 times with DCM.

A resin sample was drawn and dried for the determination of resin loading. Three samples of 5-10 mg dry resin were weighed in reaction tubes and treated with 1 mL deprotection solution (20 % piperidine in DMF) for 1 h under shaking. The resin was allowed to settle and the supernatant was diluted for photometrical measurement at λ = 301 nm. The loading of each sample was then calculated according to the following equation: resin load [mmol/g] = (A × 1000) / (m [mg] × 7800 × df) with A as measured

absorbance, m as exact mass and df as the dilution factor. The mean value of three samples was used as final resin loading.

The remaining resin was treated four times with 20 % piperidine in DMF to remove the Fmoc protection group. The reaction progress was monitored using the Kaiser test.[3] Afterwards, the resin was washed three times with DMF and DCM and dried *in vacuo*.

Synthesis of lipopeptides

The artificial amino acid Fmoc-Stp(Boc)$_3$-OH was synthesized according to the protocol published in Schaffert et al.[1] Oligoaminoamides were synthesized using a 2-chlorotrityl resin preloaded with Tyr(tBu)-OH (resin loading above). The sequence (C → N) [Y(tBu)]$_3$-[Stp(Boc)$_3$]$_2$-K(Dde)-[Stp(Boc)$_3$]$_2$-[Y(tBu)]$_3$ was synthesized with a SyroWave^{TM} synthesizer (Biotage, Uppsala, Sweden). Double coupling steps were carried out twice for 12 min at 50 °C each using 4 eq. Fmoc-amino acid, 4 eq. HOBt, 4 eq. HBTU, and 8 eq. DIPEA in NMP/DMF (5 mL g^{-1} resin). Equivalents were calculated relative to free resin-bound amines (1 eq.). Fmoc deprotection was accomplished by 5 × 10 min incubation with 20 % piperidine in DMF (7 mL g^{-1} resin). Washing was accomplished by 6 × 1 min DMF (8 mL g^{-1} resin) after each coupling and deprotection step.The remaining couplings steps were performed manually using syringe microreactors and an overhead shaker. Coupling steps were carried out with 4 eq. Fmoc-amino acid, 4 eq. HOBt, 4 eq. PyBOP, and 8 eq. DIPEA in DCM/DMF (50 /50) (10 mL g^{-1} resin) for 90 min. Fmoc deprotection was accomplished by 4 × 10 min incubation with 20 % piperidine in DMF (10 mL g^{-1} resin). A washing procedure comprising 3 × 1 min DMF, 3 × 1 min DCM incubation (10 mL g^{-1} resin each) and a Kaiser test was performed after each coupling and deprotection step. When the Kaiser test yielded a positive result after coupling, the last coupling step was repeated. In the case of a negative result after deprotection, the last deprotection step was repeated.

Fmoc-Lys(N$_3$)-OH was coupled to the backbone and after the removal of the Fmoc protecting group, the N-terminal NH$_2$-group was protected with 10 eq. Boc$_2$O and 10 eq. DIPEA in DCM/DMF (50/50 v/v). Dde-deprotection was performed 15 times with the automatic SyroWave^{TM} synthesizer. A hydrazine/DMF solution (2/98 v/v) was

added and vortexed for 2 min. The reaction solvent was drained and fresh solution was added again. Afterwards, the resin was washed with 5 × 1 min DMF, 5 × 1 min DIPEA/DMF (10/90) and 3 × 1 min DCM (10 mL g^{-1} resin each). After the coupling of a Fmoc-Gly-OH, a symmetrical branching point was introduced by using Fmoc-Lys(Fmoc)-OH. In the final coupling step, the respective fatty acid was coupled (5β-cholanic acid (CholA) for *1106*; oleic acid (OleA) for *1169*; linoleic acid (LinA) for *1171*; stearic acid (SteA) for *1172*; linolenic acid (LenA) for *1195*; gondoic acid (GonA) for *1204*; arachidonic acid (AraA) for *1205*, eicosapentaenoic acid (EPA) for *1206*; docosahexaenoic acid (DHA) for *1207*).

Synthesis of Pip6a-azide

The original Pip6a-PMO conjugate, as reported in the literature, is assembled by conjugation of the C-terminus of Pip6a (Ac-RXRRBRRXRYQFLIRXRBRXRB) to the 3'-amine of a PMO via amidation reaction.[4] To adapt this composition and orientation to the click-chemistry approach used in this work, a Pip6a-azide derivative (Ac-RXRRBRRXRYQFLIRXRBRXRBK(N$_3$-Hx)-NH$_2$) carrying a C-terminal azide function for conjugation with the 3'-DBCO of a PMO was synthesized. The solid-phase synthesis was conducted on a Rink-amide resin to generate a C-terminal carboxamide in order to produce a Pip6a-PMO conjugate with equal peptide charge as the original conjugate. Synthesis of the peptide backbone RXRRBRRXRYQFLIRXRBRXRBK(Dde) with a C-terminal N^ϵ-Dde protected lysine was synthesized using a SyroWave^{TM} synthesizer (Biotage, Uppsala, Sweden). Double coupling steps were carried out twice for 10 min at 60 °C each using 4 eq. Fmoc-amino acid, 4 eq. HOBt, 4 eq. HBTU, and 8 eq. DIPEA in NMP/DMF (5 mL g^{-1} resin). Equivalents were calculated relative to free resin-bound amines (1 eq). Fmoc deprotection was accomplished by 4 × 10 min incubation with 20 % piperidine in DMF (7 mL g^{-1} resin). Washing was accomplished by 6 × 1 min DMF (8 mL g^{-1} resin) after each coupling and deprotection step. N-terminal acetylation was accomplished by 60 min incubation with 10 eq. acetic anhydride in DCM (5 mL g^{-1} resin) at room temperature followed by 6 × 1 min DMF wash (8 mL g^{-1} resin). Subsequently, Dde-deprotection was performed 15 times with the automatic SyroWave^{TM} synthesizer. A hydrazine/DMF solution (2/98 v/v) was added and vortexed for 2 min. The reaction

solvent was drained and fresh solution was added again. Afterwards, the resin was washed with 5 × 1 min DMF, 5 × 1 min DIPEA/DMF (10/90 v/v) and 3 × 1 min DCM (10 mL g^{-1} resin each). Finally, the azide-function was introduced at the ε-amine of the C-terminal lysine by incubating the resin with 4 eq. 6-azido-hexanoic acid, 4 eq. HOBt, 4 eq. Pybob, and 8 eq. DIPEA in DCM/DMF (5 mL g^{-1} resin) for 60 min at room temperature. The resin was washed 3 × 1 min with DMF and 3 × 1 min with DCM (8 mL g^{-1} resin).

Peptide cleavage and purification

Peptide cleavage off the resin was performed by incubation with TFA/TIS/H$_2$O (95 /2.5 /2.5 v/v/v) (10 mL g^{-1} resin). To avoid side-reactions with lipopeptides containing unsaturated fatty acids, the cleavage solution was cooled to 4 °C prior to addition and incubation was terminated after 30 min followed by immediate precipitation in 40 mL of pre-cooled MTBE/*n*-hexane (50/50 v/v).[5, 6] Other lipopeptides and Pip6a-azide were cleaved during 90 min incubation with the cleavage solution at room temperature followed by precipitation in 40 mL of pre-cooled MTBE/*n*-hexane (50/50 v/v). The peptides were purified by size exclusion chromatography using an Äkta purifier system (GE Healthcare Bio-Sciences AB, Sweden) based on a P-900 solvent pump module, a UV-900 spectrophotometrical detector, a pH/C-900 conductivity module, a Frac-950 automated fractionator, a Sephadex G-10 column and 10 mM HCl in H$_2$O/ACN (70/30 v/v) as solvent. The pooled fractions containing the peptides were combined, snap-frozen and freeze-dried. Pip6a-azide was additionally purified by preparative RP-HPLC using a VWR LaPrep system (VWR International GmbH, Darmstadt, Germany), a Waters SymmetryPrep C18 column (7 µm, 19x150mm) and a water/acetonitrile solvent gradient containing 0.1 % TFA.

2.3.3 Analytical methods

Proton ^{1}H NMR spectroscopy

^{1}H NMR spectra were recorded using an Advance III HD 400 MHz Bruker BioSpin (400 MHz) or an Advance III HD 500 MHz Bruker BioSpin (500 MHz) with CryoProbe™ Prodigy probe head. All spectra were recorded without TMS and chemical shifts were calibrated to the residual proton signal of the solvent and are reported in ppm. The spectra were analyzed using MestreNova (MestReLab Research). Integration was performed manually.

MALDI mass spectrometry

1 µL matrix solution containing 10 mg/mL Super-DHB (90/10 m/m mixture of 2,5-dihydroxybenzoic acid and 2-hydroxy-5-methoxybenzoic acid) in 69.93/30/0.07 (v/v/v) H_2O/ACN/TFA was spotted on an MTP AnchorChip (Bruker Daltonics, Bremen, Germany). After the matrix crystallized, 1 µL of sample solution (10 mg/mL in water) was added to the matrix spot. Samples were analyzed using an Autoflex II mass spectrometer (Bruker Daltonics, Bremen, Germany). All spectra were recorded in positive ion mode.

2.3.4 PMO functionalization

Synthesis of PMO-DBCO

For the DCBO functionalization of morpholino oligomers (PMOs), 2 µmol of PMO with 3' primary amine modification (Gene Tools, USA) was dissolved in 600 µL water-free DMSO. 5 mg DBCO-NHS ester (Sigma-Aldrich, Germany) was dissolved in 200 µL water-free DMSO. The dissolved components were mixed and 4 µmol DIPEA was added. The reaction was incubated overnight in a shaker at 25 °C and 300 rpm. The DBCO-modified PMO was purified by size exclusion chromatography (SEC) using an Äkta purifier system based on a P-900 solvent pump module, a UV-900 spectrophotometrical detector, a pH/C-900 conductivity module, a Frac-950 automated fractionator, a Sephadex G-10 column and 30 % acetonitrile as solvent. The pooled PMO-DBCO fractions were lyophilized after SEC, dissolved in water and analyzed by MALDI-MS. The concentration of the resulting PMO solution was determined photometrically at 265 nm using the extinction coefficient provided by the PMO supplier.

Synthesis of AF647-PMO-DBCO

PMO (IVS2-705) containing a 5' azide modification (PMO-N$_3$) and 3' primary amine was labeled with 1.5 eq. AF647-DBCO and subsequently functionalized with DBCO-NHS by the following procedure. PMO-N$_3$ (1.17 µmol) was dissolved in 234 µL water-free DMSO. 2 mg AF647-DBCO (1.76 µmol) was dissolved in 266 µL water-free DMSO and mixed with the PMO-N3 solution to a final volume of 500 µL. The solution was incubated overnight at room temperature under constant shaking. On the next day, 100 µL water-free DMSO containing 3 mg DBCO-NHS ester and 0.35 µL DIPEA (2.34 µmol) was added to the PMO solution, the solution was vortexed and incubated for 24 h under constant shaking. The obtained product was first purified by dialysis (Spectrapor MWCO 3.5 kDa, Repligen GmbH, Ravensburg, Germany) against water (overnight, 4 °C). The A647N-PMO-DBCO was further purified by RP-HPLC using a Waters RP 8 column (5 µm, 150 x 4.6 mm) connected to a VWR Hitachi Chromaster HPLC system (5160 pump module, 5260 auto sampler, 5310 column oven, 5430 diode array detector). A gradient from 5 % acetonitrile (0.1 % TFA) to 100 % acetonitrile (0.1 % TFA) over 22.5 min was used and product elution was monitored photometrically at 214 nm. Fractions containing A647N-PMO were pooled and freeze-dried.

PMO-lipopeptide conjugation

For cell culture experiments, FCS and TEM measurements, conjugation of PMO and lipopeptide was carried out by diluting PMO-DBCO (stock solution in water ~700 µM) with HBG to a concentration of 100 µM. Lipopeptides were diluted with HBG to 100 µM for the 1:1 formulations. For formulations with excess of free LP, the concentration of LP was increased accordingly (e.g. 300 µM for 1:3 ratio of PMO to LP). Equal volumes of both components were mixed and incubated overnight at room temperature under constant shaking, resulting in a 50 µM PMO-LP conjugate solution without (1:1) or with (e.g. 1:3) additional free LP. For *in vivo* experiments, conjugation was carried out analogously at higher concentration.

2.3.5 AF488-labeling of LP LenA

To label the free fraction of LP LenA in formulations containing an excess of free lipopeptide, LP LenA was reacted with Alexa Fluor 488 (AF488-DBCO) at the azide function. The resulting labeled LP LenA is not able to undergo covalent reaction with PMO-DBCO and therefore stays free in the formulation. 2.38 mg LP LenA was dissolved in 250 µL water. 1 mg AF488-DBCO was dissolved in 250 µL water, the two components were mixed and incubated overnight under constant shaking at room temperature. Uncoupled dye was removed by dialysis (Spectrapor MWCO 2 kDa, Repligen GmbH, Ravensburg, Germany) against water (overnight, 4 °C) and the purified product was freeze-dried.

2.3.6 Statistical azide-functionalization of oligo- and polymers

For an initial library screening, amine-containing oligo- and polymers were statistically modified with 1.5 eq. azidobutyric acid N-hydroxysuccinimidyl ester and subsequently used for conjugation with PMO-DBCO and cell experiments. Two days prior to transfection, the samples were diluted with 10 mM HEPES buffer to a final concentration of 200 µM, azidobutyric acid N-hydroxysuccinimidyl ester was diluted to a concentration of 300 µM. Equal volumes of both solutions were mixed and incubated overnight under constant shaking, resulting in a 100 µM oligo- or polymer solution. One day prior to transfection, an equal volume of 100 µM PMO-DBCO solution was added and incubated overnight. Transfections were performed as described in paragraph 2.3.10 for the luciferase activity assay *in vitro*.

Table 2. Oligo- and polymers used in the library screening

Compound ID	Type	Sequence	Publication
PAMAM G5	Dendrimer	Commercially available	-
PPI G2	Dendrimer	Commercially available	-
LPEI	Polymer	-	Rödl et al.[7]
454	T-shape	C-Y_3-Stp_2-K(K-$OleA_2$)-Stp_2-Y_3-C	Troiber et al.[8]
784	4-arm	KK[HK(H-SPH-K)$_3$-H-C)$_2$]$_2$	Beckert et al.[9]
689	3-arm	C-H-(Stp-H)$_3$-K-[H-(Stp-H)$_3$-C]$_2$	Kos et al.[10]
552	Comb-like	C-[K-(Stp)-H]$_8$-C	Scholz et al.[11]
734	PEG 4-arm	K-(PEG_{24}-Glu)-K-[k-(Stp_4-C)$_2$]$_2$	He et al.[12]
991	T-shape	Y_3-Stp_2-K(G-K(CholA)CholA)-Stp_2-Y_3	Klein et al.[13]

2.3.7 Fluorescence correlation spectroscopy (FCS)

The fluorescence correlation measurements were performed on a home-built microscope as described elsewhere.[14] A pulsed laser diode at 470-nm wavelength (LDH-P-C-470, PicoQuant) was used for excitation of the Alexa fluorophore 488 (AF488)-dye labeled LP LenA and a pulsed laser diode at 635-nm (LDH-P-C-635b, PicoQuant) was used for excitation of the Alexa fluorophore 647 (AF647)-dye labeled-PMO. Laser powers of ~ 4.5 µW for both the 470 and 635-nm lasers were used, measured at the sample with a slide power meter (S170C-Thorlabs). The measurements were performed using a 60x water immersion objective, NA 1.27 (Plan Apo 60 x WI, Nikon). The raw optical data and subsequent correlation analysis were performed with our home written software PIE analysis with Matlab (PAM).[15] PAM is a stand-alone program (MATLAB; The MathWorks GmbH) for integrated and robust analysis of fluorescence ensemble, single-molecule, and imaging data.

The FCS data were acquired by recording the detected photons of the single photon avalanche photodiodes (SPADs) on time correlated single photon counting cards (TCSPC, SPC-150 Becker and Hickl) for a period of 15 minutes. Lifetime measurements were performed to investigate whether the self-association of the AF488-LP LenA drastically changes its photophysical properties (Figure S13). From both the FCS data and the lifetime measurements (Figure S13), aggregate formation with quenching of the fluorescence is observable at concentrations of 10 µM and above. The corresponding intensities traces are shown in Figure S14. The lifetime decay of AF647-PMO was also investigated in formulations with LP LenA at ratios of 1:1 and 1:3 (Figure S15). Incorporation of AF647-PMO into nanoparticles was observed at 1.25 µM concentration for the 1:3 formulation and at 5 µM for the 1:1 formulation. An increase in the fluorescence lifetime of the AF647-PMO was observed upon association into nanoparticles. The corresponding intensities traces are shown in Figure S16. Measurements were conducted in HBG buffer for simulating physiological body conditions.

2.3.8   Transmission electron microscopy (TEM)

PMO-LP conjugates were prepared in water as described in paragraph 2.3 for the PMO-lipopeptide conjugation. Samples either contained PMO alone or PMO with LP LenA at a 1:1 or 1:3 ratio. Carbon coated copper grids (Ted Pella, Inc. USA, 300 mesh, 3.0 mm O. D.) were hydrophilized with a plasma cleaner under argon atmosphere (420 V, 1 min). The grids were placed with the activated face down on top of 10 µL sample droplets for 20 s. Afterwards, the sample was removed with a filter paper and stained using a two-step process: first, the grid was washed with 5 µL staining solution (1.0 % uranyl formate in water), which was removed immediately. Second, 5 µL of the same solution was left on the grid for 5 s. Afterwards, it was removed with a filter paper and grids were allowed to dry for 20 min. Grids were stored at room temperature. The samples were measured on a JEOL JEM-1100 electron microscope using 80 kV acceleration voltage.

2.3.9   Cell culture

HeLa pluc/705 cells were grown in RPMI-1640 medium (L-alanyl-glutamine and sodium bicarbonate) supplemented with 10 % FBS, 100 U/mL penicillin and 100 µg/mL streptomycin. The cells were cultured in ventilated flasks in the cell incubator at 37 °C and 5 % CO_2 in a humidified atmosphere. Cells were passaged at a confluency of approx. 80 %.

2.3.10   Splice-switching and luciferase activity assay *in vitro*

Splic- switching experiments were performed in triplicates in 96-well plates. 24 h prior to transfection, the plates were coated with collagen and 5.000 HeLa pLuc/705 cells were seeded per well. Before transfection, 50 µM PMO-LP solutions were diluted with HBG buffer to 25 µM, 12.5 µM and 6.25 µM. The medium was replaced with 90 µL fresh serum-containing growth medium. 10 µL PMO-LP solution was added to each well and incubated at 37 °C. The medium was removed after the indicated incubation time and cells were treated with 100 µL cell lysis buffer per well. Luciferase activity in 35 µL cell lysate was measured in a luciferin-LAR buffer solution (20 mM glycylglycine, 1 mM $MgCl_2$, 0.1 mM EDTA, 0.051 % (w/v) DTT, 0.0278 %

(w/v) ATP, 0.5 % (v/v) Coenzyme A stock solution, pH 8-8.5) using a Centro LB 960 plate reader luminometer (Berthold Technologies, Bad Wildbad, Germany). Light emission from each well was integrated over 10 s. The relative light units (RLU) were normalized to buffer-treated cells and the results are presented as fold increase in luminescence.

2.3.11 RT-PCR

40.000 HeLa pLuc/705 cells per well were seeded in 24-well plates 48 h before transfection. PMO-LP solution was prepared as described above. On the day of transfection, the medium was replaced with 270 µL fresh serum-containing medium. The PMO-LP to be tested was diluted with HBG to the intended concentration and 30 µL of sample solution was added to each well. After 24 h of incubation, the medium was removed, cells were collected and the total RNA was isolated with Tri-Reagent® (Sigma-Aldrich) according to the manufacturer's protocol. 200 nanograms of RNA was used for the cDNA synthesis with the High-Capacity cDNA Reverse Transcription Kit (Applied Biosystems) according to the manufacturer's protocol. PCR was performed using the HotStarTaq Plus DNA polymerase kit (QIAGEN) following the manufacturer's protocol.

Primers had the following sequence:
forward: 5' TTGATATGTGGATTTCGAGTCGTC
reverse: 5' TGTCAATCAGAGTGCTTTTGGCG

PCR program:

1 x	95 °C	5 min
29 x	95 °C	30 sec
	55 °C	30 sec
	72 °C	30 sec
1 x	72 °C	10 min

RT-PCR products were analyzed on a 1.25 % agarose gel in TBE buffer and visualized using SYBRgold (Invitrogen). Electrophoresis was run at 90 V for 45 minutes and analyzed on a Fluor-S gel documentation system (Bio-Rad) with the Quantity One software (Bio-Rad).

2.3.12 Cell viability assay (MTT)

Cell viability after treatment of HeLa pLuc/705 cells with PMO formulations was determined using a MTT assay. Transfections were carried out as described in paragraph 2.9 for the luciferase activity assay *in vitro*. HeLa pLuc/705 were seeded in 96-well plates at a density of 5.000 cells/ well. After 24 h medium was replaced with 90 µL fresh medium. Before transfection, 50 µM PMO-LP solutions were diluted with HBG buffer to 25 µM, 12.5 µM and 6.25 µM. 10 µL PMO-LP solution was added to each well. Cells were incubated for 24 h or 48 h at 37 °C and 5 % CO_2 in a humidified incubator. 10 µL MTT (3-(4,5-dimethylthiazol-2-yl)-2,5-diphenyltetrazolium bromide) (5 mg/mL) was added to each well. After an incubation time of 2 h, unreacted dye and medium were removed, and the 96-well plates were frozen at −80 °C for at least 30 min. To dissolve the purple formazan product, 100 µL DMSO was added per well and the plate was incubated for 30 min at 37 °C under constant shaking. Each well was quantified by measuring the absorbance at 590 nm with background correction at 630 nm using a microplate reader (Tecan Spark 10M, Tecan, Switzerland). All studies were performed in triplicate. The relative cell viability (%) was calculated relative to control wells treated with HBG as ([A] test/[A] control) × 100 %. Means are reported +/- standard deviation.

2.3.13 Flow cytometry

One day prior to uptake experiments, HeLa pLuc/705 cells were seeded into 24-well plates (Corning ® Costar, Sigma-Aldrich, Germany) at a density of 50.000 cells/well and a 12.5 µM PMO-DBCO solution in HBG (pH 7.4), which was prepared with 5 % AF647 labeled and 95 % unlabeled PMO-DBCO. The concentrations of the lipopeptide solutions were calculated according to the indicated equivalents used. Equivalents represent the molar ratio of PMO to cationic lipopeptide in the PMO-LP solutions. Equal volumes of both components were mixed (end concentration 6.25 µM PMO-LP in HBG) and incubated overnight under constant shaking. On the next day, the medium in each well was replaced with 450 µL fresh medium and 50 µL PMO-LP solution (5 % AF647-PMO-LP) resulting in a concentration of 0.625 µM PMO-LP (5 % AF647-PMO-LP). Control experiments were performed with 50 µL HBG buffer or PMO-DBCO (containing 5 % AF647-PMO-DBCO) without the addition

of lipopeptide. Cells were incubated for the indicated time at 37 °C and 5 % CO_2 in a humidified incubator, collected and resuspended in PBS buffer containing 10 % FBS. All samples were analyzed by flow cytometry using a LSR Fortessa flow cytometer (BD Biosciences, Singapore). 1 ng/µL 4′,6-diamidino-2-phenylindole (DAPI) was added shortly before the measurement and used to discriminate between viable and dead cells. The cellular fluorescence was assayed by excitation of DAPI at 405 nm and detection of emission at 450 nm and the excitation of AF647 at 640 nm and detection of emission at 670 nm. Only isolated viable cells were evaluated. Flow cytometry data were analyzed using FlowJo 7.6.5 flow cytometric analysis software by FlowJo, LLC (Ashland, OR, USA). All experiments were performed in triplicate.

2.3.14 Confocal laser scanning microscopy (CLSM)

15.000 HeLa pLuc/705 cells were seeded in collagen-coated 8 well-Ibidi µ-slides (Ibidi GmbH, Planegg/Martinsried, Germany) in a total volume of 300 µL medium per well. Cells were incubated at 37 °C and 5 % CO_2. A 25 µM PMO-LP solution in HBG containing 20 % AF647 labeled and 80 % unlabeled PMO-DBCO were prepared and incubated overnight under constant shaking. The amount of the lipopeptide was calculated according to the indicated equivalents used. Equivalents represent the molar ratio of PMO to cationic lipopeptide in the PMO-LP solutions. For the co-localization experiments, 20 % of the lipopeptide was substituted by an AF488-labeled version. On the next day, the medium was replaced with 240 µL fresh medium. The PMO-LP solutions were diluted with HBG buffer and 60 µL PMO-LP (20 % AF647-PMO-LP) was added to each well resulting in a final concentration of 0.625 µM PMO-LP. After the indicated time, each well was washed twice with 300 µL PBS and cells were subsequently fixed with 4 % paraformaldehyde in PBS (40 min incubation at RT). After fixation, each well was again washed two times with 300 µL PBS, the cell nuclei were stained with DAPI (2 µg/mL) and F-actin was labeled with rhodamine-phalloidin (1 µg/mL). After 20 min of incubation (light protected at RT), the staining mixture was aspirated and replaced with 300 µL PBS per well. Images were recorded utilizing a Leica-TCS-SP8 confocal laser scanning microscope (CLSM) equipped with an HC PL APO 63x 1.4 objective (Germany). DAPI emission was recorded at 460 nm, AF488-LP at 519nm, rhodamine at 580 nm and AF647-PMO-LP

at 665 nm. Afterwards, all images were processed using the LAS X software from Leica.

2.3.15 Calcein release assay by CLSM

24 hours prior to the PMO conjugate addition, 15.000 HeLa pLuc/705 cells were seeded per well in collagen-coated 8-well Ibidi µ-slides (Ibidi GmbH, Planegg/Martinsried, Germany). The cells were incubated with 30 µL of PMO-LP conjugate (50 µM) in a 1:3 ratio along with 0.45 mg/ml calcein in 270 µL RPMI medium containing 10 % FBS for 4 hours. Afterwards, the cells were washed three times with PBS and the medium was replaced with 300 µL RPMI medium containing 10 % FBS without phenol red. Images were recorded by confocal laser scanning microscopy with 488 nm laser excitation (TCS-SP8 confocal laser scanning microscope equipped with an HC PL APO 63x 1.4 objective, Leica Microsystems, Germany).

2.3.16 Calcein release assay by flow cytometry

24 hours prior to the PMO conjugate addition, 50.000 HeLa pLuc/705 cells per well were seeded in collagen-coated 24-well plates in a total volume of 1 mL per well. The cells were incubated with 50 µL of PMO-LP conjugate (50 µM) in a 1:3 ratio along with 0.45 mg/ml calcein in 450 µL RPMI medium containing 10 % FBS for 4 hours. Cells were incubated for 4 h at 37 °C and 5 % CO_2 in a humidified incubator, washed three times with PBS, collected and resuspended in PBS buffer containing 10 % FBS. All samples were analyzed by flow cytometry using a LSR Fortessa flwo cytometer (BD Biosciences, Singapore) as described in paragraph 2.12. The cellular calcein emission was assayed at 519 nm. Flow cytometry data were analyzed using FlowJo 7.6.5 flow cytometric analysis software by FlowJo, LLC (Ashland, OR, USA). All experiments were performed in triplicate.

2.3.17 Erythrocyte leakage assay

EDTA-blood was washed with phosphate-buffered saline (PBS) containing 25 mM sodium citrate. The washed erythrocyte suspension was centrifuged and the pellet was diluted to 5×10^7 erythrocytes per mL with PBS (pH 7.4, 6.5 and 5.5). A volume of 75 µL of erythrocyte suspension and 75 µL of PMO-LP solution (previously diluted with PBS of the respective pH) were added to each well of a V-bottom 96-well plate (NUNC, Denmark), resulting in the stated PMO-LP concentration. The plates were incubated at 37 °C under constant shaking for 1 h. After centrifugation, 80 µL of the supernatant was analyzed for hemoglobin release by monitoring the absorption at 405 nm wavelength using a microplate reader (Spectrafluor Plus, Tecan Austria GmbH, Grödig, Austria). PBS-treated erythrocytes were set to 0 %. Erythrocytes treated with 1 % Triton X-100 (previously diluted with PBS of the respective pH) served as positive control and was set to 100 %. Data are presented as the mean value (± SD) of four independent measurements.

2.3.18 Splice-switching and luciferase activity assay *in vivo*

All animal studies were performed according to guidelines of the German Animal Welfare Act and were approved by the animal experiments ethical committee of the "Regierung von Oberbayern", District Government of Upper Bavaria, Germany.

Eight-week-old, female, nude mice, Rj: NMRI-nu (nu/nu) (Janvier, Le Genest-Saint-Isle, France), were housed in isolated ventilated cages under pathogen-free condition with a 12 h light/dark interval and were acclimated for seven days prior to experiments. Water and food were provided ad libitum. 5×10^6 HeLa pLuc/705 cells were injected subcutaneously into the left flank. The tumor volume was measured using a caliper and calculated as [0.5 × (longest diameter) × (shortest diameter)^2] and the body weight was recorded daily.

The PMO solutions were prepared 24 h before injection and contained 450 µg PMO (~15 mg/kg body weight) unconjugated or conjugated with 1 eq. LP LenA (*1195*), Pip6a-azide, respectively formulated with 3 eq. LP LenA (*1195*), LP OleA (*1169*), LP LinA (*1171*), LP AraA (*1205*) in a total volume of 50 µL HBG. Equivalents represent the molar ratio of PMO to cationic lipopeptide in the PMO-LP solutions. When tumors

reached 500-700 mm^3, the animals were randomly divided into groups (n=3), anesthetized with 3 % isoflurane in oxygen and injected with 50 µL PMO solution intratumorally. All mice were euthanized by cervical dislocation 48 h after intratumoral injection. Tumors were collected and homogenized in cell culture lysis buffer (Promega, Germany) using a tissue and cell homogenizer (MP FastPrep®-24, Hyland Scientific, USA). The samples were subsequently centrifuged at 3000 g at 4 °C for 10 minutes to separate insoluble cell components. Luciferase activity was determined in the supernatant using a luciferin-LAR (20 mM Glycylglycine, 1 mM MgCl$_2$, 0.1 mM EDTA, 0.051 % (w/v) DTT, 0.0278 % (w/v) ATP, 0.5 % (v/v) Coenzyme A Stock solution, pH 8-8.5) buffer solution and measured with a Centro LB 960 plate reader luminometer (Berthold Technologies, Germany).

2.3.19 Cultivation, treatment and RT-PCR analysis of H2K-*mdx*52 cells

H2K-*mdx*52 cells were cultivated at 33 °C and 10 % CO$_2$ in growth media containing DMEM (Thermo Fisher Scientific, Waltham, MA) supplemented with 20 % FBS (FBS Gold, PAA Laboratories), 2 % chicken embryo extract (Seralab), 1 % penicillin/streptomycin (P/S) (Life Technologies) and 20 U/ml of γ-interferon (PeproTech). For exon skipping experiments, 35.000 cells were seeded in 24-well gelatine-coated plates in growth medium. On the next day, the media was changed to differentiation media containing DMEM supplemented with 5 % horse serum (Life Technologies) and 1 % P/S and cultured at 37 °C and 5 % CO$_2$. On day 3, the media was exchanged to fresh differentiation media and directly afterwards splicing compounds were added in the stated concentration. After 48 h, total RNA was extracted from the cells by RNeasy MiniKit (Qiagen, Hilden, Germany) according to the manufacturer's instructions.

200 ng of extracted RNA was used for cDNA synthesis using the High Capacity cDNA Reverse Transcription Kit (Applied Biosystems, Warrington, UK) according to the manufacturer's instructions. For one RT-PCR reaction, 1 µL of cDNA template was mixed with 14.9 µL of water, 0.2 µL of 10 µM forward primer, 0.2 µL of 10 µM reverse primer, 1.6 µL of 2.5 mM dNTPs, 2 µL of 10 × Ex Taq Buffer, and 0.1 µL Ex Taq DNA polymerase (Takara Bio, Shiga, Japan).

Primers for amplification of cDNA from exons 49–54 had the following sequence:

Ex49F 5′-AAACCAAGCACTCAGCCAGT-3′
Ex54R 5′-CAGCAGAATAGTCCCGAAGAA-3′

PCR program:

1 x	95 °C	4 min
35 x	94 °C	1 min
	58 °C	1 min
	72 °C	1 min
1 x	72 °C	7 min

PCR products were detected using MultiNA, a microchip electrophoresis system (Shimadzu, Kyoto, Japan). Exon-skipping efficiency (%) was calculated as (exon-skipped transcript molarity)/(unskipped + exon-skipped transcript molarity) × 100 % using MultiNA.

2.3.20 Statistical analysis

Data were analyzed with GraphPad prism 5. The statistical significance of experiments was estimated using the two-tailed student's t-tests, *** $p \le 0.001$, ** $p \le 0.01$, * $p \le 0.05$.

2.4 Results and Discussion

2.4.1 Conjugate design and evaluation

Since PMOs are uncharged nucleic acid analogs, they are not prone to the formation of ionic complexes with positively charged transfecting reagents. Strain-promoted azide-alkyne cycloaddition (SPAAC), initially established by Carolyn R. Bertozzi,[202] was used for the covalent linkage of dibenzocyclooctyne (DBCO) modified PMO and azide-containing artificial peptides. For activity screenings and structural optimizations, a PMO sequence against a thalassemicβ-globin intron mutation IVS2-705 was selected to enable quantitative evaluation of splicing correction in different cell lines containing the pLuc/705 construct developed by RyszardKole's lab in the 1990s. The cells contain a luciferase reporter which is interrupted by the globin IVS2-705 resulting in increased luciferase activity depending on successful splice-switching (Figure 6).[203] Since the construct exhibits a certain background luciferase activity, luminescence levels were always normalized to the background of untreated cells and expressed as 'fold increase in luminescence'.
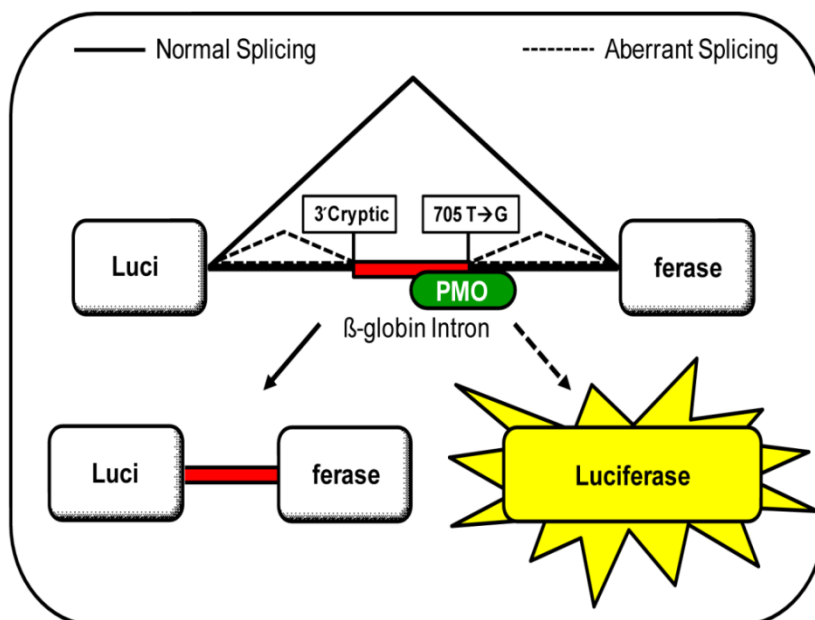
Figure 6. Schematic illustration of PMO induced splicing correction in HeLa pLuc/705 cells.[203] The construct in the top represents luciferase pre-mRNA interrupted by a human ß-globin intron 2 carrying an A-to-G mutation at nucleotide 705. This mutation creates an additional 5' splice site and activates a cryptic 3' splice site. PMO targeted to the splice site around nucleotide 705 prevents aberrant splicing (solid arrow) and restores correct splicing (dashed arrow) resulting in expression of functional luciferase protein.

2.4.2 Lead identification

To assess the general potential of oligo(ethylenamino) amides for PMO delivery, a first library screen was conducted with a statistical azide-functionalization approach (Figure 7).
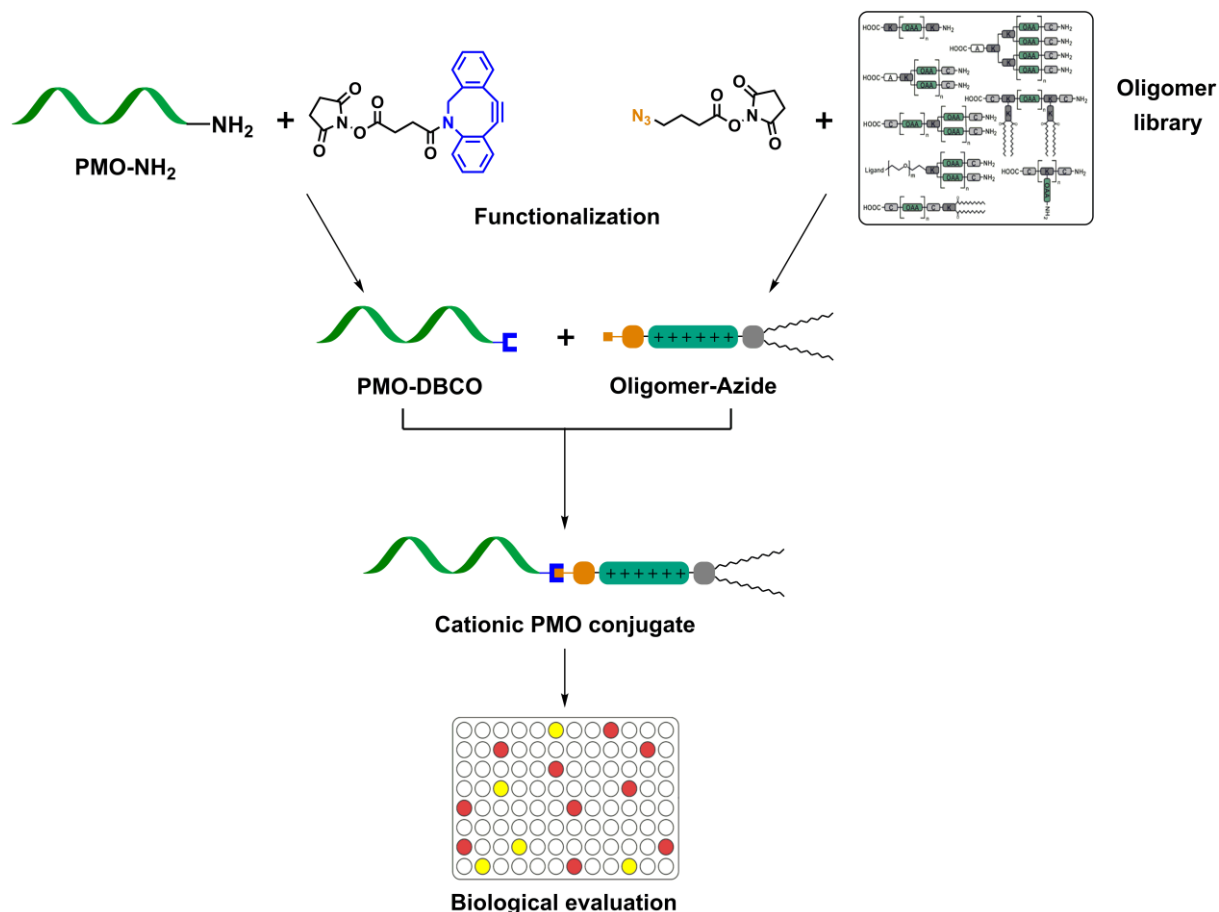
Figure 7. Schematic illustration of an oligomer library screening for lead PMO conjugates. An initial oligomer screening was carried out by statistical azide-modification of cationic oligomers. PMO with a 3' primary amine was functionalized with DBCO-NHS ester (top, left) and purified by size exclusion chromatography. Representatives of oligomers with different architectures were statistically functionalized with 1.5 eq. azidobutyric acid NHS ester (top, right), conjugated with PMO-DBCO and used for transfection of HeLa pLuc/705 cells. The splice-switching activity of the different PMO conjugates was evaluated by luciferase activity assays to identify lead structures for PMO delivery.

Selected representatives of cationic polymers (PAMAM dendrimer G5, PPI dendrimer G3, LPEI 22 kDa) and artificial peptides with different architectures (branched 3-arm,[162] 4-arm,[158, 197] comb-like,[204] PEGylated[153] and lipid-modified[113, 205]) were first functionalized with 1.5 eq. of azidobutyric acid NHS ester, subsequently click-conjugated to PMO-DBCO and finally used for transfection of HeLa pLuc/705 cells

41

(Figure 8). Here, the lipopeptide (LP) *#991* was identified as the most efficient facilitator of PMO-mediated splice-switching. It contains the oligo(ethylenamino) acid succinyl-tetraethylenepentamine (Stp) as a cationic building unit, cholanic acid as a hydrophobic modification and tyrosine, which previously showed beneficial effects on charged nucleic acid delivery.[205-208]
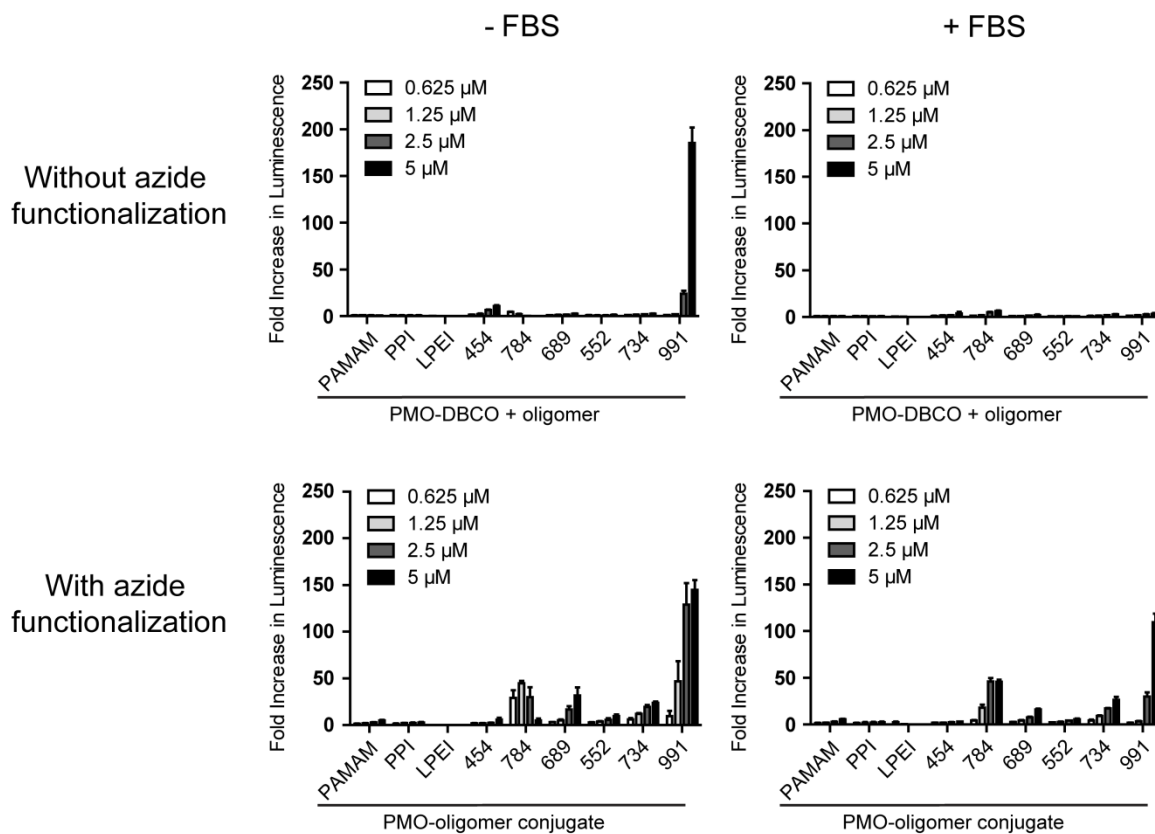
Figure 8. Luciferase activity assay results of oligomer library screening. The increase in luminescence in HeLa pLuc/705 cells was determined 24 h after transfection of PMO-DBCO with representatives of different oligomer groups. Oligomers were tested without azide-functionalization (top graphs) and with statistical azidobutyric acid-functionalization. Transfections were performed under serum-free conditions (4 h serum-free followed by 20 h serum containing conditions, left graphs) as well as under serum containing conditions (right graphs). Data are presented as the mean ± SD (n=3).

For further validation of this screening hit, a *#991* analog with azide-group at a defined position, oligomer *#1106* (LP CholA)[167], was used for transfections in comparison to unmodified *#991* and at different PMO to oligomer ratios (Figure 9). Here, 1:1 represents the ratio of PMO to LP in the reaction resulting in an equimolar mixture of PMO-DBCO + LP CholA (noncovalent, *#991*) or the PMO-LP CholA

conjugate (covalent, *#1106*). Surprisingly, noncovalent PMO formulations with *#991* were also able to mediate increased luciferase activity, but only at higher oligomer to PMO ratios. Covalent formulations (PMO-LP CholA) were superior in all cases, but also here a beneficial effect of additional unconjugated LP was evident.
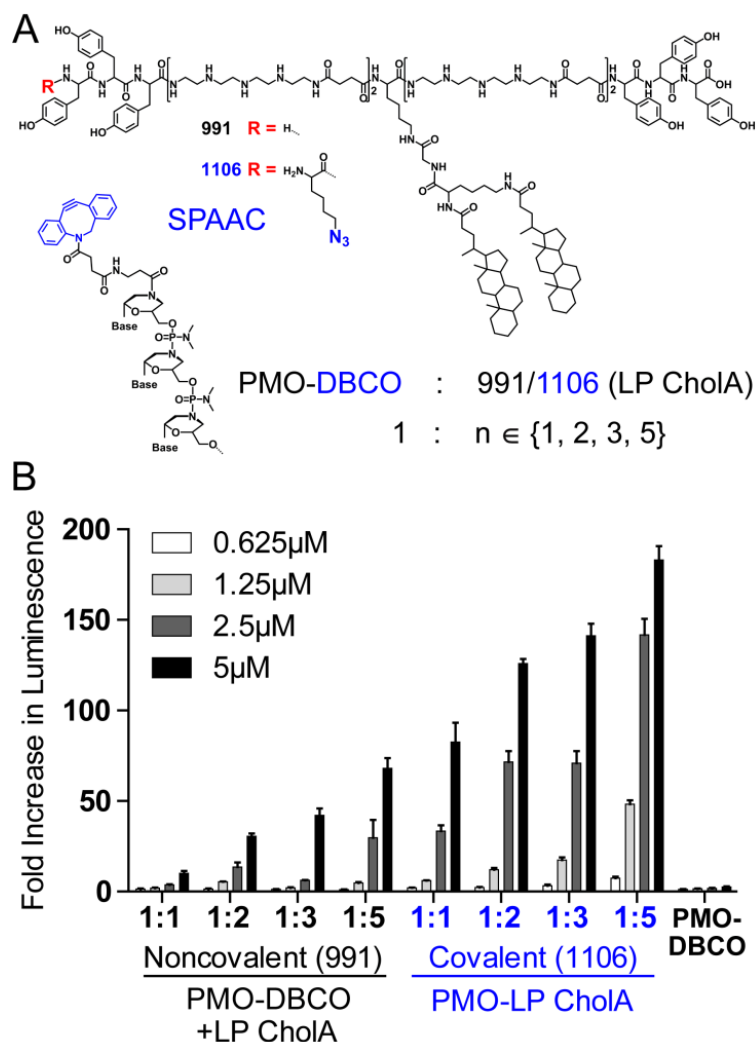
Figure 9. PMO-LP conjugation and evaluation. (A) The chemical structure of the lipopeptide*#991* and its analog *#1106* with *N*-terminal azidolysinefor conjugation to PMO-DBCO via strain-promoted azide-alkyne cycloaddition (SPAAC). (B) The increase in luminescence in HeLa pLuc/705 cells 24 h after transfection with noncovalent *#991* or covalent *#1106* formulations at different PMO-DBCO to oligomer ratios. The fold increase in luminescence represents arbitrary light units normalized to the mean background level of buffer treated cells. Data are presented as mean ± SD (n=3). Additional cell viability data (MTT) are provided in Figure 23.

To validate the formulation via click reaction, HeLa pLuc/705 cells were treated side by side with the PMO-LP CholA 1:1 formulation and the purified PMO-LP CholA conjugate (Figure 10). Both PMO formulations mediated comparable levels of luciferase activity which confirms the reliability of the formulation approach.
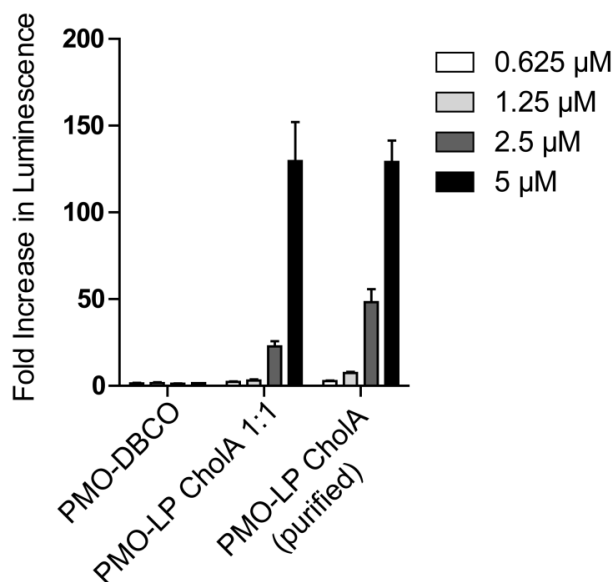
Figure 10. Comparison of PMO-LP CholA 1:1 formulation to purified PMO-LP CholA conjugate. Increase in luminescence in HeLa pLuc/705 cells was determined 24 h after transfection of PMO-LP CholA at a 1:1 ratio and compared to the HPLC purified conjugate. CholA: cholanic acid. Data are presented as the mean ± SD (n=3).

2.4.3 Structural variations

First, the impact of the repeated aminoetylene motif in the identified lipopeptide architecture was assessed in systematic variations of the lead structure *#1106* by replacement of the contained oligoamino acid Stp with basic α-amino acids lysine, arginine, histidine, their combinations, or a 6-aminohexanoic acid-arginine motif (RXR).[118, 184] Although the derivatives were designed to contain an equal number of protonatable amines in the biologically relevant pH range above pH 5, the substitution of Stp resulted in a complete loss of activity (Figure 11).
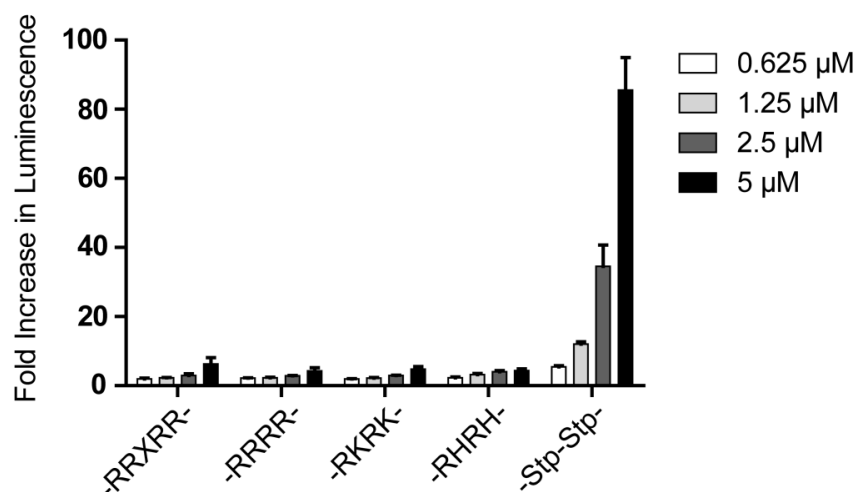
Figure 11. PMO-LP CholA (#1106) backbone variation. Increase in luminescence in HeLa pLuc/705 cells was determined 24 h after transfection of PMO-DBCO conjugated to different lipopeptides at a 1:1 ratio. The lead structure #1106 (-Stp-Stp-) was varied by replacement of the artificial oligoamino acid Stp with basic α-amino acids lysine (K), arginine (R), histidine (H) and combinations thereof or an arginine - aminohexanoic acid - arginine (RRXRR) motif. CholA: cholanic acid. Data are presented as the mean ± SD (n=3).

This indicates that the artificial oligoamino acid Stp is an essential part of this particular lipopeptide architecture,presumably due the unique endosomal protonation characteristics of repeated aminoethylene motifs.In contrast, substitution of unsaturated fatty acids for the cholanic acid part resulted in improved activity (Figure 12).
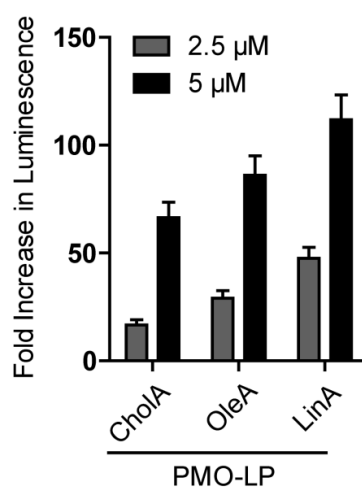
Figure 12. PMO-LP fatty acid variation. The increase in luminescence in HeLa pLuc/705 cells was determined 24 h after transfection of PMO-DBCO conjugated to lipopeptides containing different fatty acids at a 1:1 ratio. CholA, cholanic acid; OleA, oleic acid; LinA, linoleic acid. Data are presented as the mean ± SD (n=3).

This is in line with previous findings that the hydrophobic core of Pip6a derivatives is a critical element for efficient PMO delivery.[103] Based on this observation, a series of *#1106* analogs containing fatty acids with different numbers of unsaturated bonds was synthesized and functional luciferase expression was assessed in a kinetic study 12 to 72 h after transfection (Figure 13). Here, a distinct dependence of splice-switching activity on the contained fatty acids and the degree of unsaturation was observed: the luminescence increases gradually with increasing number of unsaturated bonds up to three (Figure 13B, left, top). The PMO conjugate containing linolenic acid with three double bonds (PMO-LP LenA) promoted the highest splice-switching at 5 µM concentration. The high activity of PMO-LP LenA was not exceeded by conjugates containing fatty acids with four to six double bonds (Figure 13B, left, bottom).
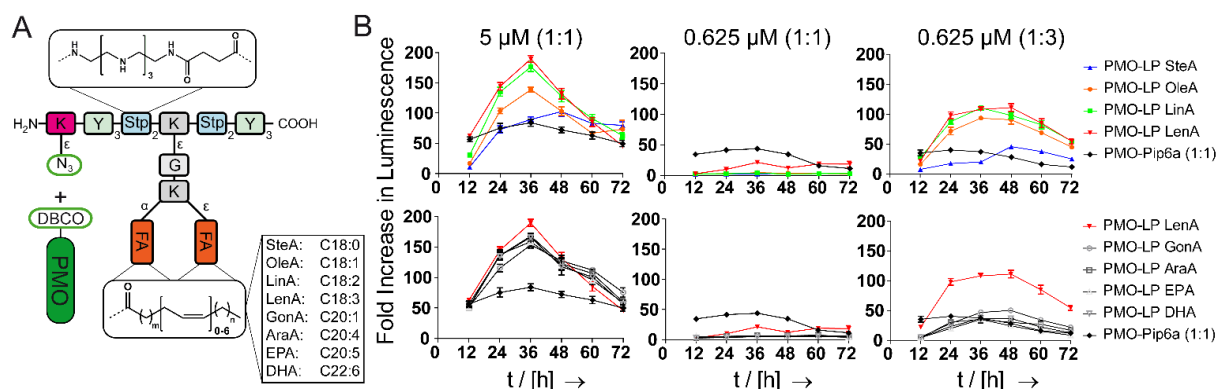
Figure 13. Structure- and formulation-activity relationships of PMO-LP conjugates.(A) A schematic illustration of artificial lipopeptides (LP) with systematic variation of contained fatty acids (FA) with 0 (stearic acid, SteA, C18:0) to 6 (docosahexaenoic acid, DHA, C22:6) all-*cis* double bonds. (B) Kinetics of the increase in luminescence between 12 to 72 h after transfection with PMO conjugate formulations in 1:1 (left, middle) or 1:3 (right) PMO-DBCO to LP ratio. Fold increase in luminescence represents arbitrary light units normalized to the mean background levels of buffer treated cells. Figures show a comparison between LP containing 0 to 3 (top) or 3 to 6 *cis* double bonds (bottom). A Pip6a-azide derivative served as a positive control in the same PMO-DBCO conjugation protocol at a 1:1 ratio. Data are presented as mean ± SD (n=3). A complete set of PMO formulations at different concentrations are provided in Figure 24 and Figure 25.

In addition to HeLa, three other cell lines were treated with the same set of PMO conjugates to confirm the general ability to mediate splice-switching of thalassemic β-globin IVS2-705 (Figure 14). Similar structure-activity relationships and significant splice-switching activities were also observed in pLuc/705 based human hepatoma (Huh7), murine neuroblastoma (Neuro2A) and murine myoblast (C2C12) cells.[209-210]
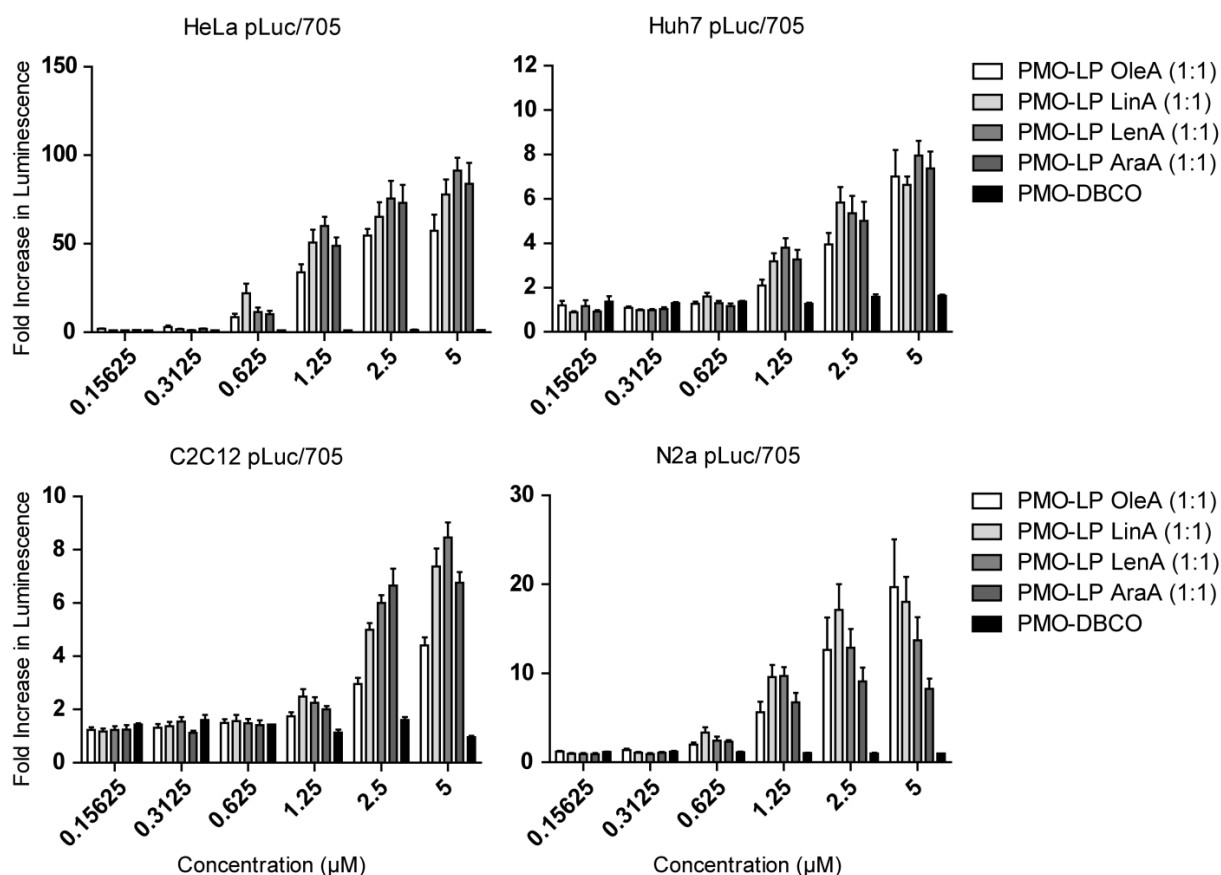
Figure 14. Splice-switching activity of PMO-LP formulations in different pLuc/705 based cell lines.[209-210] The increase in luminescence was determined 24 h after transfection of PMO-LP formulations at a 1:1 ratio. Figures show a comparison between PMO-LPs containing fatty acids with 1 (OleA), 2 (LinA), 3 (LenA) or 4 (AraA) double bonds. 50 µM PMO-LP formulations in HBG were produced at the LMU Munich and freeze-dried. Transfections of human hepatoma (Huh7), murine neuroblastoma (N2a), murine myoblast (C2C12) as well as human cervix carcinoma cells HeLa, all containing the pLuc/705 construct, were carried out at the Karolinska Institute in Stockholm after reconstitution of the freeze-dried samples. Data are presented as the mean ± SD (n=3).

The PMO-sequence specificity was assessed in HeLa pLuc/705 treatments with PMO-LP LenA1:1 and 1:3 formulations containing eitherPMO IVS2-705or 51D (Figure 15). The data illustrate a high increase in luminescence mediated by the specific PMO-705 in contrast to a very low unspecific response towards the PMO-51D formulations.
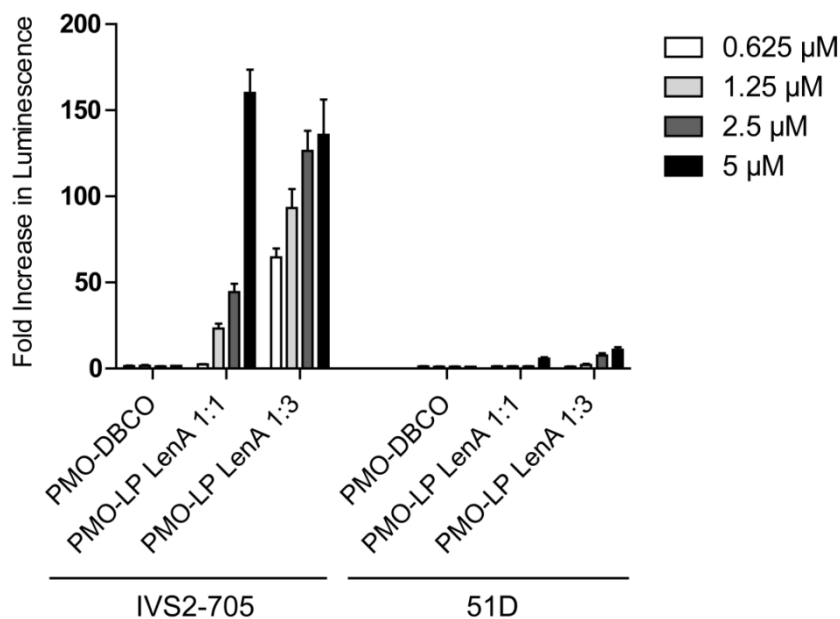
Figure 15. PMO-sequence specific splice-switching mediated by PMO-LP LenA formulations. Increase in luminescence in HeLa pLuc/705 cells was determined 24 h after transfection of two different PMO-DBCO sequences formulated with LP LenA at 1:1 and 1:3 ratio. PMOs targeting the T to G point mutation at position 705 in intron 2 of the human β-globin gene (IVS2-705), and 51D targeting the splice donor site of Dmd exon 51 were used. Data are presented as the mean ± SD (n=3).

In all transfections the activities of PMO-LP conjugates showed a strong dose-dependency. Upon decreasing the concentration of PMOs to 0.625 µM, the activity and increase in luminescence dropped to low levels (Figure 13B, middle). As observed before (Figure 9B), additional unconjugated peptide enhanced the splice-switching activity and a high increase in luminescence was achieved by the PMO-LP 1:3 formulations at low PMO concentrations (Figure 13B, right, Figure 24).

A systematic dose titration clearly illustrated the shifted splice-switching activities of PMO-LP LenA at 1:1 or 1:3 ratio on the RNA and protein activity level (Figure 16). The ratio between aberrant and corrected splicing was determined by RT-PCR specific for a sequence surrounding the β-globin IVS2 (Figure 16A). The band intensities of related PCR products (268 bp aberrant, 142 bp corrected) indicate that complete splicing-correction was achieved with PMO-LP LenA 1:3 at a concentration of 1.25 µM PMO whereas, at a 1:1 ratio, 2.5 µM PMO were required. This also correlates with the dose-response at the luciferase activity level (Figure 16B). Bare PMO-DBCO, up to a concentration of 10 µM, was not able to increase luciferase activity significantly. Dose titrations of both PMO-LP LenA 1:1 and 1:3 formulations side by side revealed equal maximum levels between 2.5 and 5 µM and an enhanced potency for the 1:3 formulation at lower concentrations due to the additional fraction of free LP. At the high concentration of 10 µM, the excess of unconjugated LP (20 µM) also mediated cytotoxicity (Figure 16C), which was responsible for the drop of luciferase activity. An azide-containing derivative of the efficient CPP Pip6a served as a positive control and benchmark compound; the PMO-DBCO conjugation was carried out analog to the LP formulations at a 1:1 ratio. In direct comparison to Pip6a-PMO, PMO-LP LenA 1:3 showed a comparable potency at low concentrations, higher maximal luciferase activity and reduced cytotoxicity at higher concentrations. PMO-LP LenA 1:1 exhibited the best tolerability and no observable signs of cytotoxicity or reduced luciferase activity up to a concentration of 10 µM PMO. Notably, all formulations clearly outperformed the commercial noncovalent PMO delivery reagent 'Endo-Porter' which was supplemented at constant 6 µM concentration, as recommended by the distributor.[122, 211]
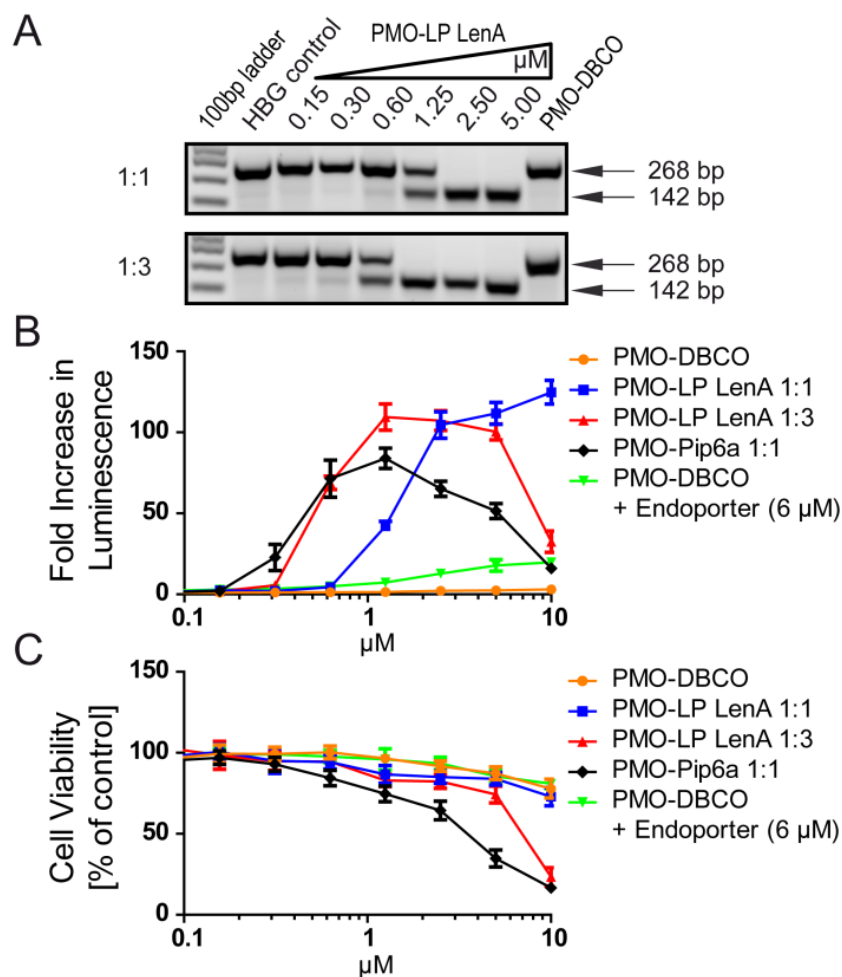
Figure 16. Dose-response effects of PMO formulations on HeLa pLuc/705 cells. (A) Detection of corrected β-globin intron splicing by RT-PCR. The total RNA was extracted from cells 24 h after PMO-LP LenA 1:1 (top) or 1:3 (bottom) treatment and amplified using RT-PCR specific for a sequence surrounding β-globin IVS2. Arrows indicate the PCR products resulting from unchanged aberrant (268 bp) and corrected (142 bp) mRNA splicing. PMO-DBCO was used at 5 µM concentration. (B) Fold increase in luminescence and (C) metabolic activity 24 h after treatment with PMO-DBCO formulations containing 0.156 to 10 µM PMO. Free PMO-DBCO, PMO-DBCO formulations with constant 6 µM 'Endo-Porter' reagent (Gene Tools, LLC) and PMO-Pip6a served as references. Data are presented as mean ± SD (n=3).

Next, to understand if these structure-activity relationships identified under cell culture conditions would also translate to a more complex *in vivo* environment, PMO-LP formulations were locally injected into subcutaneous HeLa pLuc/705 xenograft tumors in mice (Figure 17). The quantification of *ex vivo* luciferase activity in the tumor confirmed the two key findings of the previous *in vitro* studies: first, the fraction of free peptide in PMO-LP 1:3 formulations enhances splice-switching activity (Figure 17A), and second, LP LenA containing linolenic acid with three unsaturated bonds is superior to analogs containing fatty acids with one (OleA), two (LinA) or four (AraA) double bonds (Figure 17B). The studies demonstrate that PMO-LP LenA 1:3 represents a potent formulation with significant splice-switching activity in the investigated models.
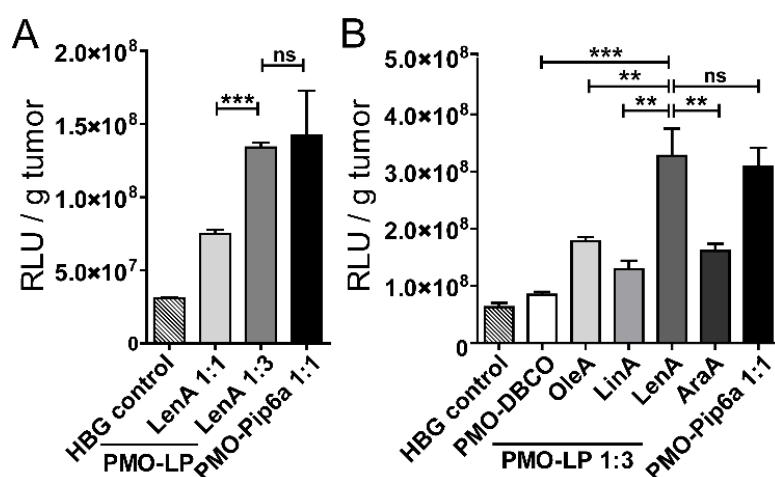
Figure 17. *Ex vivo* **luciferase activity in subcutaneous HeLa pLuc/705 tumors 48 h after local injection.** (A) Comparison of PMO-LP LenA formulations at a 1:1 or 1:3 ratio. (B) Comparison of PMO-LP (1:3) formulations with fatty acids containing 1 (OleA), 2 (LinA), 3 (LenA) or 4 (AraA) double bonds. A Pip6a-azide derivative served as a benchmark in the same PMO-DBCO conjugation protocol at a 1:1 ratio. All formulations contained 450 µg PMO. Data are presented as mean ± SD (n=3).

The exclusive investigation of luminescence levels as final result of a complex transfection process is not sufficient to elucidate the underlying mechanisms. Therefore, specific mechanistic studies were conducted to clarify the impact of free LP (Figure 18) and unsaturated fatty acids (Figure 19) in the PMO-LPs.

2.4.4   Particle formation

To investigate the formation of PMO-LP nanoparticles, fluorescence correlation spectroscopy (FCS) experiments with PMO-LP LenA 1:1 and 1:3 formulations at various PMO-LP concentrations each containing 50 nM Alexa Fluor 647 labeled PMO (AF647-PMO) were carried out (Figure 18A). FCS is based on the diffusion of fluorescent molecules through a small confocal volume (~1 fL), where the fluorescence signal is recorded and the fluctuations analyzed.[212-214] Changes in the rate of diffusion due to the assembly of PMO-LP nanoparticles causes a shift in the temporal autocorrelation function (ACF) of the FCS signal to slower timescales. Already at 1.25 µM PMO, a significantly slower ACF decay of the PMO-LP 1:3 formulation was observed, which did not significantly change at higher concentrations. Although, a decrease in the decay time of the ACF of the PMO-LP 1:1 formulation was observed at a concentration of 2.5 µM, it was only at a concentration of 5 µM that the decay time of the ACF approached that of the 1.25 µM of the 1:3 formulation.

These observations indicate a dose-dependent self-association and complex formation of PMO-LP formulations. In this process, the fraction of free LP in 1:3 formulations seems to contribute to the complex assembly at low PMO concentrations. Interestingly, neither labeled PMO-DBCO (at 1 µM and 50 µM concentrations, Figure 26) nor LP LenA alone (below 10 µM concentrations) showed substantial supramolecular assembly (Figure 27 and Figure 28), compared to the PMO-LP LenA formulations. The conjugation seems to change the assembly tendency compared to the unconjugated reaction partners.Similar findings were obtained by transmission electron microscopy (TEM, Figure 18B). At a PMO concentration of 5 µM, spherical nanomicelles were detected in both PMO-LP 1:1 and 1:3 formulations, whereas, at 1.25 µM PMO, similar complexes could only be observed in the 1:3 formulation. Free PMO-DBCO did not form particles at any concentration. To address the impact of unconjugated LP on the PMO transfection process, cellular uptake of PMO-LP 1:1 and 1:3 was investigated by confocal laser scanning microscopy (CLSM, Figure 18C) and flow cytometry (Figure 18D). Already 5 min after addition of the formulations to HeLa pLuc/705 cells, cellular association could be observed in the 1:3 formulation, which rapidly increased over time. Despite the same PMO concentration, cellular uptake was significantly enhanced 15 min after

transfection by the fraction of free peptide in the 1:3 formulation compared to 1:1 (Figure 18D), which presumably is a result of the facilitated complex formation and nanoparticle internalization.[132] The resulting higher PMO uptake after 24 h (Figure 35) is in line with the enhanced splice-switching activity mediated by PMO-LP 1:3 formulations.The intracellular fate of PMO-LP and free LP was assessed in an additional CLSM experiment with a PMO-LP LenA 1:3 formulation containing AF647-PMO and Alexa Fluor 488 labeled free LP LenA (Figure 18E). The images verify that both separate components co-localize within the cells and seem to remain associated up to 24h after transfection.
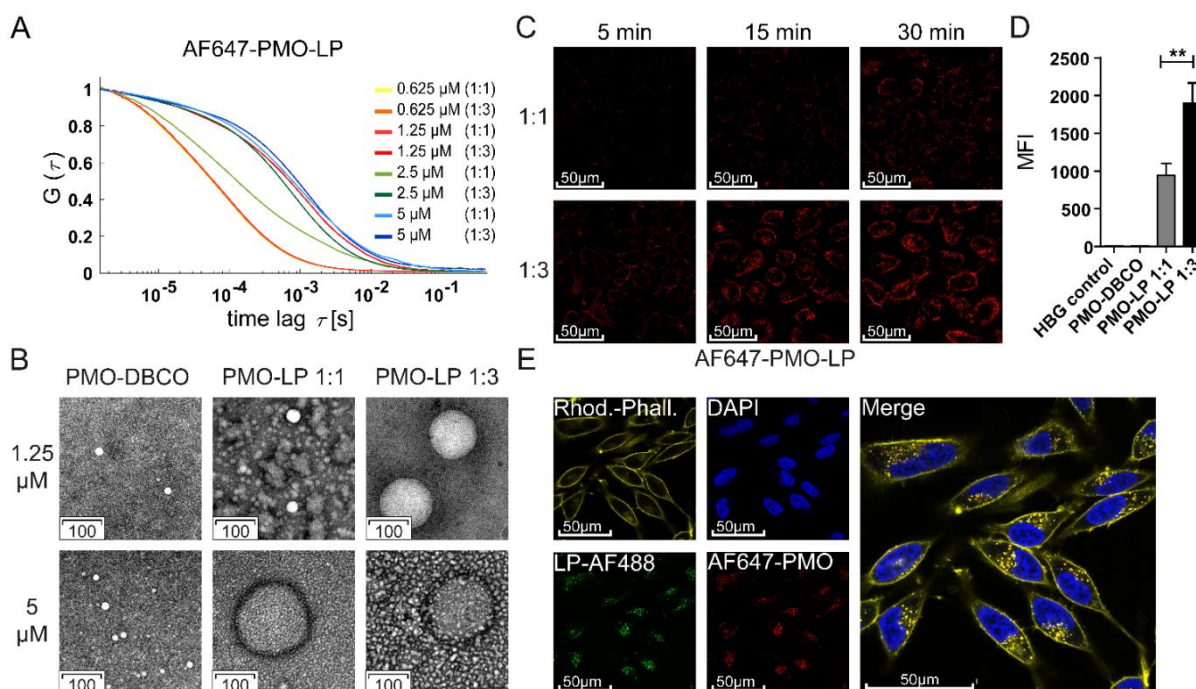
Figure 18. Impact of free LP in the PMO formulations. (A) Fluorescence correlation spectroscopy (FCS) measurements of PMO-LP LenA 1:1 and 1:3 formulations at different concentrations where 50 nM of Alexa Fluor 647 labeled PMO-DBCO (AF647-PMO) was included. The slower decay of the autocorrelation function represented by a shift toward higher time lag τ indicates the slower diffusion of AF647-PMO-LP nanoparticles. (B) Transmission electron microscopy (TEM) images of bare PMO-DBCO or formulations with LP LenA at 1:1 and 1:3 ratio. (C) Confocal laser scanning microscopy (CLSM) images of HeLa pLuc/705 cells 5 min, 15 min or 30 min after transfection with PMO-LP LenA 1:1 or 1:3 (0.625 µM PMO) containing 20 % AF647-PMO. (D) The uptake of PMO-LP LenA 1:1 and 1:3 (0.625 µM PMO) containing 5 % AF647-PMO into HeLa pLuc/705 cells 15 min after transfection determined by flow cytometry (median fluorescence intensity, MFI, n=3) is shown. (E) CLSM images of HeLa pLuc/705 cells 24 h after transfection with PMO-LP LenA 1:3 containing 20 % AF647-PMO and 20 % Alexa Fluor 488-labeled free LP-LenA (LP-AF488). Nuclei were stained with DAPI (blue), actin filaments with rhodamine phalloidin (yellow). The merged channel indicates co-localization (yellow) of AF647-PMO-LP and free LP-AF488. Additional FCS, TEM, CLSM and flow cytometry data are provided in Figure 26 - Figure 35.

2.4.5   Membrane interaction

From additional flow cytometry studies, it is evident that the beneficial effect of the unconjugated LP in 1:3 formulations on the cellular uptake is independent of the different lipid or fatty acid modifications (Figure 35). 1:1 formulations with LP containing cholanic acid or fatty acids with 1 to 4 unsaturated bonds mediated comparable levels of cellular PMO uptake. In all cases, a distinct PMO uptake enhancement was observed in the corresponding 1:3 formulations. Obviously, enhanced cellular uptake can explain the advantage of free LP in the formulations, but not the advantage of a specific fatty acid content.Therefore, the high efficacy of LP LenA must be the result of a different mechanism associated with the intracellular PMO trafficking. The lipid modifications turn the cationic conjugates into amphiphilic structures and provide the potential for membrane interactions. It has been shown previously that unsaturated fatty acids can mediate pH-dependent membrane lytic activity in nucleic acid transfecting agents.[161, 164, 201] For this reason, we hypothesize membrane interaction and endosomal release after endocytotic internalization as being a potential explanation for the superiority of PMO-LP LenA. An endosomal membrane integrity and release assay[197, 215-216] was carried out with fluorescent calcein being loaded into endosomes during transfection with PMO-LP SteA (saturated) or PMO-LP LenA (unsaturated) formulations (Figure 19A). In both cases, calcein was taken up efficiently (Figure 19B) but it was only in the case of PMO-LP LenA that a broad and homogenous distribution of fluorescence intensity were evident over the cell indicating release of the fluid phase marker calcein from the endosomes. An erythrocyte leakage assay verified the pH-dependent membrane interactive potential of PMO-LP containing unsaturated fatty acids (Figure 19C).The set of PMO-LP formulations containing CholA or fatty acids with zero to four double bonds was incubated with erythrocytes at physiological pH 7.4 or endolysosomal pH 6.5 and 5.5. A clear trend showed an increasing erythrocyte leakage, particularly at acidic pH, with an increasing number of double bonds. The highest lytic activity was observed with PMO-LP LenA and AraA, which altogether supports the initial hypothesis of increased endosomal membrane interaction and release of the PMO-LP formulation containing unsaturated bonds.
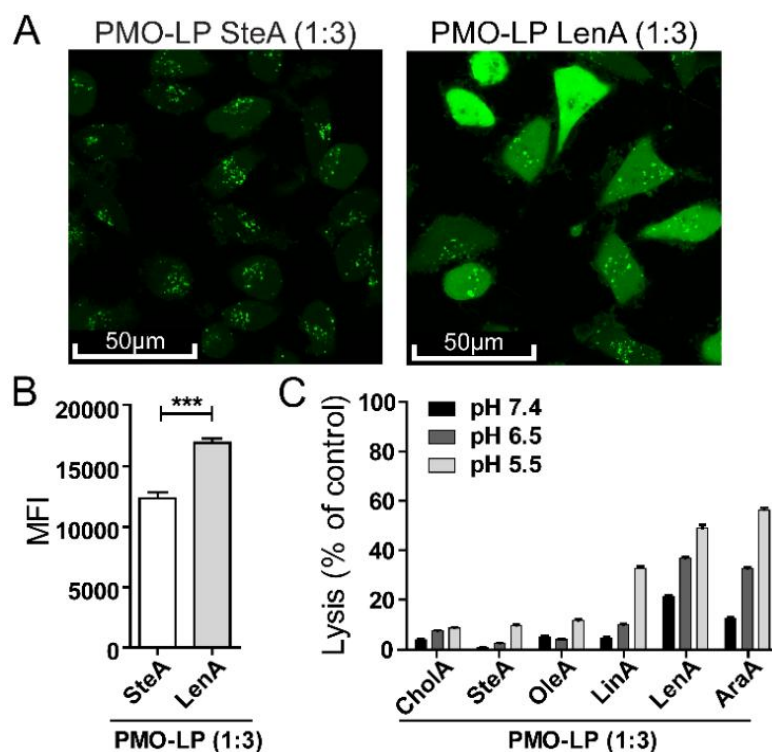
Figure 19. Impact of unsaturated fatty acids on cellular membrane interactions. (A) CLSM images of HeLa pLuc/705 cells treated with 0.45 mg/mL calcein and 5 µM PMO-LP SteA (1:3) or PMO-LP LenA (1:3) for 4 h. (B) The cellular calcein fluorescence intensity determined by flow cytometry (median fluorescence intensity, MFI, n=3) is shown. (C) Hemoglobin release was determined photometrically for 3.75×10^6 erythrocytes that were incubated for 60 min with 2.5 µM PMO-LP (1:3) at pH 7.4, 6.5 and 5.5. Values were normalized to positive control samples treated with 1 % Triton X-100 (100 % lysis). Data are presented as mean ± SD (n=4).

Additional erythrocyte leakage assays were conducted to clarify the contribution of free LP in PMO-LP 1:3 formulations (1 eq. PMO-LP conjugate, 2 eq. free LP) on membrane disruption (Figure 20). Erythrocytes were treated with free LP SteA or LenA (2.5 µM, 5 µM, 7.5 µM), PMO-LP SteA or LenA 1:1 (2.5, 7.5 µM) and PMO-LP SteA or LenA 1:3 (2.5 µM) formulations. The concentrations were chosen to enable direct comparison of equal free and total LP contents. Here, several significant observations were made. First, the higher lytic activity of LP LenA compared to LP SteA was confirmed in all three different states: free LP, PMO-LP 1:1 and 1:3 formulations. Second, free LP mediated by far the highest erythrocyte leakage in all cases which indicates a reductionof lytic potential due toconjugation. Third, PMO-LP 1:3 (2.5 µM) exhibited lower lytic activity than the corresponding samples with equal amount of free (5 µM) or total (7.5 µM) LP content. Apparently, the presence of PMO-

LP reduces lytic potential of free LP which can be explained by the observed co-assembly into nanomicelles. Finally, the initially speculated contribution of free LP on membrane disruption was confirmed: in both cases (LP SteA, LP LenA), PMO-LP 1:3 formulations mediated higher lytic activity than the corresponding 1:1 formulations.
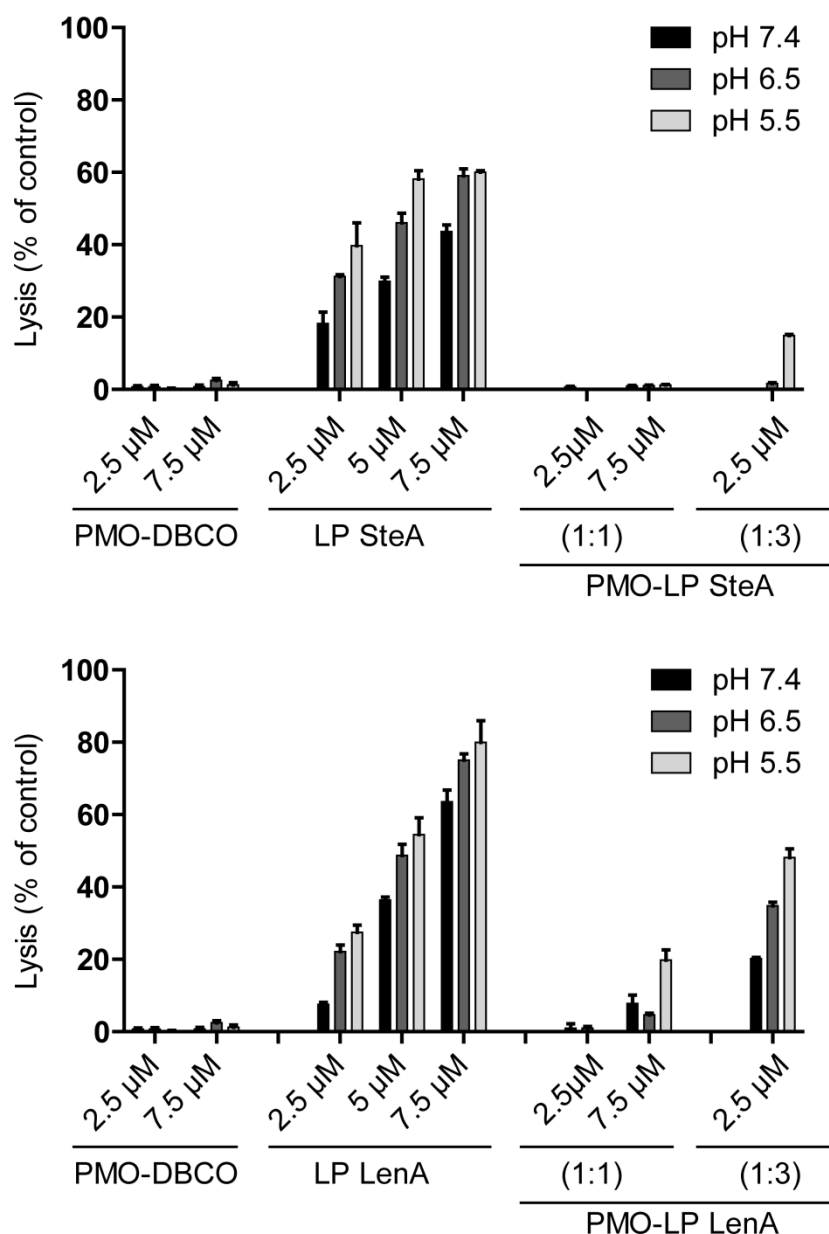
Figure 20. Impact of free LP in PMO-LP 1:3 formulations on membrane disruption. Hemoglobin release was determined photometrically for 3.75×10^6 erythrocytes that were incubated for 60 min with indicated amounts of PMO-DBCO, LP LenA and formulations of the two components at pH 7.4, 6.5 and 5.5. Values were normalized to positive control samples treated with 1 % Triton X-100 (100 % lysis). Data are presented as mean ± SD (n=4).

2.4.6 DMD myotube treatment

As an additional model with clinical relevance, an alternative PMO sequence 51D[217] mediating exon skipping in H2K-*mdx*52 dystrophic skeletal myotubes was selected (Figure 21). In *mdx*52 mice, a deletion of dystrophin exon 52 was generated by gene targeting,[218] which belongs to the 'deletion mutation hotspot'[219] of human DMD. H2K-*mdx*52 myotubes were treated with varying concentrations of PMO-LP LenA 1:1 (12.5 – 50 nM) or 1:3 (2 – 50 nM) and Pip6a at 50 nM. After 48 h, the exon skipping rate of extracted RNA was determined by RT-PCR amplification of dystrophin exons 49–54 and microchip electrophoresis. In this *in vitro* DMD exon skipping model the PMO-LP formulations displayed remarkably high activity. Both the 1:1 and 1:3 formulations achieved > 85 % exon skipping at a concentration of 50 nM. The exon skipping rate mediated by the 1:1 formulation dropped to approx. 43 % at 25 nM and 24 % at 12.5 nM concentrations. Consistent with the findings obtained in HeLa pLuc/705 cells, also in H2K-*mdx*52 dystrophic mytobes the PMO conjugates strongly benefit from the additional free LP in the formulation.
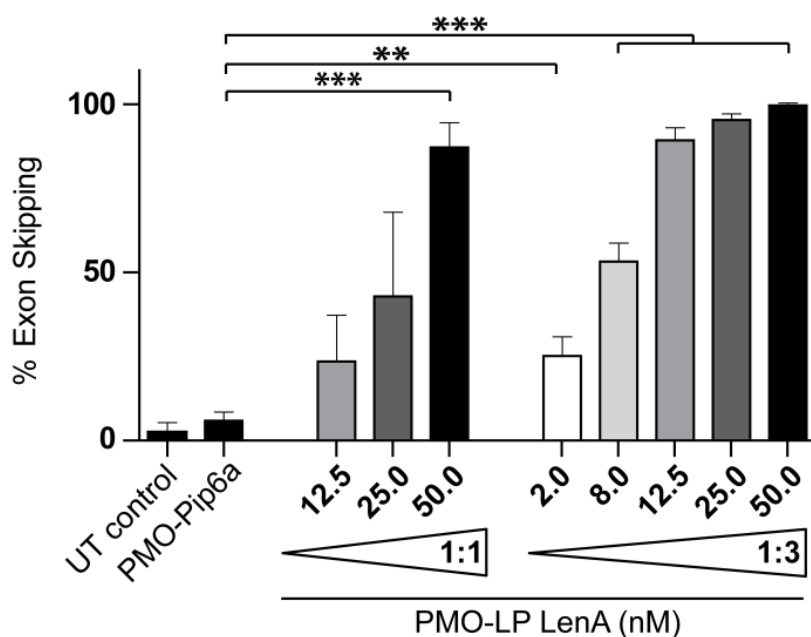
Figure 21. Exon skipping efficiency in H2K-*mdx*52 myotubes. H2K-*mdx*52 myoblasts were differentiated for 3 days and treated with varying concentrations of PMO-LP LenA 1:1 or 1:3. PMO-Pip6a 1:1 at 50 nM concentration and untreated cells (UT) served as controls. After 48 h, the total RNA was extracted from the cells and RT-PCR amplifying cDNA from exons 49–54 was carried out. PCR products were detected using a microchip electrophoresis system. Exon-skipping efficiency (%) was calculated as (exon-skipped transcript molarity) / (unskipped + exon-skipped transcript molarity) × 100 %. Data are presented as mean ± SD (n=3). Additional data of PMO-LP LenA 1:1 and PMO-Pip6a are provided in Figure 22.

PMO-LP LenA 1:3 mediated significantly higher exon skipping (approx. 25 % at 2 nM, approx. 100 % at 50 nM) compared to PMO-Pip6a (approx. 6 % at 50 nM, approx. 77 % at 400 nM, Figure 22).
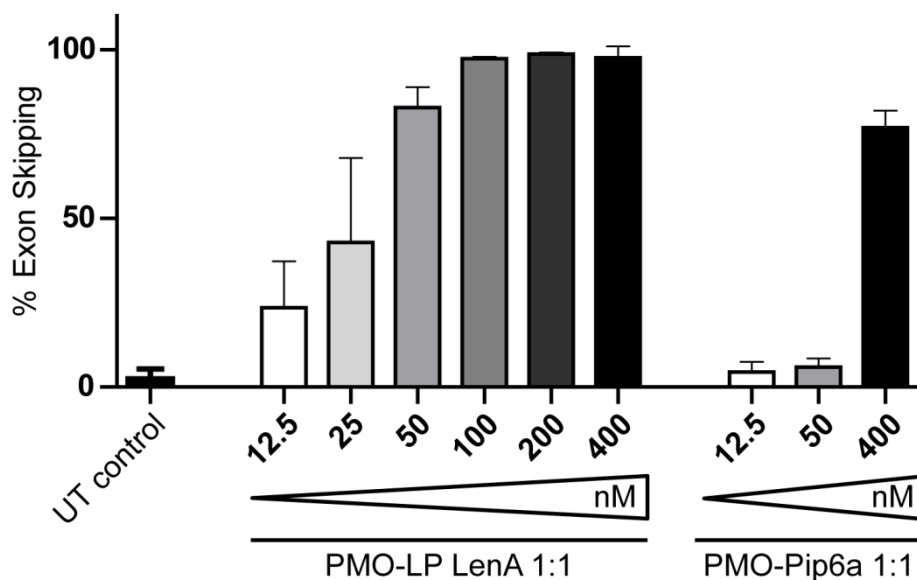
Figure 22. Exon skipping efficiency in H2K-*mdx*52 myotubes. H2K-*mdx*52 myoblasts were differentiated for 3 days and treated with varying concentrations of PMO-LP LenA 1:1 or PMO-Pip6a 1:1 and untreated cells (UT) served as controls. After 48 h total RNA was extracted from the cells and RT-PCR amplifying cDNA from exons 49–54 was carried out. PCR products were detected using a microchip electrophoresis system. Exon-skipping efficiency (%) was calculated as (exon-skipped transcript molarity) / (unskipped + exon-skipped transcript molarity) × 100 %. Data are presented as mean ± SD (n=3). Subset of the data is shown in Figure 21.

2.5   Conclusion

In summary, we report novel aminoethylenelipopeptide-PMO conjugates with a high potential for promoting splice-switching PMO delivery. During the screening and optimization process, two key parameters of highly active formulations were identified: (1) PMO-LP conjugates containing linolenic acid mediate the highest effects, and (2) additional unconjugated LP in the formulation enhances the potency and activity at low concentrations. The PMO-LP conjugatesself-associate into nanocomplexes in a concentration-dependent fashion and a fraction of additional free LP in the formulation contributes to the particle formation. The content of unsaturated fatty acid LenA was found to facilitate endosomal release after cellular internalization, most likely via membrane interactions. The splice-switching activity of the PMO-LP formulations was confirmed in human cervix carcinoma (HeLa), human hepatoma (Huh7), murine neuroblastoma (Neuro2A) and murine myoblast (C2C12) pLuc/705 cells *in vitro* as well as after local injection into HeLa pLuc/705 tumors *in vivo*. The encouraging splice-switching activity was additionally confirmed in H2K-*mdx*52 dystrophic skeletal muscle cells where the identified PMO-LP formulation exhibited remarkably high potency and mediated significant exon skipping at low concentration < 10 nM. The presented LP conjugates and formulations are considered a highly potent platform for the delivery of PMO therapeutics with antisense or splicing-modifying mechanism.

2.6   Acknowledgements

2.7 Supporting information figures

Figure 23. HeLa pLuc/705 cell viability after treatment with PMO-LP CholA. Metabolic activity of HeLa pLuc/705 cells was determined using a MTT assay 24 h after transfection with noncovalent *#991* or covalent *#1106* formulations at different concentrations and PMO to lipopeptide ratios. Data are presented as % cell viability with respect to the control cells ± SD (n=3).
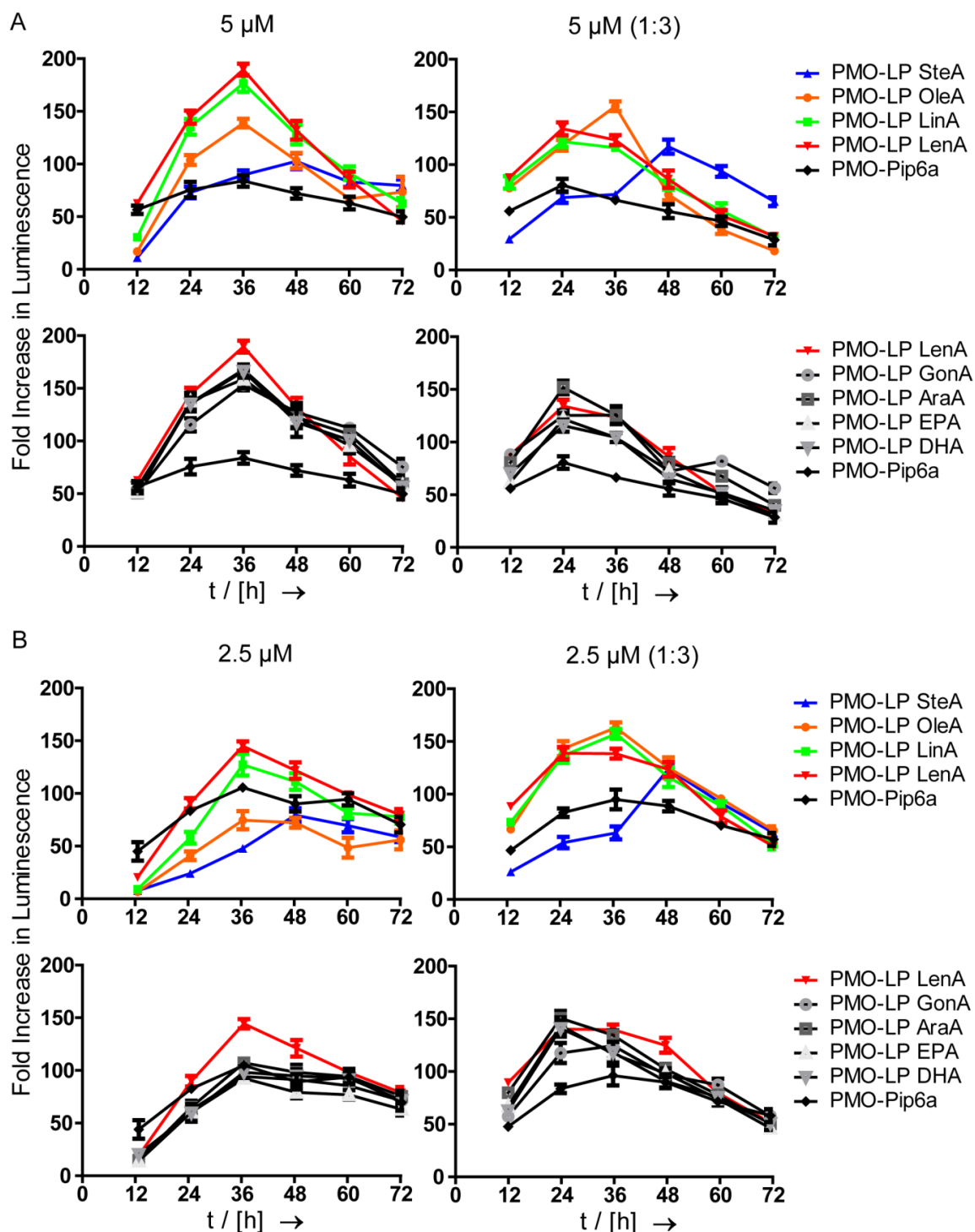
Figure 24. Luciferase activity kinetic in HeLa pluc/705 cells after PMO-LP transfection. The kinetics of the increase in luminescence from 12 to 72 hours [h] after transfection with PMO conjugate formulations containing 5 µM (A) or 2.5 µM (B) PMO at a 1:1 (left graphs) or 1:3 (right graphs) PMO-DBCO to LP ratio. Luciferase activity was measured every 12 hours. Figures show a comparison between LP containing 0 to 3 (top A and B) or 3 to 6 double bonds (bottom A and B). A Pip6a-azide derivative served as a positive control in the same PMO-DBCO conjugation protocol at a 1:1 ratio. Data are presented as the mean ± SD (n=3). Subset of the data is shown in Figure 13 of the main manuscript.
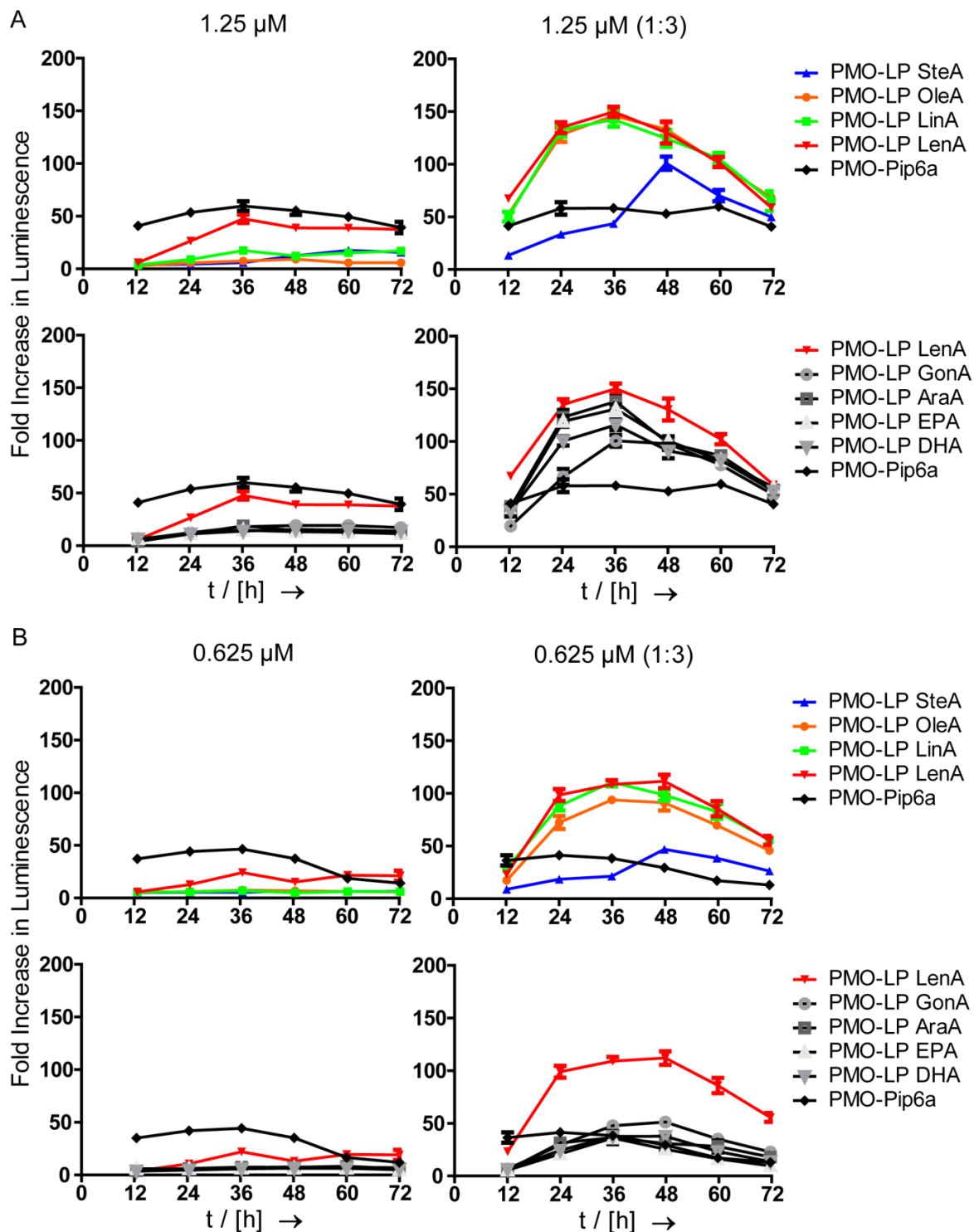
Figure 25. Luciferase activity kinetics in HeLa pluc/705 cells after PMO-LP transfection. The kinetics of the increase in luminescence from 12 to 72 hours [h] after transfection with PMO conjugate formulations containing 1.25 μM (A) or 0.625 μM (B) PMO at a 1:1 (left graphs) or 1:3 (right graphs) PMO-DBCO to LP ratio. Luciferase activity was measured every 12 hours. Figures show a comparison between LP containing 0 to 3 (top A and B) or 3 to 6 double bonds (bottom A and B). A Pip6a-azide derivative served as a positive control in the same PMO-DBCO conjugation protocol at a 1:1 ratio. Data are presented as the mean ± SD (n=3). Subset of the data is shown in Figure 13 of the main manuscript.
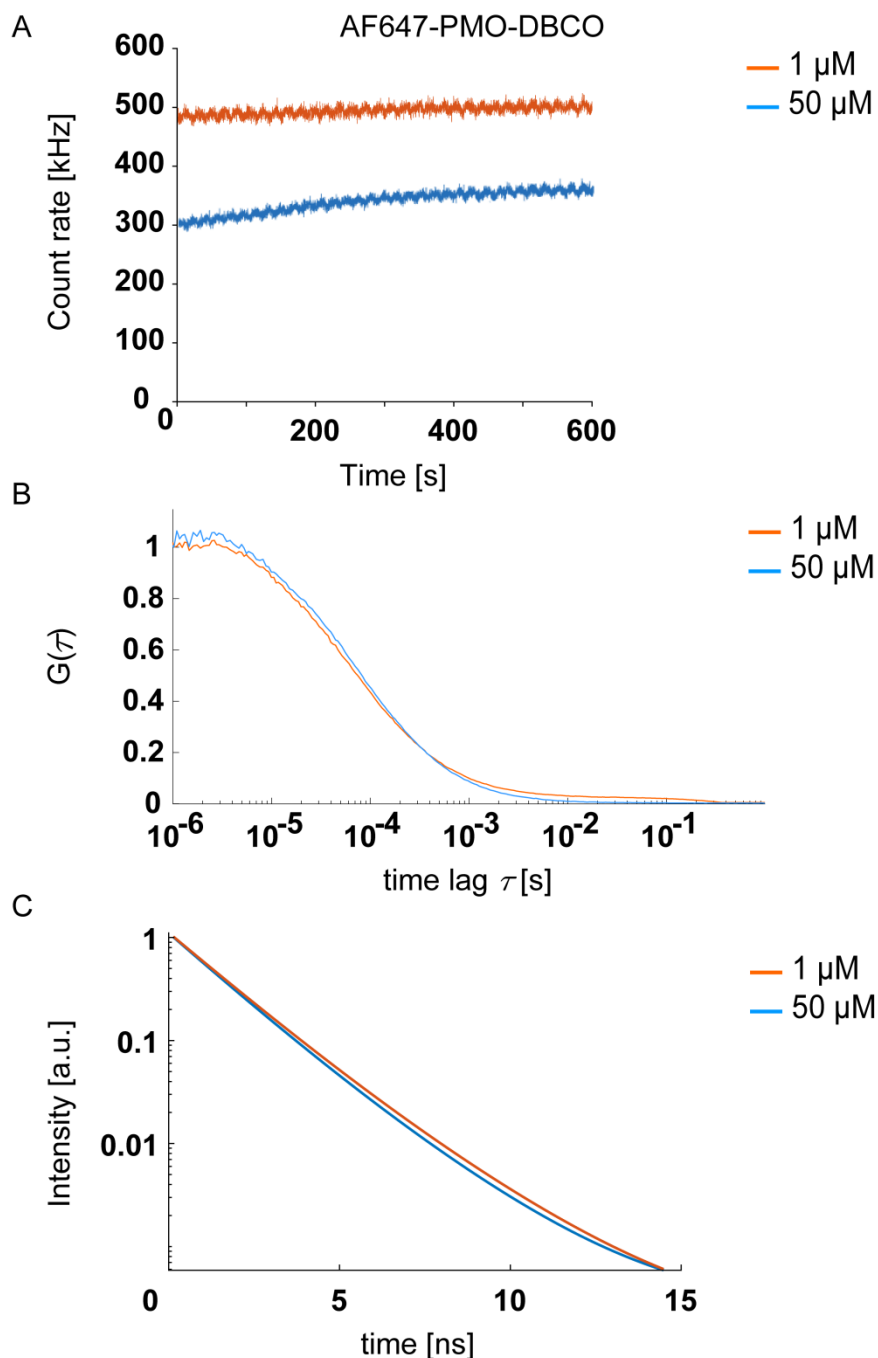
Figure 26. The absence of interactions between PMOs at two different concentrations monitored using FCS and fluorescence lifetime. (A) Fluorescence intensity traces, (B) FCS measurements, and (C) lifetime decay traces of AF647-PMO mixed with two different concentrations of unlabeled PMOs: 100 nM AF647-PMO was spiked with 0.9 µM (orange trace) and 49.9 µM (blue trace) unlabeled PMO. The high resemblance in both the autocorrelation function and lifetime decay indicates the absence of PMO interactions. The binning time is 100 ms.
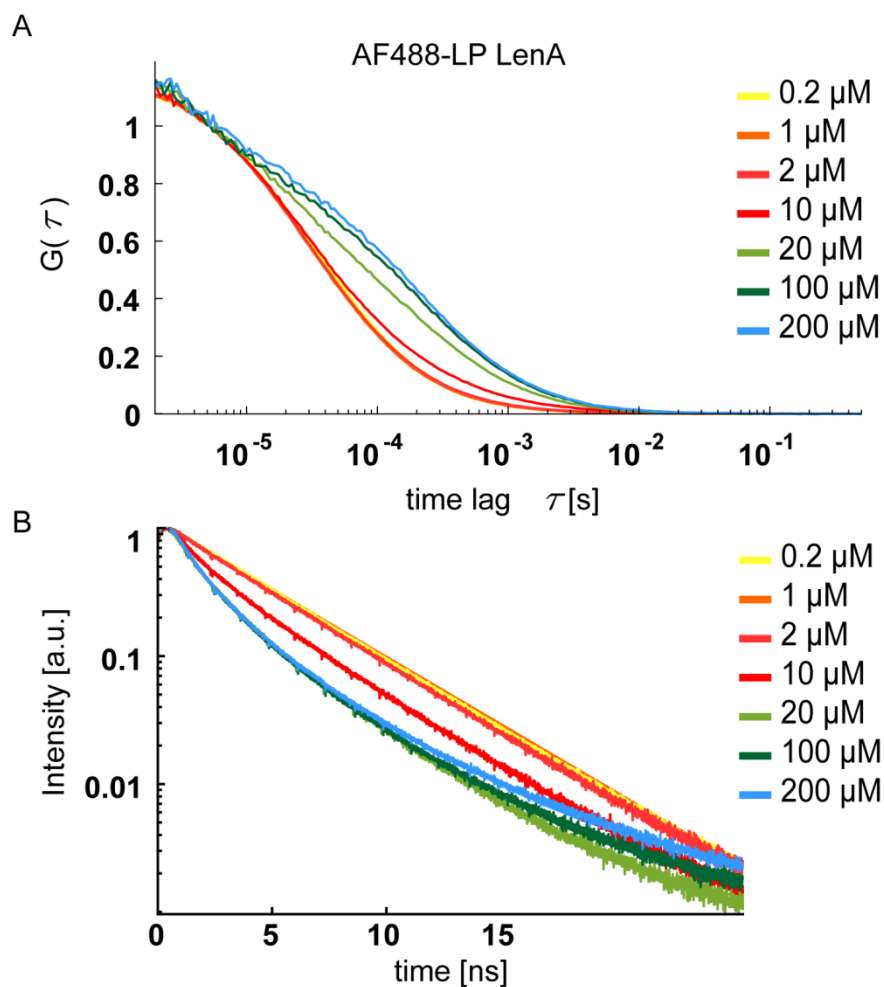
Figure 27. Interactions between LP LenA oligomers at different concentrations monitored using FCS and fluorescence lifetime. (A) FCS measurements and (B) fluorescence lifetime decay of 100 nM AF488-LP LenA spiked with different LP LenA concentrations as given in the figure legend. The lifetime showed a consistent mono-exponential decay for LP LenA concentrations below 10 µM with a lifetime $\tau \sim 4.1$ ns. A bi-exponential decay, with lifetimes of $\tau_1 \sim 1.3$ ns and $\tau_2 \sim 3.7$ ns, was observed for LP LenA concentrations of 10 µM and above indicating the interaction of LP LenA at higher concentrations.
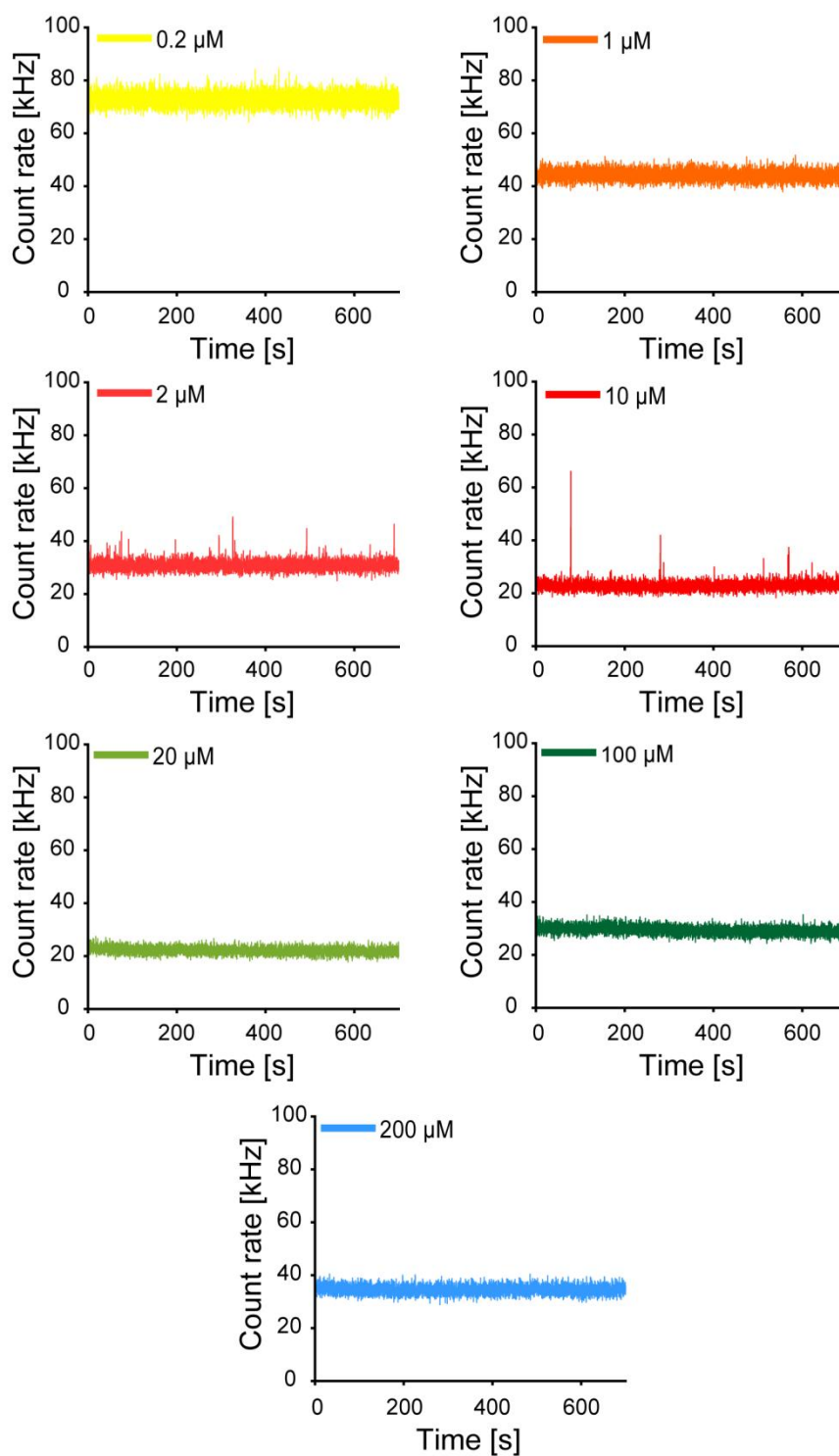
Figure 28. Fluorescence intensity traces of AF488-LP LenA at different concentrations of unlabeled LP LenA. 100 nM AF488-LP LenA was spiked with different concentrations of unlabeled LP LenA as given in the figure legend. The binning time is 100 ms. The spikes visible in the intensity traces at 2 and 10 µM total concentration of LP LenA indicates that the peptide starts to aggregate. Above 10 µM, the aggregates prevail and a more homogenous signal is observed. These results are supported from the FCS experiments in Figure 27A.

A

AF647-PMO-LP LenA

B
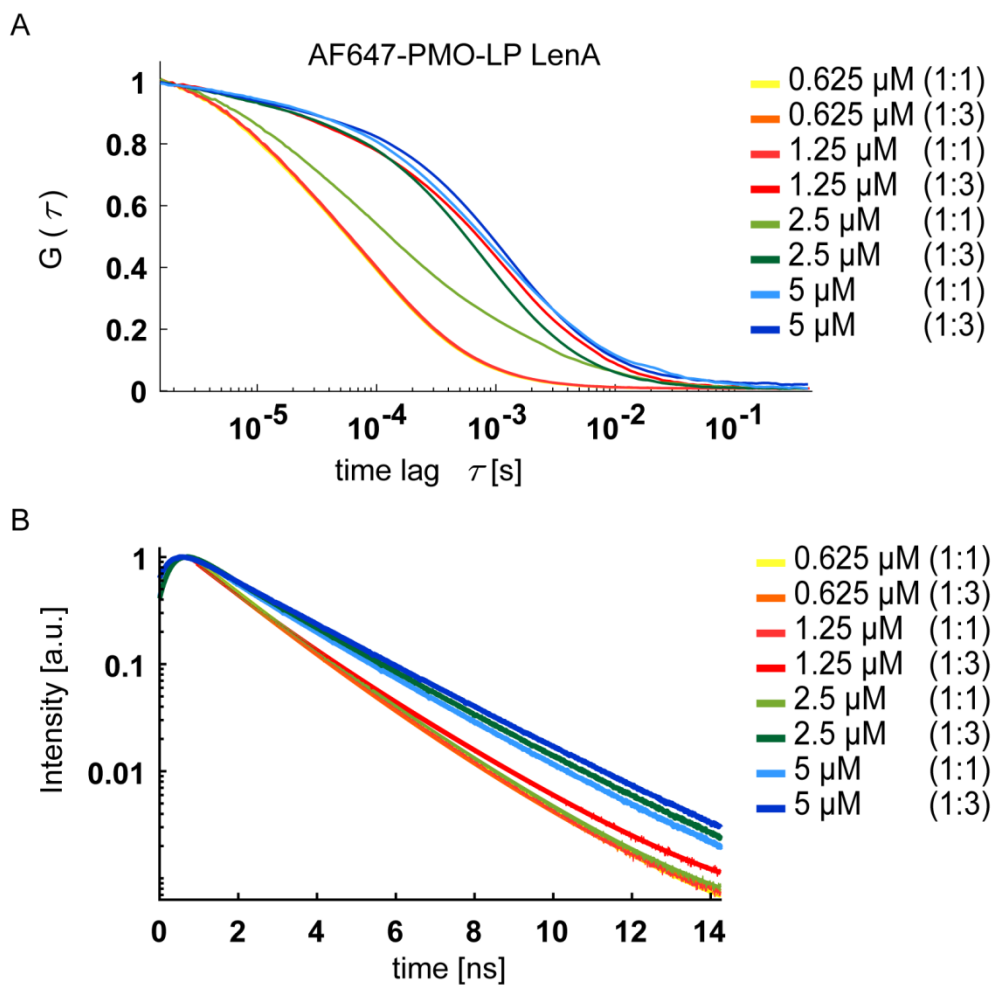
Figure 29. Interactions between PMO and LP LenA oligomer at different concentrations monitored using FCS and fluorescence lifetime. (A) The FCS measurements and (B) lifetime decay traces of 50 nM AF647-PMO LP spiked with different PMO and LP LenA concentrations in ratios of 1:1 and 1:3 PMO-LP LenA. The lifetime showed a bi-exponential decay with lifetimes of $\tau_1 \sim$ 1.5 ns and $\tau_2 \sim$ 2.2 ns, where the fraction of the longer 2.2 ns lifetime component increases with increasing PMO-LP LenA concentration. Subset of the data is shown in Figure 18 of the main manuscript.
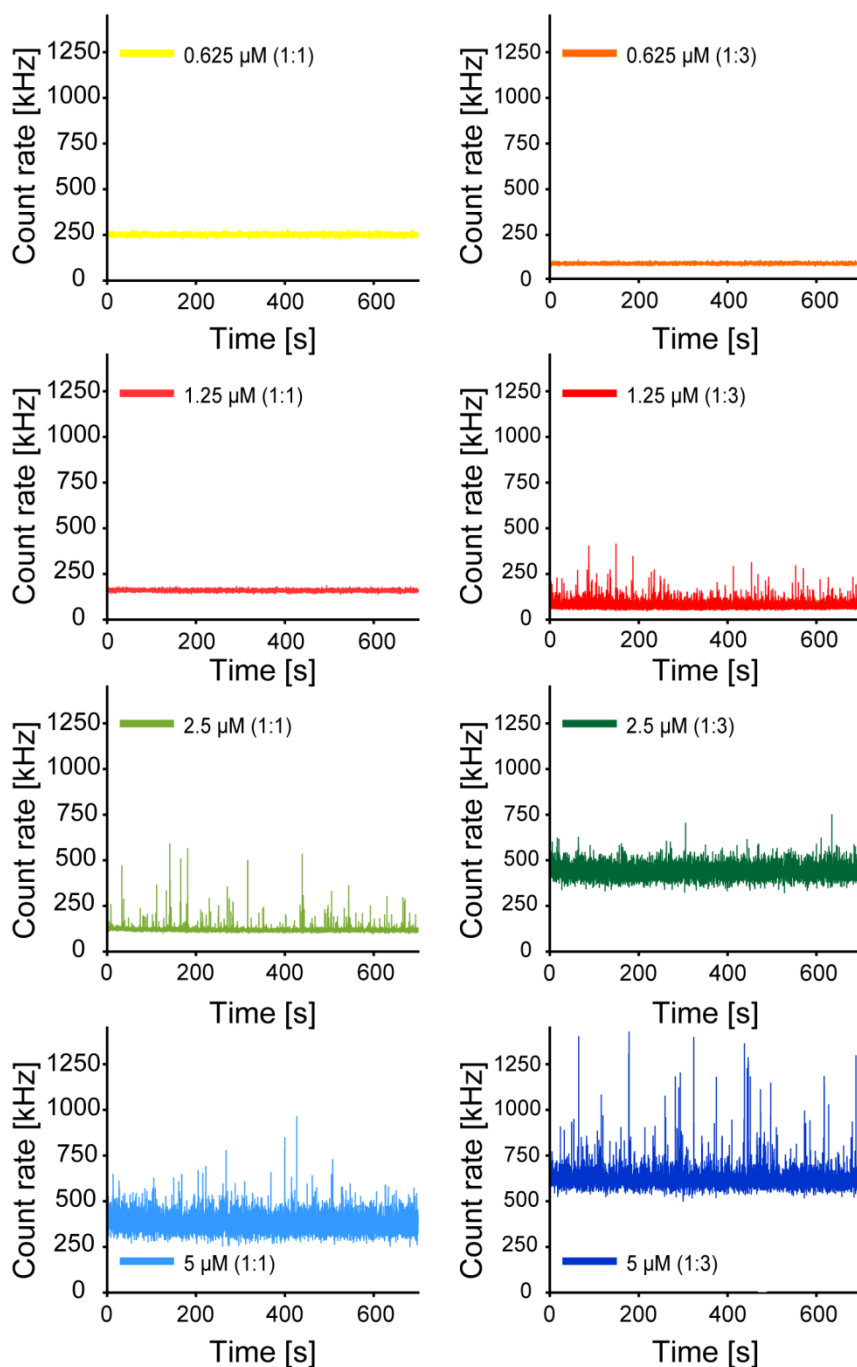
Figure 30. Fluorescence intensity traces of AF647-PMO in combination with different concentrations of 1:1 PMO-LP LenA (left) and 1:3 PMO-LP LenA (right). 50 nM AF647-PMO was spiked with different concentrations of unlabeled PMO and LP LenA as given in the legend for each measurement condition. The binning time is 100 ms. Spikes in the intensity traces indicate the formation of heterogenous aggregates.
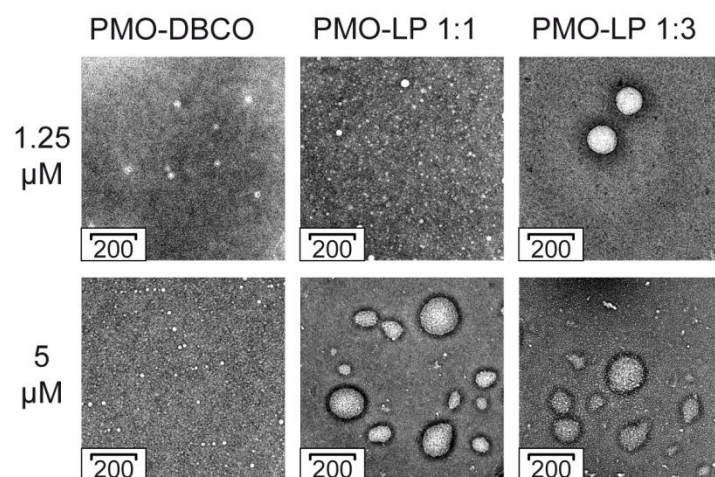
Figure 31. Transmission electron microscopy (TEM) images of free PMO-DBCO (left) or PMO-LP LenA formulations at 1:1 (middle) and 1:3 (right) ratio. Scale bars represent 200 nm.
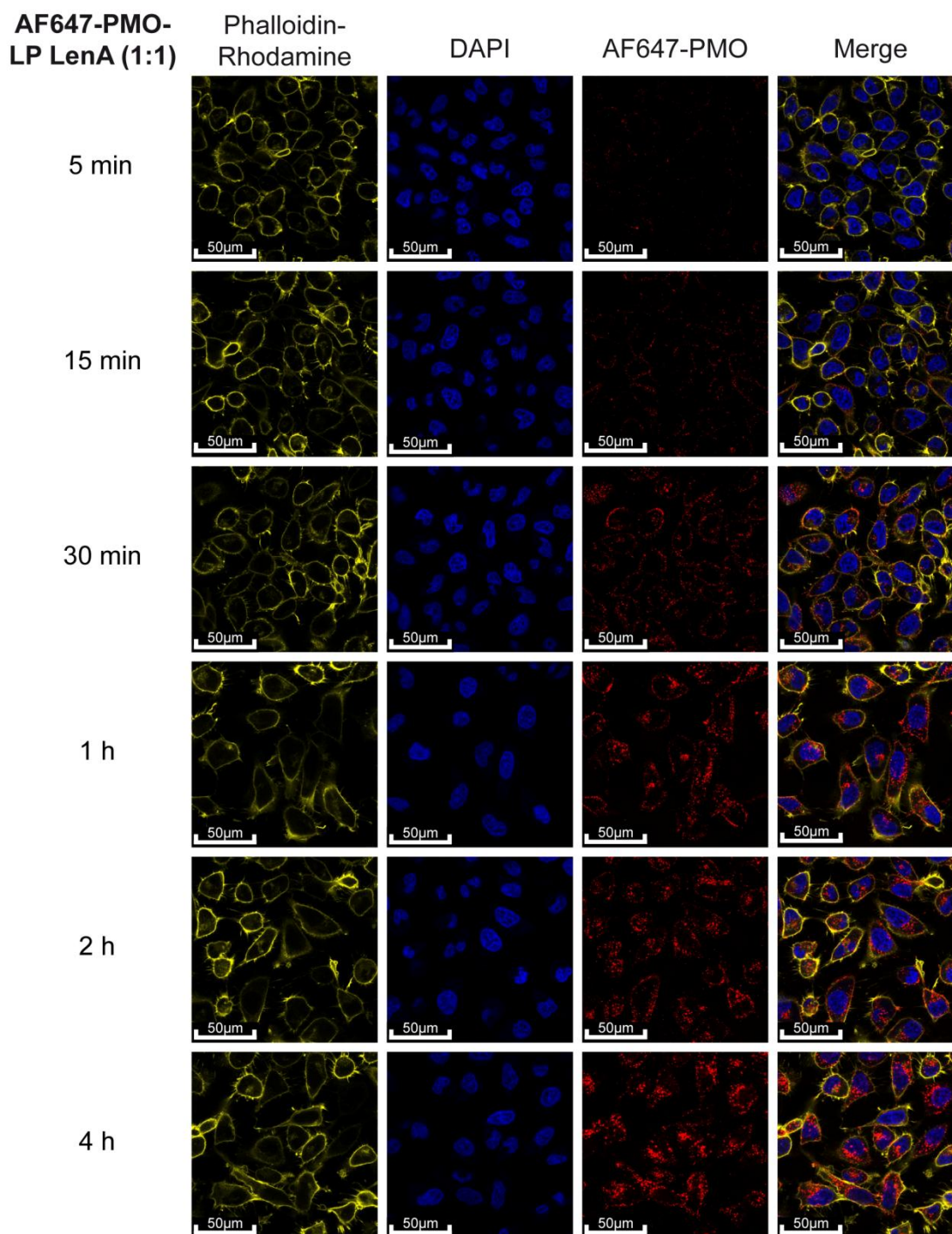
Figure 32. Confocal laser scanning microscopy (CLSM) images of AF647-PMO-LP LenA (1:1) uptake kinetics. HeLa-pLuc/705 cells were incubated with 0.625 µM PMO-LP LenA at a 1:1 ratio containing 20 % AF647-labeled PMO. Images were recorded after 5 min, 15 min, 30 min, 1 h, 2 h and 4 h. First column: fluorescence of phalloidin-rhodamine stained actin filaments; second column: nuclear staining with DAPI; third column: fluorescence of AF647-labeled PMO; fourth column: merge of all three channels. Subset of the data is shown in Figure 18 of the main manuscript.
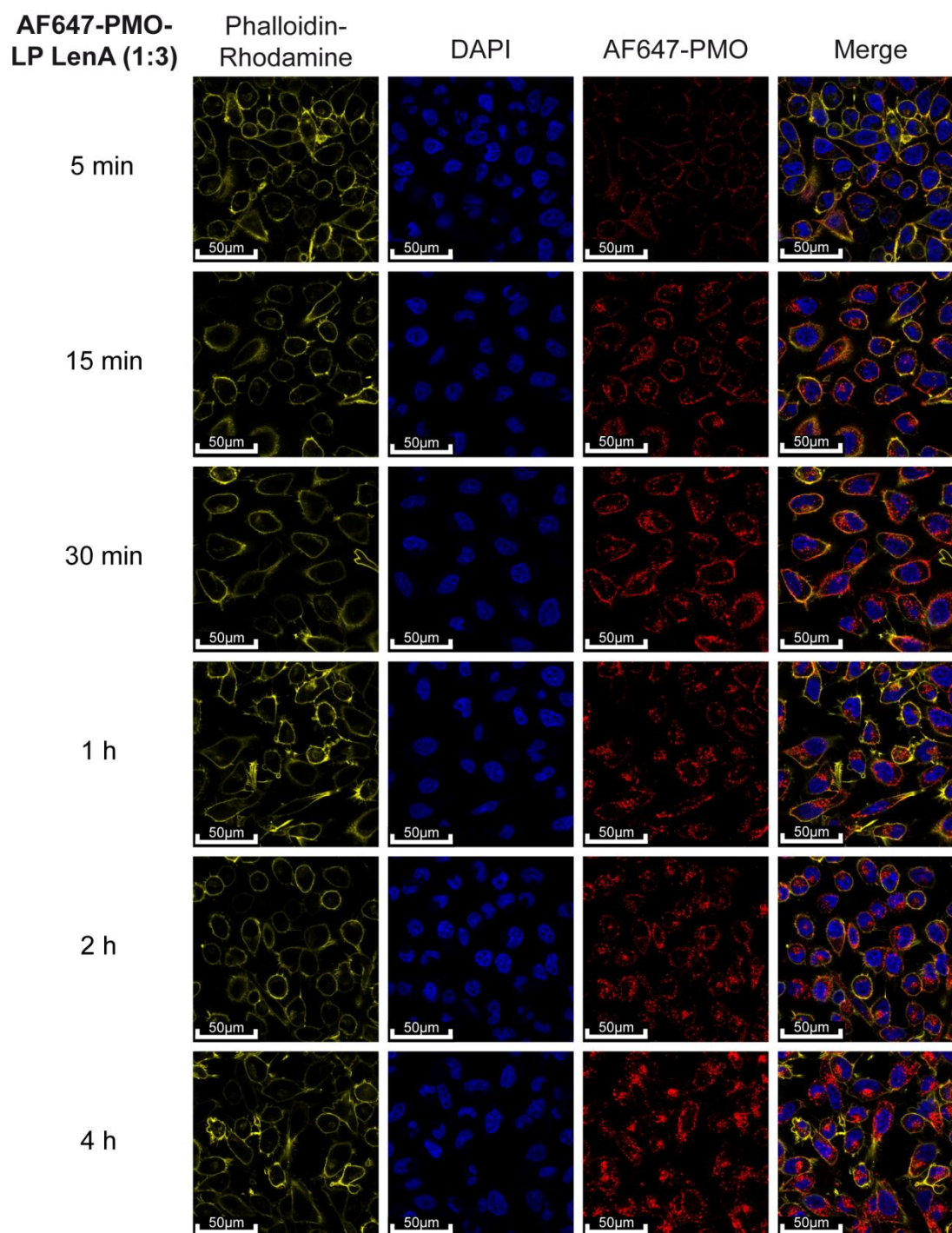
Figure 33. Confocal laser scanning microscopy (CLSM) images of AF647-PMO-LP LenA (1:3) uptake kinetics. HeLa-pLuc/705 cells were incubated with 0.625 µM PMO-LP LenA at a 1:3 ratio containing 20 % AF647-labeled PMO. Images were recorded after 5 min, 15 min, 30 min, 1 h, 2 h and 4 h. First column: fluorescence of phalloidin-rhodamine stained actin filaments; second column: nuclear staining with DAPI; third column: fluorescence of AF647-labeled PMO; fourth column: merge of all three channels. Subset of the data is shown in Figure 18 of the main manuscript.
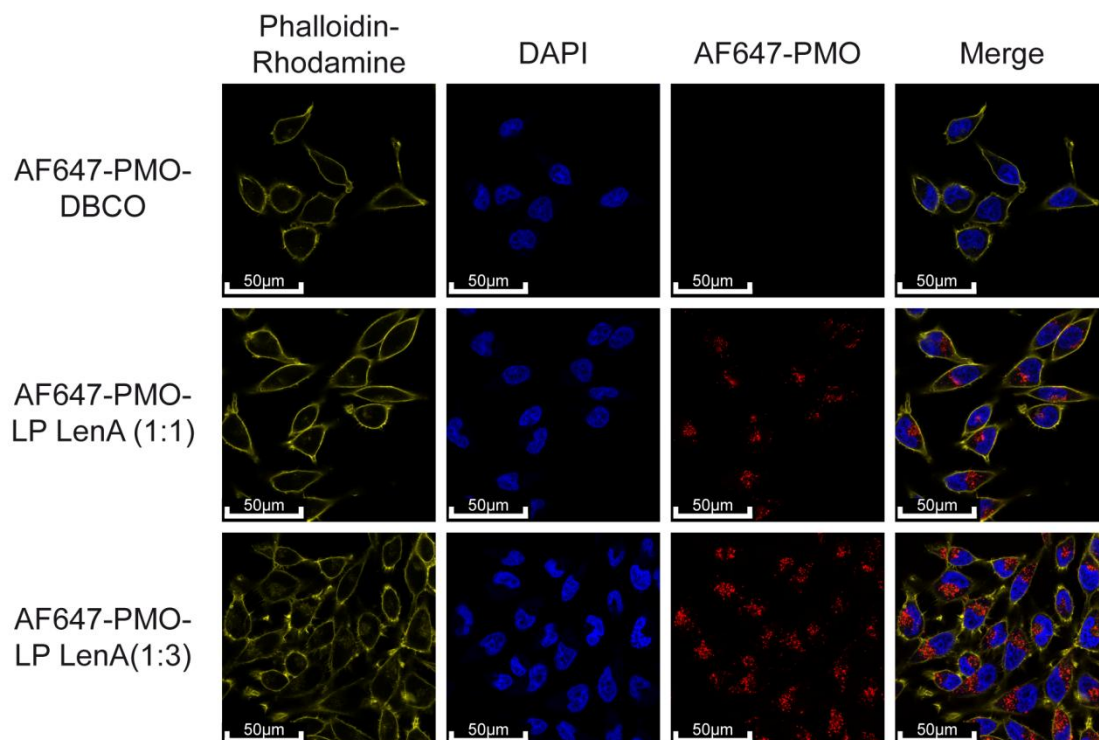
Figure 34. Confocal laser scanning microscopy (CLSM) images of AF647-PMO-LP LenA uptake 24 h after transfection. HeLa-pLuc/705 cells were incubated with 0.625 µM PMO-DBCO (top) as well as PMO-LP LenA formulations at a 1:1 (middle) or 1:3 (bottom) ratio, each containing 20 % AF647-labeled PMO. Images were recorded 24 h after transfection. First column: fluorescence of phalloidin-rhodamine stained actin filaments; second column: nuclear staining with DAPI; third column: fluorescence of AF647-labeled PMO; fourth column: merge of all three channels.

A

Sample:	Ratio:	MFI:	SD:
HBG control		12,8	± 0,3
PMO-DBCO		149,7	± 1,5
PMO-LP CholA	1:1	39066,7	± 503,3
PMO-LP CholA	1:3	48666,7	± 1115,1
PMO-LP OleA	1:1	41133,3	± 2400,7
PMO-LP OleA	1:3	71333,3	± 3412,2
PMO-LP LinA	1:1	44766,7	± 1800,9
PMO-LP LinA	1:3	67066,7	± 5254,8
PMO-LP LenA	1:1	40600,0	± 608,3
PMO-LP LenA	1:3	71233,3	± 3023,8
PMO-LP AraA	1:1	36400,0	± 500,0
PMO-LP AraA	1:3	56200,0	± 100,0

B
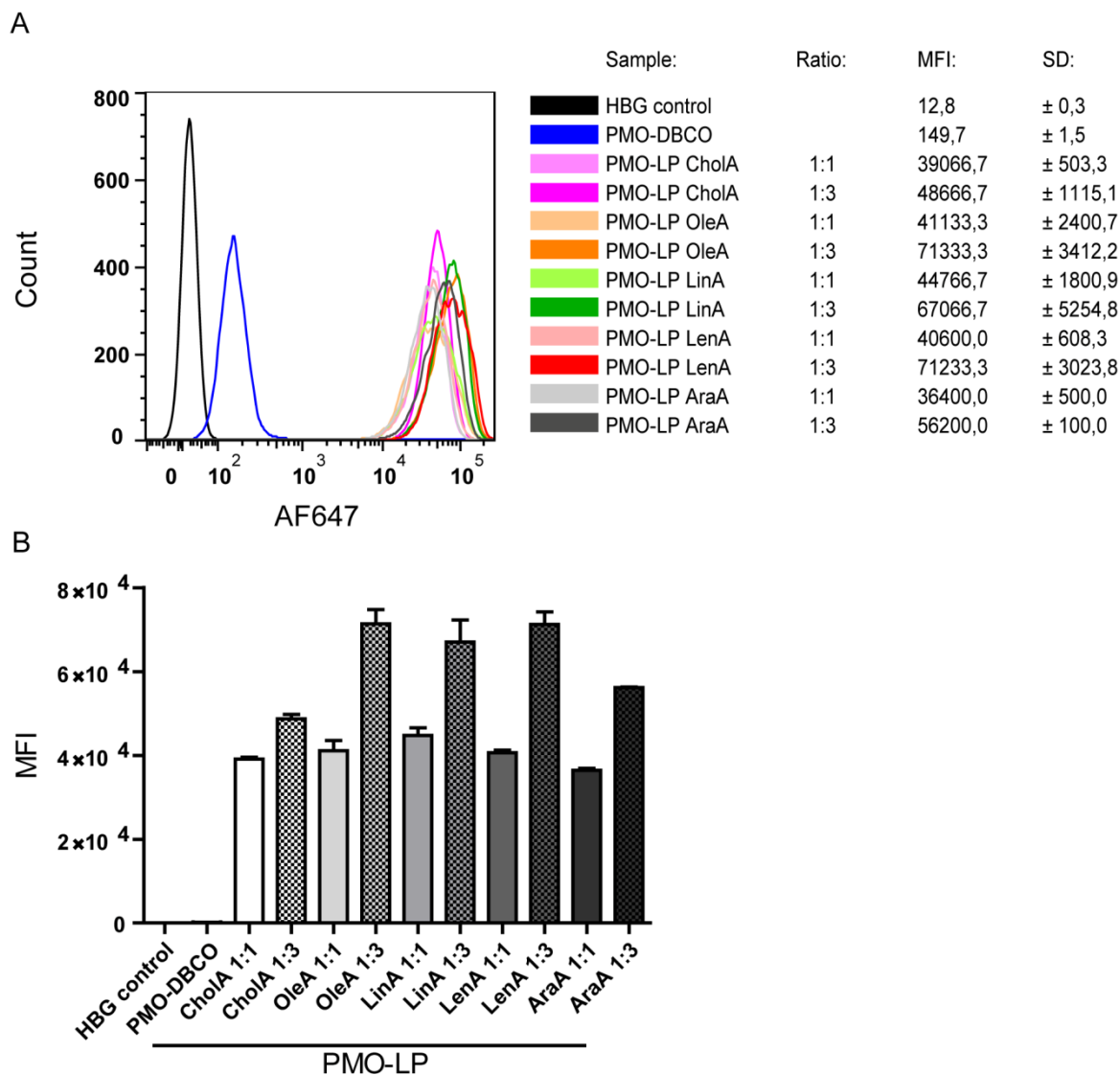
Figure 35. Cellular uptake of PMO-LP formulations containing different fatty acids determined by flow cytometry. HeLa-pLuc/705 cells were incubated with 0.625 µM PMO-DBCO (5% AF647-labeled) as well as with PMO-LP formulations at a 1:1 or 1:3 ratio containing different fatty acids. Flow cytometry was conducted 24 h after PMO transfection. (A) A FACS histogram plot of each sample group. (B) A comparison of the measured median fluorescence intensities. The data are presented as the mean ± SD (n=3).

3 Chapter II:

Delivery of Cas9/sgRNA Ribonucleoprotein Complexes via Hydroxystearyl Oligoamino Amides

Jasmin Kuhn[1], Yi Lin[1], Ana Krhac Levacic[1], Nader Al Danaf[2], Lun Peng[1], Miriam Höhn[1], Don C. Lamb[2], Ernst Wagner[1], and Ulrich Lächelt[1]

[1]Department of Pharmacy and Center for NanoScience (CeNS), LMU Munich, 81377 Munich, Germany
[2]Department of Chemistry and Center for NanoScience (CeNS), LMU Munich, 81377 Munich, Germany

The following sections are directly adapted from the submitted manuscript.

Sections may have been moved for consistency.

Contributions: JK was engaged in planning and conductance of all experiments and wrote the manuscript. YL supported knock out experiments, performed sequencings and DLS measurements. AKL supported knock out experiments. NAD and the group of DCL performed the fluorescence correlation spectroscopy. LP synthesized the sequence-defined oligo(ethylenamino) amides. MH captured the confocal laser scanning microscopy pictures. EW conceived the study and provided conceptual advice. UL conceived the study and wrote the manuscript. All authors contributed to the manuscript and conclusions of this work.

3.1   Abstract

The programmable endonuclease activity and simple usage of CRISPR/Cas9 revolutionized the field of genome editing. The binding of single guide RNA (sgRNA) by the Cas9 protein results in the formation of negatively charged ribonucleoprotein (RNP) complexes. The presence of this functional complex inside cells is imperative for intended specific genome modifications. Direct intracellular delivery of Cas9/sgRNA RNP complexes would be of great utility. A compound library of sequence-defined oligo(ethylenamino) amides containing structural motifs for stable nanoparticle formation, cellular uptake and endosomal release was utilized for the screening and development of suitable Cas9 RNP delivery vehicles. Lipid containing oligoaminoamides (lipo-OAAs) were identified as most efficient carriers for intracellular Cas9/sgRNA delivery and gene disruption. Fluorescence correlation spectroscopy measurements indicated that the lipo-OAAs only interact with sgRNA-loaded Cas9 protein which suggest exclusive ionic interaction with the negatively charged RNPs. The type of contained fatty acid turned out to have a critical impact on the knock out efficiency: the presence of one hydroxy group in the fatty acid dramatically changes the properties and performance of resulting Cas9/sgRNA lipo-OAA complexes. The lipo-OAA containing hydroxy-stearic acid (OHSteA) was superior to the analogs with saturated or unsaturated fatty acids without hydroxylation; it formed smaller and more defined nanoparticles with Cas9/sgRNA, improved the cellular uptake and exhibited favorable interaction with membranes at acidic pH which is suggested to facilitate intracellular release out of endosomes. The efficient and adaptable delivery platform is considered to have high potential for the future development of therapeutics based on precise genome modification.
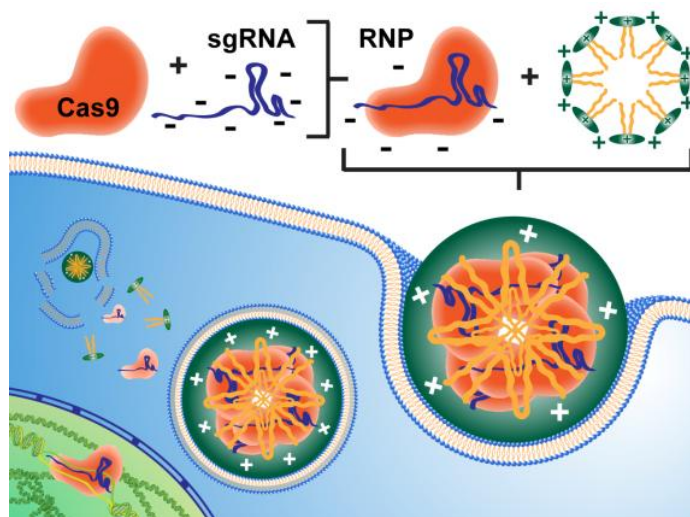
3.2   Introduction

Protein therapeutics have emerged as a major new class of biopharmaceuticals, since the discovery and approval of the first recombinant protein.[220-221] This class of drugs, which includes hormones, antibodies, cytokines, growth factors, enzymes as well as bone and blood related agents, exhibits an enormous therapeutic potential due to its involvement in various biochemical processes, its high specificity, tolerability and safety.[222]

CRISPR (clustered, regularly interspaced, short palindromic repeats) Cas (CRISPR-associated) is an adaptable DNA cleavage system found in bacteria,[62, 223] and has been utilized as an efficient RNA-guided genome-editing tool in numerous species,[224-226] as well as in human cells.[70, 227] The target sequence of the programmable nuclease Cas9 is controlled by a guide RNA (combination of crRNA and tracrRNA) or a single guide RNA (sgRNA).[62] For efficient genome editing, a successful intracellular delivery of the CRISPR/Cas9 components is essential. So far, the most common strategy is based on the delivery of the CRISPR/Cas9 encoding DNA sequences or *in vitro* transcribed RNA molecules.[228] However, the direct delivery of the Cas9 protein complexed with sgRNA has several advantages over the delivery of corresponding nucleic acid precursors, as the ribonucleoprotein (RNP) complex is immediately functional without the requirement of transcription and translation. Furthermore, there is no risk of spontaneous genome integration, and the timely degradation reduces off-target effects.[69]

Since nucleic acids and proteins are susceptible to enzymatic degradation the incorporation into a carrier system can increase their stability.[229-230] In addition, the poor membrane permeability impedes transport of Cas9/sgRNA RNPs to the intracellular target site and requires development of suitable delivery vehicles.[231] Different non-viral delivery technologies evolved for the direct delivery of the RNP complexes including cell-penetrating peptides,[145] DNA nanoclews,[232] gold nanoparticles,[146-147] polymeric systems,[233-235] as well as lipid nanoparticles.[111, 149] Nonetheless, the requirement of better carriers for stable RNP components packaging, high cellular uptake, efficient endosomal escape and nuclear entry while preserving biological activity of the protein remains.

Sequence-defined oligo(ethylenamino) amides (OAAs) based on artificial oligoamino acids and solid-phase synthesis have recently been developed as a platform for the delivery of nucleic acids,[152] proteins[230] and drugs.[154] They combine the advantages of aminoethylene based polymers with the chemical precision of peptides and enable cargo-specific optimization. OAAs with a favorable stability, biocompatibility and toxicity profile were generated.[152, 236]

In this study, lipo-OAAs were established as a new delivery platform for co-delivery of the Cas9 protein and sgRNA. Different architectures were screened to identify favorable structural motifs and the most suitable reagents. Here, the artificial oligoamino acids were intended to complex the negatively charged RNP complexes and facilitate their endosomal escape via the hypothesized proton sponge effect.[237] Additional cysteines (C) and hydrophobic motifs, like the tyrosine (Y) tripeptide, have been shown to improve nanoparticle stability in context of other delivery purposes.[166, 238] Fatty acids can enable efficient intracellular delivery by promoting membrane interaction and endosome disruption.[163-165]

3.3   Material and Methods

3.3.1   Materials

Oligoamino amides were synthesized by solid-phase synthesis[152] as described previously.[164] Detailed sequence information can be found in chapter 3.7 Supporting Information Table 3. HEPES buffered glucose (HBG) containing 20 mM HEPES (Biomol GmbH, Germany) and 5 % w/v glucose (Merck, Germany) was adjusted to pH 7.4. ATTO647N NHS-ester was purchased from ATTO-TEC (Germany), 5-(3-aminoallyl)-uridine-5'-triphosphate-ATTO488 from Jena Bioscience (Germany). Cell culture media, antibiotics, and fetal bovine serum (FBS) were purchased from Invitrogen (Germany). All solvents and other reagents were purchased from Sigma-Aldrich, Iris Biotech (Germany), Merck (Germany), or AppliChem (Germany). All flasks, dishes, and multiwell plates were manufactured by TPP (Switzerland). Deionized water was purified in-house using an Evoqua Ultra Clear® Glass Panel Systems (Germany) and was used for all experiments.

3.3.2   Cas9 protein expression and purification

Recombinant Cas9 was produced by bacterial expression of a plasmid pET28a/Cas9-Cys containing the human codon-optimized Cas9 nuclease gene with a N-terminal His-tag and a C-terminal cysteine. pET28a/Cas9-Cys was a gift from Hyongbum Kim (Addgene plasmid # 53261).[239] The plasmid pET28a/Cas9-Cys was transformed into RosettaBL21(DE3)pLysS (Merck Millipore, Germany), as recommended by the manufacturer.

An overnight culture of RosettaBL21(DE3)pLysS (pET28a/Cas9-Cys) was grown in lysogeny broth (LB) medium containing 34 µg/mL chloramphenicol and 50 µg/mL kanamycin at 37 °C under constant shaking. On the next day, the bacterial culture was 1:100 diluted with LB medium (34 µg/mL chloramphenicol and 50 µg/mL kanamycin) and incubated at 37 °C under constant shaking until an optical density of 0.5-0.7 (600 nm) was reached. Afterwards, the bacterial suspension was cooled down to room temperature (RT), protein expression was induced by adding 1 mM isopropyl β- *D*-1-thiogalactopyranoside (IPTG) and the culture was incubated overnight at RT under constant shaking.

Bacteria were harvested by centrifugation (20 min, 5000 x g, 4 °C). The supernatant was discarded and the pellet was resuspended in bacterial lysis buffer (20 mM trizma-base, 0.2 M NaCl, 20 % sucrose, 10 mM $MgCl_2$, pH 7.5). The final concentrations added were 10 µg/mL RNase, 30 µg/mL DNase, 1 mg/mL lysozyme and 1 mM phenylmethylsulfonyl fluoride (PMSF). The lysed bacterial suspension was frozen in liquid nitrogen, thawed on ice and sonicated (3 x 20 sec on ice, full power). The bacterial lysate was ultracentrifuged (1 h, 20.000 rpm, 4 °C) and filtered using a 0.45 µm syringe filter.

The Cas9 protein was purified by nickel chromatography (HisTrap HP column, GE Healthcare, Sweden) using a gradient from binding buffer (20 mM trizma-base, 0.5 M NaCl, pH 7.4, 20 mM imidazole) to elution buffer (20 mM trizma-base, 0.5 M NaCl, pH 7.4, 0.5 M imidazole). Afterwards, the Cas9 containing fractions were concentrated with Amicon Ultra centrifugal filter units (MWCO=100 kDa, Millipore, USA). Finally, the protein solution was subjected to size exclusion chromatography (SEC) using an Äkta purifier system based on a P-900 solvent pump module, a UV-900 spectrophotometrical detector, a pH/C-900 conductivity module, a Frac-950 automated fractionator, a Superdex 200 size exclusion column and storage buffer (20 mM HEPES, 200 mM KCl, 10 mM $MgCl_2$, 1mM DTT) as solvent. The pooled fractions containing the Cas9 protein were combined, the amount of purified protein was quantified using a Nanodrop photometer (Thermo Scientific, USA) and an extinction coefficient of $\varepsilon/1.000 = 120$ $M^{-1}cm^{-1}$. The solution was snap-frozen and stored at -80 °C. Protein purity was analyzed on a Coomassie Brilliant Blue stained 10 % SDS-PAGE gel (Chapter 3.7 Supporting Information Figure 42A).

3.3.3 ATTO647N-labeling of Cas9 protein

Cas9 protein was diluted in HEPES (adjusted to pH 8.0 with 0.2 M sodium bicarbonate solution) to a concentration of 2 mg/mL. ATTO647N NHS-ester was solubilized in DMSO (10 mM) and a twofold molar excess of reactive dye were added to the protein solution. The mixture was incubated under constant stirring for 1 h at RT. Uncoupled dye was removed by size exclusion chromatography (Äkta purifier system GE Healthcare Bio-Sciences AB, Sweden) with a Superdex 200 size exclusion column using storage buffer (20 mM HEPES, 200 mM KCl, 10 mM MgCl$_2$, 1 mM DTT) as mobile phase. The pooled fractions containing the Cas9 protein were combined, the amount of purified protein was quantified using a Nanodrop photometer (Thermo Scientific, USA) and an extinction coefficient of $\varepsilon/1.000= 120$ M^{-1}cm^{-1}. The solution was snap-frozen and stored at -80 °C.

3.3.4 *In vitro* transcription of sgRNAs

The general sgRNA design was based on Larson et al.[240] Specific sgRNA sequences were derived from Qi et al. (sgGFP)[241] and Sun et al. (cgRNA).[232] The DNA template for the *in vitro* transcription of sgRNA was assembled from two single-stranded oligonucleotides with 21 nucleotide overhangs which were annealed and extended with T4 DNA polymerase (NEB, Germany). The template was purified using a QIAquick PCR Purification Kit (QIAGEN, Germany) and stored in RNase-free water. The linear DNA fragments containing the T7 promoter followed by the sgRNA sequence were analyzed on an agarose gel and transcribed *in vitro* using the HiScribeT7 High Yield RNA Synthesis Kit (NEB, Germany) according to the manufacturer's instructions.

ATTO488-labeled sgRNA was synthesized by substitution of 7 % of the UTPs with aminoallyl-UTP-ATTO488 (Jena Bioscience, Germany) during *in vitro* transcription. After transcription, 1 µL DNase was added and incubated for 15 min at 37 °C. The *in vitro* transcribed sgRNA was purified using the peqGOLD Mikro RNA kit (peqLab, Germany) according to the manufacturer's instructions. The purified sgRNA was heated to 80 °C for 2 min, directly snap frozen in liquid nitrogen and stored at -80 °C. Purity of the sgRNA was analyzed on a GelRed stained 10 % DNA-PAGE gel (Figure 42B).

ssDNA oligonucleotides for assembly of dsDNA templates:

F-sgGFP: 5´-GCGGCCTCTAATACGACTCACTATAGGACCAGGATGGG
             CACCACCCGTTTTAGAGCTAGAAATAGCA-3`

F-cgRNA: 5´-GCGGCCTCTAATACGACTCACTATAGGGTAACCGTGCGG
             TCGTACGTTTTAGAGCTAGAAATAGCA-3`

F-sgFolR1:   5´-TTCTAATACGACTCACTATAGAGGGTTTAACAAGTGCGCAG
             GTTTTAGAGCTAGA-3´

R-sgRNA: 5´-AAAAAAAGCACCGACTCGGTGCCACTTTTTCAAGTTGATAA
             CGGACTAGCCTTATTTTAACTTGCTATTTCTAGCTCTAAAAC-3´

sgRNA sequences after *in vitro* transcription:

sgGFP: 5´-GACCAGGATGGGCACCACCCGTTTTAGAGCTAGAAATAG
             CAAGTTAAAATAAGGCTAGTCCGTTATCAACTTGAAAAAGTG
             GCACCGAGTCGGTGCTTTTTTT-3´

cgRNA: 5´-GGGTAACCGTGCGGTCGTACGTTTTAGAGCTAGAAATAG
             CAAGTTAAAATAAGGCTAGTCCGTTATCAACTTGAAAAAGTG
             GCACCGAGTCGGTGCTTTTTTT-3´

sgFOLR1:   5´-GGGTTTAACAAGTGCGCAGTGTTTTAGAGCTAGAAATAG
             CAAGTTAAAATAAGGCTAGTCCGTTATCAACTTGAAAAAGTG
             GCACCGAGTCGGTGCTTTTTTT-3´

3.3.5 *In vitro* cleavage assay to test the RNP functionality

To confirm the functionality of Cas9 and sgRNA *in vitro*, 300 ng of a linearized plasmid or PCR amplicon containing the sgRNA target site was generated. The linear DNA fragment was then incubated with the precomplexed RNPs (150 ng Cas9 protein and 60 ng sgRNA)for 2 h at 37 °C. The reaction mixture was analyzed by agarose gel electrophoresis (1.5 % agarose gel). Due to the asymmetric location of the sgRNA-target sequence within the amplicon, successful cleavage by the Cas9/sgRNA complex results in two bands on the agarose gel(Figure 42C).

3.3.6 Cell culture

Neuro2a eGFP-Luc, HeLa eGFP-Tub and HeLa pLuc/705 cells were grown in DMEM medium supplemented with 10 % FBS, 100 U/mL penicillin and 100 µg/mL streptomycin. The cells were cultured in ventilated flasks in the cell incubator at 37 °C and 5 % CO_2 in a humidified atmosphere. Cells were passaged at approximately 80 % confluency.

3.3.7 Formulation of RNP oligomer complexes

To formulate RNP oligomer complexes, the indicated amount of Cas9 protein and sgRNA were mixed and pre-incubated for 15 min at RT. For the uptake studies, 20 % of the Cas9 protein was substituted by ATTO647N-Cas9 and 20 % of the sgRNA by ATTO488-sgRNA. The calculated amount of oligomer at the indicated lipo-nanoparticle (N/P) ratio was diluted in a separate tube (total volume 10 µL) in HBG buffer. After 15 min incubation of Cas9 and sgRNA, the RNP complex solution is diluted to a volume of 10 µL and added to the oligomer solution, mixed by pipetting and incubated for another 15 min at RT.

3.3.8   Cellular treatments under serum-free conditions

For an initial library screening, 5.000 Neuro2a eGFP-Luc cells per well were seeded into 96-well plates the day before cell treatment. 15 min prior the treatment, the full serum medium (DMEM containing 10 % FBS) was substituted by 80 µL fresh prewarmed serum-free medium. 20 µL of the RNP oligomer complexes formed as described above was added to each well. After 4 h of serum free incubation, 100 µL medium containing 20 % serum was added and the cells incubated for another 44 h. After 48 h total incubation time, the cells were transferred into 24-well plates and incubated for additional 72 h. All treatments were performed in triplicates. The knock out efficiency was determined by flow cytometry as the percentage of GFP negative cells after subtraction of unspecific GFP negative population in HBG treated cells. Data are presented as the mean value (± SD) of three independent measurements.

3.3.9   Cellular treatment under standard conditions

RNP lipo-nanoparticle treatments were performed in triplicates in 96-well plates. 5.000 cells were seeded per well 24 h prior transfection. On the next day, the medium was replaced by 80 µL fresh prewarmed medium containing 10 % FBS. The nanoparticles were prepared as described above and 20 µL of the transfection mix were added. After 48 h treatment, the cells were transferred into 24-well plates and further incubated for 72 h. The knock out efficiency was determined by flow cytometry as the percentage of GFP negative cells after subtraction of unspecific GFP negative population in HBG treated cells. Data are presented as the mean value (± SD) of three independent measurements. The relative cell number (%) was calculated relative to control wells treated with HBG as ([A] test/[A] control) × 100 %. Means are reported +/- standard deviation.

3.3.10 Particle size and zeta potential

Particle sizes and zeta potentials of Cas9/sgRNA ribonucleoprotein lipo-nanoparticles were determined by dynamic and electrophoretic light scattering in folded capillary cells (DTS 1070) using a Zetasizer Nano ZS (Malvern Instruments, UK). RNP lipo-nanoparticles containing 12.5 µg Cas9 protein and 2.5 µg sgRNA at N/P 24 were formed in 200 µL HBG. For size measurements, each sample was measured three times with 13 subruns at RT. For zeta potential measurements, the sample was diluted to 800 µL with 20 mM HEPES pH 7.4 buffer and measured three times with 10 to 15 subruns. Zeta potentials were calculated by the Smoluchowski equation.[242]

3.3.11 Fluorescence (cross-) correlation spectroscopy (FCS/FCCS)

The fluorescence correlation spectroscopy and dual-color fluorescence cross-correlation spectroscopy measurements (FCCS) were performed on a home-built microscope as described elsewhere.[243] A pulsed laser diode at 470-nm wavelength (LDH-P-C-470, Pico Quant) was used for excitation of the ATTO488 labeled sgRNA (ATTO488-sgRNA) and a pulsed laser diode at 635-nm (LDH-P-C-635b, Pico Quant) was used for excitation of the ATTO647N labeled Cas9 protein (ATTO647N-Cas9). Laser powers of ~ 4.5 µW for both the 470 and 635-nm lasers were used, measured at the sample with a slide power meter (S170C-Thorlabs). The measurements were performed using a 60x water immersion objective, NA 1.27 (Plan Apo 60 x WI, Nikon).

The correlation analyses were performed with our home written software PIE analysis with Matlab (PAM).[244] PAM is a stand-alone program (MATLAB; The Math Works GmbH) for integrated and robust analysis of fluorescence ensemble, single-molecule, and imaging data. The FCS data were acquired by recording the photons with a single APD on a time-correlated single-photon-counting card (TCSPC, SPC-150 Becker and Hickl) for a period of 15 minutes. The FCCS data were acquired by recording the detected photons of two single photon avalanche photodiodes (SPADs) on two separate but synchronized TCSPC cards for a period of 15 minutes. Measurements were conducted in HBG buffer for simulating physiological body conditions.

The autocorrelation functions (ACFs) were fit using a single or two-component model with a triplet fraction, assuming a 3D Gaussian focus shape.

$$G(\tau) = \frac{\gamma}{(A_1 + A_2)^2} \cdot \left[\left(A_1 \left(1 + \frac{4D_1 \cdot \tau}{\omega_r{}^2}\right)^{-1} \cdot \left(1 + \frac{4D_1 \cdot \tau}{\omega_z{}^2}\right)^{-\frac{1}{2}} \right) + \left(A_2 \left(1 + \frac{4D_2 \cdot \tau}{\omega_r{}^2}\right)^{-1} \cdot \left(1 + \frac{4D_2 \cdot \tau}{\omega_z{}^2}\right)^{-\frac{1}{2}} \right) \right]$$

$$\cdot \left[1 + \frac{T}{1-T} \cdot e^{\frac{\tau}{\tau_T}} \right]$$

where *A* is the size-weighted relative-amplitude of particles in the observation volume. The A_1 fraction refers to the unbound, freely diffusing labeled sgRNA or Cas9 protein, while A_2 corresponds to the RNP complex bound-labeled sgRNA or Cas9 protein. D_1 and D_2 refer to the respective diffusion coefficients of A_1 and A_2, respectively. The time delay of the autocorrelation is represented by τ. ω_r and ω_z are the lateral and axial focus sizes, respectively, defined as the distance from the focus center to the point where the signal intensity has decreased to $1/e^2$ of the maximum. The shape factor γ is $2^{-3/2}$ for a 3D Gaussian.

The triplet dynamics were accounted for by an additional factor, where *T* is the triplet fraction and τ_T is the triplet time constant. The fitting was used to extract the fraction of freely diffusing vs. complex bound ATTO488-sgRNA / ATTO647N-Cas9, in the absence and presence of the T-OHSteA oligomer. The unbound freely diffusing ATTO488-sgRNA and ATTO647N-Cas9 diffusion coefficients D_1 and D_2 were fixed in the fitting to the value of 56.0 and 18.2 μm^2/s, respectively, which was previously determined by measuring ATTO488-sgRNA and ATTO647N-Cas9 alone, respectively.

3.3.12 Flow cytometry

After the specified treatments, the cells were collected and resuspended in phosphate-buffered saline(PBS) buffer containing 10 % FBS (FACS buffer). All samples were analyzed by flow cytometry using a LSR Fortessa flow cytometer (Becton, Dickinson and Company Biosciences, Singapore). 1 ng/µL 4′,6-diamidino-2-phenylindole (DAPI) was added shortly before the measurement and used to discriminate between viable and dead cells. The cellular fluorescence was assayed by excitation of DAPI at 405 nm and detection of emission at 450 nm and the excitation of ATTO647N at 640 nm and detection of emission at 670 nm. ATTO488 as well as the cellular eGFP expression was assayed by excitation at 488 nm and the detection of emission at 530 nm. Only isolated viable cells were evaluated. Flow cytometry data were analyzed using FlowJo 7.6.5 flow cytometric analysis software by FlowJo, LLC (Becton, Dickinson and Company, USA). All experiments were performed in triplicates.

3.3.13 Confocal laser scanning microscopy (CLSM)

15.000 Neuro2a eGFP-Luc cells were seeded in 8 well-Ibidi µ-slides (Ibidi GmbH, Germany) in a total volume of 300 µL medium per well. Cells were incubated at 37 °C and 5 % CO_2. On the next day, the medium was replaced with 240 µL fresh medium. 60 µL of Cas9/sgRNA RNP (20 % ATTO647N labeled Cas9, 20 % ATTO488 labeled sgRNA) lipo-nanoparticles was added to each well resulting in a final concentration of 75 nM RNP complex. After 4 h, each well was washed twice with 300 µL PBS followed by a 20 min incubation on ice with 300 µLPBS containing 500 I.U./mL of heparin. The cells were washed twice with 300 µL PBS and subsequently fixed with 4 % paraformaldehyde in PBS (40 min incubation at RT). After fixation, each well was washed twice with 300 µL PBS, the cell nuclei were stained with DAPI (2 µg/mL) and F-actin was labeled with rhodamine-phalloidin (1 µg/mL). After 20 min of incubation (light protected at RT), the staining mixture was aspirated and replaced with 300 µL PBS per well.

Images were recorded with a Leica-TCS-SP8 confocal laser scanning microscope (CLSM) equipped with a HC PL APO 63x 1.4 objective (Germany). DAPI emission was recorded at 460 nm, ATTO488-sgRNA at 519nm, rhodamine at 580 nm and

ATTO647N-Cas9 at 665 nm. All images were processed using the LAS X software from Leica.

3.3.14 Erythrocyte leakage assay

EDTA-blood was washed with PBS buffer containing 25 mM sodium citrate. The washed erythrocyte suspension was centrifuged and the pellet was diluted to 5×10^7 erythrocytes per mL with PBS (pH 7.4, 6.5 and 5.5). A volume of 75 µL of erythrocyte suspension and 75 µL of oligomer solution (diluted with PBS at the respective pH) was added to each well of a V-bottom 96-well plate (NUNC, Denmark), resulting in the indicated oligomer concentration. The plates were incubated at 37 °C under constant shaking for 1 h. After centrifugation, 100 µL of the supernatant was analyzed for hemoglobin release by monitoring the absorption at 405 nm using a microplate reader (Spectrafluor Plus, Tecan Austria GmbH, Austria). PBS-treated erythrocytes were set to 0 %. Erythrocytes treated with 1 % (v/v) Triton X-100 (diluted with PBS at the respective pH) served as positive control and was set to 100 %. Data are presented as the mean value (± SD) of four independent measurements.

3.3.15 Folate receptor expression levels

To examine the folate receptor (FolR1) expression of the different cell lines, 500.000 cells were collected in 100 µL FACS buffer. For the detection of the FolR1, 5 µL allophycocyanin (APC)-conjugated α-FolR1 IgG$_1$ antibody was added and incubated on ice for 1 h. As a negative control, allophycocyanin (APC)-conjugated anti control IgG1 antibody with no specific target was used. After the incubation on ice, cells were washed twice with 1 mL FACS buffer, resuspended in 600 µL FACS buffer and analyzed by flow cytometry using a LSR Fortessa flow cytometer (BD Biosciences, Singapore). 1 ng/µL DAPI was added shortly before the measurement and used to discriminate between viable and dead cells. The amount of folic acid receptor positive cells was analyzed through excitation of the dye at 640 nm and detection of emission at 670 nm. Flow cytometry data were analyzed using FlowJo 7.6.5 flow cytometric analysis software by FlowJo, LLC (Becton, Dickinson and Company, USA).

3.3.16 DNA sequencing

Single cell clones were generated from treated cells as described above using limiting dilution method in 96-well plates. Genomic DNA of the isolated single cell clones was extracted by QIAamp® DNA Mini Kit (QIAGEN, Germany) following the manufacture's protocol. The target regions of eGFP or FolR1 gene were amplified with One*Taq*® DNA polymerase (NEB, Germany) using primers eGFP-F/eGFP-R or FolR1-F/FolR1-R. The amplicons were purified by gel extraction with QIAquick® Gel Extraction Kit (QIAGEN, Germany). Purified amplicons at concentrations of 10-30 ng/μL were sequenced by Eurofins GATC Biotech (Germany) with primer eGFP-S or FolR1-R.Sequences of the Primers can be found in the Supporting Information.

PCR and sequencing primer sequences:

eGFP-F: 5'-GGTGAGCAAGGGCGAGGAGCTGTTCAC-3'

eGFP-R: 5'-GCGGTCACGAACTCCAGCAGGACCATG-3'

FolR1-F: 5'-GACCATGGAGCAGGAACC-3'

FolR1-R: 5'-CAGCTCCAGTTCTATTCGG-3'

eGFP-S: 5'-TCGGCCATGATATAGACGTT-3'

3.3.17 Statistical analysis

Data were analyzed with GraphPad prism 5. The statistical significance of experiments was determined using the two-tailed student's t-tests, *** $p \leq 0.001$, ** $p \leq 0.01$, * $p \leq 0.05$.

3.4   Results and Discussion

3.4.1   Lead structure identification

To assess the general potential of oligo(ethylenamino) amides (OAAs) for Cas9/sgRNA RNP delivery, a first library screen was conducted. Sequence-defined OAAs with different architectures and structural motifs were selected, which showed efficient intracellular delivery of other cargos such as small interfering RNA (siRNA), plasmid DNA (pDNA) and proteins in previous studies.[101, 152, 159, 238] GFP reporter gene was used as read-out to assess the knock-out efficiency for the identification of the best performing structures. Neuro2a eGFP-Luc cells were treated with Cas9/sgRNA RNP formulations for 4 h without serum. Subsequently, serum was added and cells were incubated for additional 44 h. All samples were analyzed by flow cytometry 3-4 days after the cell treatment. As expected, the bare RNP complex did not induce substantial GFP knock out (Figure 36). Commercially available lipofectamine 3000 (LF 3) achieved reporter gene knock out of approximately 11 % at higher concentrations, while succinylated polyethyleneimine (PEI-Suc)[245] increased knock out levels to 15 %. Sequence-defined OAAs with comb-like architecture, which initially were designed as efficient pDNA delivery agents[159] did not induce significant GFP knock-out with Cas9/sgRNA. In contrast, branched 3- and 4-arm OAAs exhibited distinct Cas9/sgRNA delivery efficiency. In case of 3-arm OAAs, the introduction of hydrophobic tyrosine tripeptide motifs strongly improved the GFP knock out efficiency from 2 % (Stp-H-C) to 18 % (Stp-H-Y3-C). A 4-arm OAA (Sph-H-C) based on the artificial oligoamino acid succinyl-pentaethylene hexamine (Sph) mediated 23 % GFP knock out. A substitution of Sph with the shorter oligoamino acid glutaryl-triethylene tetramine (Gtt-H-C) eliminated the delivery efficiency completely which shows the critical impact of slight structural variations and optimal composition. The highest Cas9/sgRNA delivery potency and approximately 28 % GFP knock out was observed with a lipid-modified T-shape structure (T-OleA) containing the cationizable oligoamino acid stuccinyl-tetraethylene pentamine (Stp), oleic acid and stabilizing tyrosine trimers.[166] The same oligomer did not induce any reduction of GFP expression with Cas9/cgRNA RNP containing a control guide RNA (cgRNA) without specific target in the genome, which confirms the sequence specific GFP knock out.
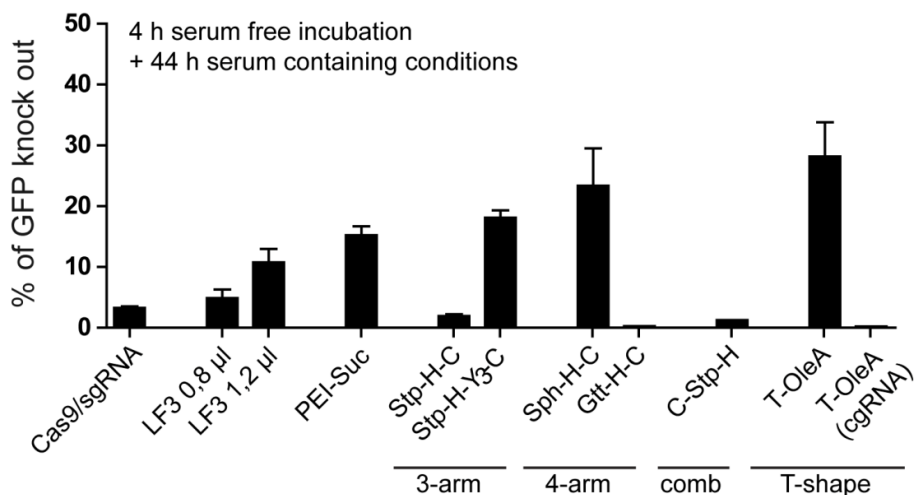
Figure 36: GFP knock out efficiency results of the oligomer library screening. The percentage of GFP knock out in Neuro2a eGFP-Luc cells was determined by FACS analysis 7 days after treatment with RNP OAA nanoparticles containing representatives of oligomer groups with different functional motifs and architectures. Naked Cas9/sgRNA complex (75 nM Cas9 protein and 150 nM sgRNA) without OAA serves as negative control. RNP complex formulated with Lipofectamine 3000 (LF3) served as a positive control. The polymeric PEI-Suc as well as 3-arm, 4-arm, comb- and T-shape structures with different functional units were compared in terms of knock out efficiency. Cas9 protein complexed with control guide RNA (cgRNA) with no specific target served as negative control. Detailed sequence information can be found in the supporting information table S1. The samples were normalized to HBG treated cells. Transfections were performed under serum free conditions (4h serum-free followed by 44 h serum containing conditions). Data are presented as mean ± SD (n=3).

3.4.2 Lipid variation

The initial library screen had identified the T-shape oligomer T-OleA as the best-performing structure for Cas9/sgRNA RNP delivery (Figure 36). The fatty acids in the delivery system are suggested to boost intracellular delivery by hydrophobic nanoparticle stabilization as well as endosomal membrane interaction and release.[163, 246-247] Based on the promising results obtained with T-OleA, which contains the unsaturated C18 fatty acid oleic acid (OleA), different T-shape lipo-OAAs with fatty acid variations were screened (Figure 37). We recently reported that the degree of unsaturation of the fatty acid moiety critically impacts the delivery of phosphorodiamidate morpholino oligomers (PMOs).[165] Analogs of T-OleA containing saturated stearic acid, bis-unsaturated linoleic acid (LinA), 8-nonanamidooctanoic acid (NonOcA) and hydroxystearic acid (OHSteA) instead of oleic acid were

synthesized (Figure 37A). To determine the influence of the fatty acid variation, Neuro2a eGFP-Luc cells were incubated with Cas9/sgRNA RNP formulations for 48 h in serum-containing medium (Figure 37B). As expected, the bare RNP complex did not induce GFP knock out. In presence of serum, which represent more challenging conditions compared to the initial library screen, neither saturated T-SteA, nor the mono-unsaturated T-OleA resulted in significant GFP knock out. In contrast, bis-unsaturated T-LinA and T-NonOcA increased the GFP knock out efficiency to around 12 % or 7 %, respectively. Notably, the hydroxylated T-OHSteA mediated the highest GFP knock out of 40 % after the single Cas9/sgRNA treatment. The cell number after the treatments with the lipo-nanoparticles was determined as a measure for nanoparticle toxicity (Figure 37C). All lipo-nanoparticles were generally well tolerated with T-NonOcA exhibiting the highest effect on the cell number.
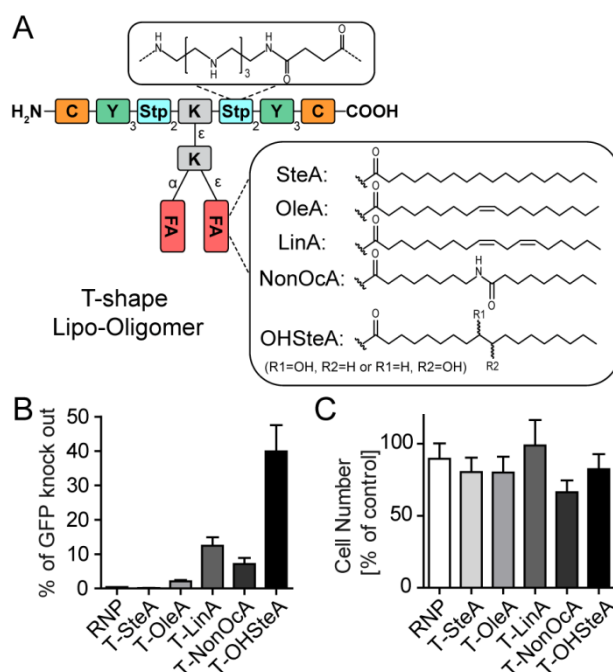
Figure 37: Lipid variation. (A) A schematic illustration of T-shape OAAs with different fatty acids (FA). SteA: stearic acid; OleA: oleic acid; LinA: linoleic acid; NonOcA: nonanamidooctanoic acid; OHSteA: hydroxystearic acid; Stp: succinyl-tetraethylene pentamine. (B) GFP knock out efficiency determined by flow cytometry and (C) cell number of Neuro2a eGFP-Luc cells 3-4 d after the 48 h treatment with 75 nM RNP lipo-nanoparticles (N/P 24) targeting the eGFP gene. Cells were normalized to HBG buffer treated cells. RNP complex without lipo-OAA served as negative control. Data are presented as mean ± SD (n = 3).

3.4.3 Impact of lipid on nanoparticle formation and membrane interaction

The lipo-nanoparticles, which were formed from T-shape lipo-OAAs containing the different lipid variations and the RNP complex, were further characterized in terms of their physicochemical properties, since they can significantly impact the *in vitro* and *in vivo* characteristics of a carrier system.[248-249] The nanoparticle size, polydispersity and the zeta potential were determined by DLS (Figure 38A-C). Lipo-nanoparticles containing Cas9/sgRNA and the saturated (T-SteA), mono- (T-OleA) and bis-unsaturated fatty acids (T-LinA) or the amide-lipid (T-NonOcA) displayed hydrodynamic sizes of 247-293 nm, whereas the more hydrophilic hydroxylated T-OHSteA counterpart produced significantly smaller nanoparticles with a z-average of 168 nm (Figure 38A). The polydispersity index (PDI) as a measure for the homogeneity of the particle population (Figure 38B), also suggested more homogenous nanoparticle formation with T-OHSteA (PDI 0.24) compared to the other four oligomers (PDI 0.45-0.56). The zeta potential of all lipo-nanoparticles ranged from +15 to +18 mV (Figure 2C), suggesting positive surface charges which are beneficial for cellular uptake via electrostatic interactions.[250]

The intracellular delivery of the Cas9/sgRNA complex formulations into Neuro2a cells was determined by confocal laser scanning microscopy (CLSM, Figure 38D). To investigate the uptake of both RNP components individually, the Cas9 protein and the sgRNA were labeled with fluorescent dyes ATTO647N and ATTO488, respectively. While cellular internalization of the Cas9 protein (top images, red channel) was observed for both formulated (RNP+T-OHSteA) as well as bare RNP complexes (RNP), intracellular sgRNA was only detected in combination with the lipo-OAA (middle images, green channel).A possible explanation for this observation is the stabilization and protection of single stranded RNA by complexation and encapsulation in the carrier system.[229] Importantly, these data show that only the lipo-nanoparticles mediate co-delivery of both functional RNP components, which are essential for genome editing activity.

The lipid modification of the T-shape lipo-OAA was shown to have a major impact on GFP knock out efficiency (Figure 37). To investigate a possible explanation for the importance of suitable lipid modification, lipo-nanoparticle uptake into Neuro2a cells was determined by flow cytometry (Figure 38E). The mono-unsaturated T-OleA and hydroxylated T-OHSteA mediated the highest levels of cellular internalization, while

all other screened compounds were inferior. Since no distinct difference between the T-OleA and T-OHSteA was observed, the superiority of T-OHSteA in terms of GFP reporter gene knock out cannot only be explained by a higher cellular uptake. Inadequate endosomal escape has often been identified as a key bottleneck in cellular delivery of biomolecules.[229, 251-252] Since the conducted cellular uptake study does not identify the intracellular localization and, in particular, does not differentiate between the endolysosomal or cytosolic compartment, the advantage of T-OHSteA lipid nanoparticles might be related to a superior endosomal release. The amphiphilic character of the lipid modified cationic oligomer provides the potential of lytic membrane interactions. Previous nucleic acids studies have shown that unsaturated fatty acids can enhance pH-dependent membrane lysis and thereby endosomal escape.[113, 166, 238] Erythrocyte leakage assays were carried out to assess the pH-dependent membrane interaction of lipo-OAAs.

The T-shape oligomers with different fatty acids were incubated with erythrocytes at physiological pH 7.4 as well as endolysosomal pH of 6.5 or 5.5. The results (Figure 38F) indicate increasing erythrocyte leakage at pH 5.5 with an increasing number of double bonds, which is consistent with previous findings.[113, 165] Highest lytic activities were observed for lipo-OAAs containing bis-unsaturated linoleic acid and hydroxy stearic acid. Comparing the lipo-OAA containing SteA and the hydroxylated version of this fatty acid (OHSteA), it is clearly visible that the fatty acid hydroxylation has an enormous effect on the lytic potential. C*is*-unsaturated fatty acids are suggested to affect the phase behavior and fluidity of biomembranes,[163, 253-254] which explains the higher lytic activity of T-OleA and T-LinA compared to T-SteA.[164] It can be speculated that the bulky hydroxyl group (-HC-OH)in OH-SteA results in a similarly sterically favored angled conformation of hydroxy-stearic acid compared to constrained *cis*-unsaturated bonds. The enhanced pH-dependent membrane lysis indicates beneficial effects on cell tolerability at neutral pH and promotes increased endosomal escape due to vesicular acidification.

Summing up, the beneficial effect of the RNP T-OHSteA formulation is suggested to rely on a combination of effects on defined particle formation (smallest z-average, lowest PDI), enhanced cellular uptake as well as a better endosomal escape due to the favorable lytic interaction with membranes at acidic pH.
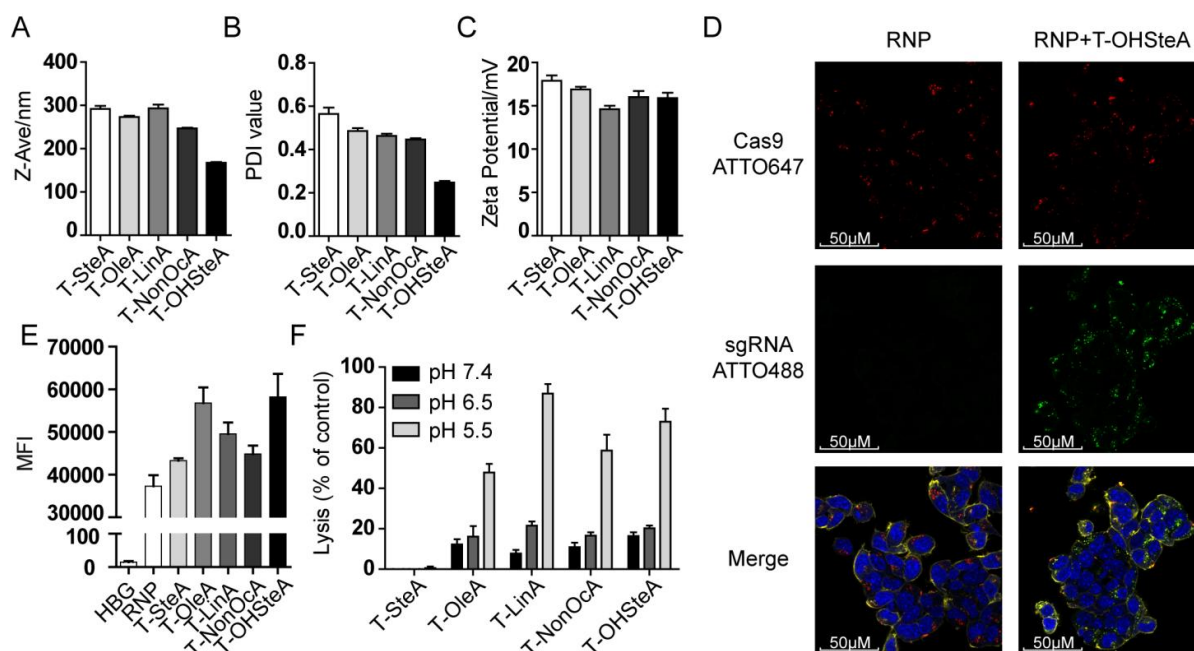
Figure 38: Impact of lipid modification on particle formation (A-C), cellular uptake (D-E) and membrane interaction (F). (A) Particle size (z-average) in nm, (B) polydispersity index (PDI) and (C) zeta potential in mV of 75nM Cas9/sgRNA solutions complexed with different lipo-OAAs at N/P 24. Particles were formed in HBG and three technical replicas were measured. (D) CLSM images of Neuro2a cells treated for 4 h with 75 nM Cas9/sgRNA RNP (Cas9:sgRNA 1:1, 20 % ATTO647N-labeled Cas9 protein, 20 % ATTO488-labeled sgRNA) with (right) or without (left) encapsulation into T-OHSteA at N/P 24. Additional data of the full set of all RNP lipo-nanoparticles can be found in in chapter 3.7 Supporting Information Figure 43. (E) The cellular ATTO647N-Cas9 fluorescence intensity determined by flow cytometry (median fluorescence intensity, MFI, $n = 3$) is shown. (F) Erythrocyte leakage assays by photometrical determination of hemoglobin that was released from 3.75×10^6 erythrocytes after 60 min incubation with 2.5 µM lipo-OAA at pH 7.4, 6.5 or 5.5. Values were normalized to positive control samples treated with 1 % (v/v) Triton X-100 (100 % lysis). Data are presented as mean ± SD ($n = 4$).

3.4.4   RNP complex formulation

GFP knock out efficiency studies (Figure 37) as well as cellular internalization experiments (Figure 38) identified the lipo-OAA T-OHSteA as the best performing structure in terms of RNP delivery. To further characterize RNP complex formulation and optimal composition, dose-titration experiments with varying RNP complex concentrations, varied Cas9 protein to sgRNA molar ratios as well as lipo-OAA nitrogen to sgRNA phosphate (N/P) ratios were performed in two reporter cell lines (Figure 39).

First, nanoparticles were formed at a fixed N/P ratio of 24. The concentration of the RNP complex in Neuro2a eGFP-Luc and HeLa GFP-Tub treatments ranged between 1 nM to 100 nM. RNP compositions of Cas9 protein to sgGFP of 1:1 (green line) and 1:2 (blue line) were applied (Figure 39A and B). In treatments of Neuro2a eGFP-Luc cells with Cas9/sgRNA RNPs at a ratio of 1:1, the GFP knock out increased with RNP concentration between 1 to 75 nM and did not improve further at the higher concentration of 100 nM (Figure 39A). In case of particles containing Cas9:sgGFP RNPs at a ratio of 1:2, the treatment with 50 nM RNP complex mediated the highest GFP knock out levels, suggesting it as the optimal concentration. Overall, differences between the Cas9/sgRNA composition ratios 1:1 or 1:2 were minor in treatments of Neuro2a eGFP-Luc cells. In contrast, treatments of HeLa GFP-Tub reporter cells resulted in a slightly different observation (Figure 39B); at both ratios the GFP knock out efficiency increases with increasing RNP concentration up to 50 nM; maximal knock out levels were reached at 50 nM with RNPs at 1:1 ratio and already at 25 nM with RNPs at 1:2 ratio. While the knock out efficiency with Cas9/sgGFP RNPs at 1:1 ratio did not decrease dramatically at higher concentrations, at 1:2 ratio it dropped to low levels at concentrations > 50 nM of RNP. The abrupt decrease of the GFP knock out efficiency could be attributed to an increased toxicity due to the double lipo-OAA concentration in case of RNPs at 1:2 ratio (Chapter 3.7 Supporting Information Figure 44). Overall, single treatments of HeLa GFP-Tub cells with both Cas9/sgGFP T-OHSteA formulations resulted in remarkably high GFP knock out levels of over 89 %. However, it has to be mentioned that the GFP fusion to tubulin in HeLa GFP-Tub cells could negatively affect proliferation which in turn could favor growth of knock out populations.

Additionally, nanoparticles were formed at different N/P ratios (Figure 39C and D). Two different lipo-OAA concentrations were kept constant and RNP levels were gradually increased. On Neuro2a eGFP-Luc cells, lipo-OAA concentrations of 9.5 µM (red line) and 14.3 µM (black line, Figure 39C) were used. GFP knock out efficiencies could be steadily improved by decreasing the N/P ratio, with a maximal effect at N/P 24 for both concentrations (indicated by arrows). Due to the higher overall GFP knock out levels on HeLa GFP-Tub cells (Figure 39B), lower lipo-OAA concentrations of 4.8 µM (blue line) and 9.5 µM (red line, Figure 39D) were chosen for this cell line. At a concentration of 4.8 µM lipo-OAA, the successive addition of RNP complex resulting

in N/P ratios of 12 increased GFP knock out levels. At lower N/P ratios the knock out efficiency dropped indicating the requirement for an optimal lipo-OAA ratio. At 9.5 µM, the transfection efficiency increased steadily to an N/P ratio of 24, where a plateau was reached. Based on these observations, an N/P ratio of 24 in Cas9/sgRNA T-OHSteA complexes was considered optimal.

To assess the RNP delivery potential of T-OHSteA at the determined formulation conditions, the delivery system was compared to other reagents in term of GFP knock out efficiency (Figure 39E). Classical transfection reagents such as succinylated polyethylenimine (PEI-Suc), linear polyethylenimine (linPEI) as well as Lipofectamine CRISPRMAX (LF CM), a commercially available reagent for Cas9/sgRNA RNP transfections, were evaluated in Neuro2a eGFP-Luc cells side-by-side with T-OHSteA. The PEI derivatives were used at published optimal polymer:nucleic ratios (linPEI 0.8 w/w, PEI-Suc 4 w/w).[245] In case of lipofectamine, four different procedures (LF CM1 to 4) with different concentrations and mixing procedures were included for a reliable comparison under the conditions suggested by the manufacturer as well as the parameters of lipo-OAA formulations. The cationizable PEI-polymers, which are known to mediate efficient intracellular delivery of nucleic acids like siRNA and pDNA,[99, 245, 255] were not able to mediate distinct effects on the GFP expression levels. The cationic lipid Lipofectamine, an otherwise potent transfection reagent, only showed up to 7 % GFP knock out at concentrations and mixing procedures suggested by the manufacturer (LF CM1 and CM2) as well as at the same concentrations used for the RNP T-OHSteA formulations (LF CM3 and CM4). In the side-by-side comparison, the Cas9/sgRNA RNP formulation containing lipo-OAA T-OHSteA outperformed all other reagents mediating highest knock out levels of 38 %.

Successful gene knock out was additionally verified on genomic level (Figure 39F). After 48 h treatment of Neuro2a eGFP-Luc cells with 75 nM RNP complexed with T-OHSteA at N/P 24, cells were diluted to generate monoclonal cell populations from single cells. 29 of the 70 monoclonal cell populations showed a complete loss of GFP expression (determined by flow cytometry), matching the knock out efficiency of previous knock out experiments. The genomic DNA of the cell populations was harvested, target region of the GFP gene amplified by PCR and analyzed by

sequencing. Figure 39F illustrates exemplary insertions and deletions (INDELS) at the expected site of the sgGFP target sequence.
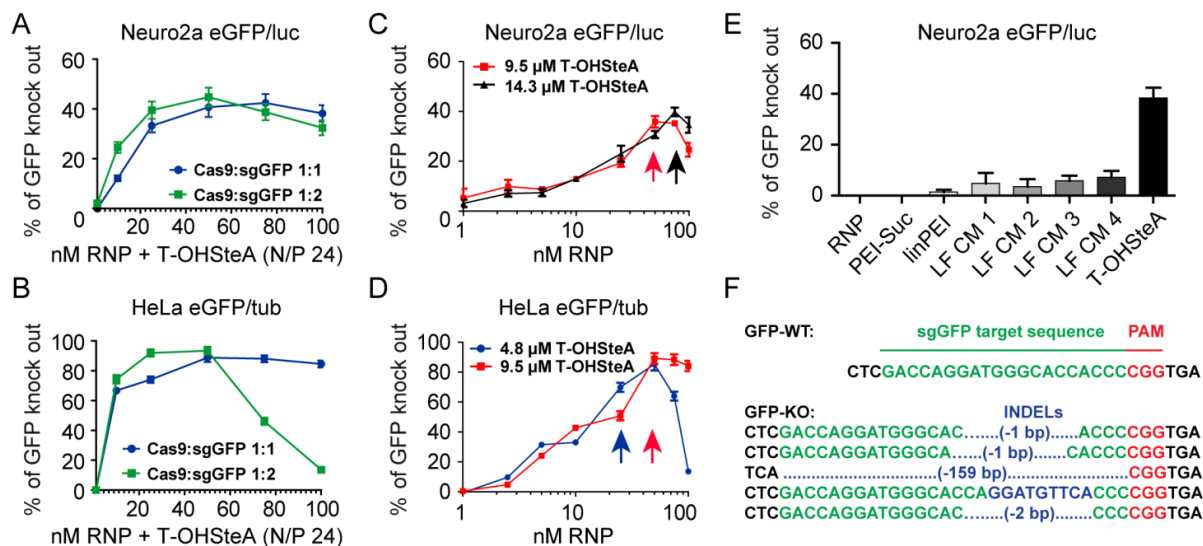
Figure 39: Dose-titration and characterization of RNP T-OHSteA formulations. (A,B) Dose-titration experiment in Neuro2a eGFP-Luc (A) or HeLa GFP-Tub (B) cells treated with 1-100 nM Cas9/sgRNA RNP complex at a 1:1 (blue) or 1:2 (green) ratio formulated with T-OHSteA at N/P 24. (C) N/P variation in Neuro2a eGFP-Luc cells by keeping T-OHSteA concentration constant (red curve: 9.5 µM; black curve: 14.3 µM) and varying the amount of RNP complex (in nM) at a 1:1 ratio. Arrows of the same color indicate an N/P of 24. (D) N/P variation experiment in HeLa GFP-Tub cells by keeping T-OHSteA concentration constant (blue curve: 4.8 µM; red curve: 9.5 µM) and varying amount of RNP complex at a 1:1 ratio. Arrows of the same color indicate an N/P of 24. (E) Comparison of RNP T-OHSteA formulations with established transfection reagents in terms of knock out efficiency. RNP complex without carrier served as negative control. Established transfection reagents included succinylated polyethylenimine (PEI-Suc) at a w/w ratio of 4, linear polyethylenimine (linPEI) at w/w 0.8 of polymer to sgRNA. Lipofectamine CRISPRMAX (LF CM) was tested at three different concentrations and with two different mixing procedures. LF CM 1 (6 nM RNP) and 2 (15 nM RNP) and 3 (75 nM RNP) were prepared as recommended by the manufacturer. LF CM 4 (75 nM RNP) as well as T-OHSteA (75 nM RNP) were mixed according to the protocol for formulation of RNP lipo-OAA formulations. All data points indicate the % knock out efficiency 3-4 d after a 48 h treatment in presence of 10 % FBS. The % of GFP knock out was normalized to HBG buffer treated cells. Data are presented as mean ± SD (*n* = 3). (F) Sequencing of monoclonal GFP knock out cells. The green sequence indicates the sgRNA target sequence in the eGFP gene next to the protospacer adjacent motive (PAM) sequence in red. Insertions and deletions caused by the DNA repair mechanisms after the Cas9 induced double strand break are highlighted in blue.

In view of addressing the interaction between sgRNA and Cas9, i.e. the RNP complex formation, and the RNP interaction with the T-OHSteA oligomer, fluorescence correlation spectroscopy (FCS) was used (Figure 40). FCS records and analyzes the intensity fluctuations through a small (≈fL) observation volume, caused by the diffusion of fluorescent particles in and out of this observation volume. From the temporal autocorrelation function (ACF) of the signal, a slower diffusion coefficient due to the building of complexes causes a shift in the temporal ACF to slower timescales.[212-213, 256] The diffusion of the single-labeled ATTO647N-Cas9 (18.2 μm^2/s) and ATTO488-sgRNA (56.0 μm^2/s) corresponds to their individual molecular weights and confirms the presence of a monomolecular species in solution (Figure 40A and B, light blue curves), (Chapter 3.7 Supporting Information Table 4 and Table 5).

Addition of the positively charged oligomer T-OHSteA to the Cas9 protein does not mediate a shift toward higher time lag τ, which indicates the absence of strong interactions between the two components (Figure 40A, orange curve). In contrast, the addition of T-OHSteA to sgRNA shows a strong shift of the autocorrelation function towards a higher time lag τ due to formation of an RNA polyplex (Figure 40B, orange curve). The appearance of a slowly diffusing component (4.02 μm^2/s) is a further indication of the RNA polyplex formation (Chapter 3.7 Supporting Information Table 4). Similarly, the mixture of sgRNA and Cas9 protein shows species with slower diffusion in both channels (~1.5 μm^2/s), suggesting the formation of Cas9/sgRNA RNP complexes (Figure 40A and B, yellow curves), (Chapter 3.7 Supporting Information Table 4 and Table 5).

Additionally, we performed fluorescence cross-correlation spectroscopy (FCCS) experiments, a dual-color extension of standard FCS.[257-258] Here, the temporal cross-correlation functions (CCFs) between the detection channels for the two fluorescently labeled ATTO647N-Cas9 and ATTO488-sgRNA proteins were analyzed. In FCCS, a cross-correlation signal is only present in the case of concerted motion of the different labels, i.e. the formation of an RNP complex. Thus, not only the temporal decay of the CCF is changed upon binding, but also the amplitude, making it much more sensitive as compared to standard FCS.[257]

The interaction of Cas9 and sgRNA and thus RNP formation is confirmed by the cross correlation of the two differently labeled components (Figure 40C, orange curve). The addition of T-OHSteA to Cas9/sgRNA RNPs results in a slightly faster diffusion coefficient, suggesting the reassembly or compaction of the RNP complexes, upon the addition of the highly positive oligomers (Figure 40A and B, purple curve). This compaction is better observable in the CCF (Figure 40C, absence vs. presence of T-OHSteA), where the diffusion coefficients of the RNP complex in the presence (~0.5 µm2/s) and the absence (~1 µm2/s) of the T-OHSteA shows the compaction resulting in a twice faster diffusion. Importantly, the addition of cationic T-OHSteA does not seem to disrupt the RNPs by detachment of sgRNA from the Cas9 protein, since the relative cross-correlation amplitude does not decrease but actually increases slightly upon addition of the oligomer (Figure 40C).
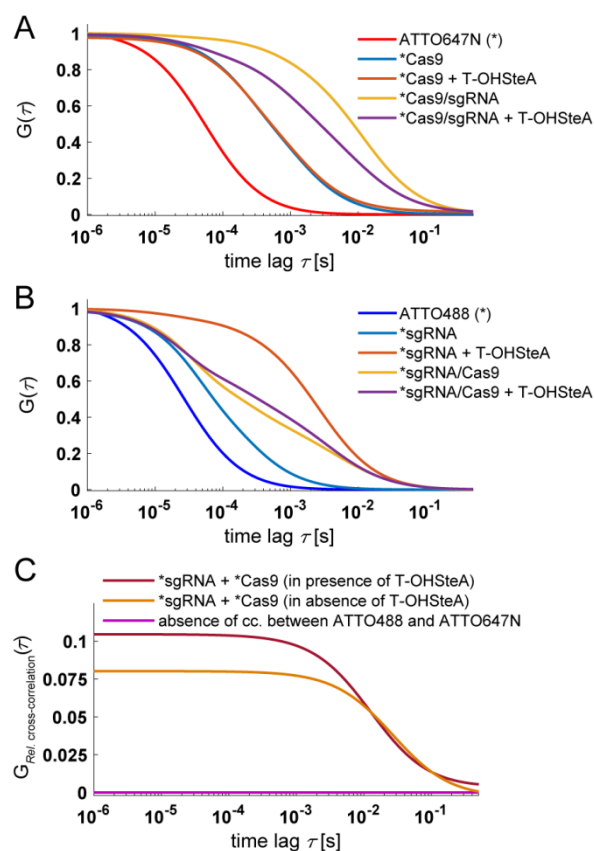
Figure 40: Interactions between sgRNA, Cas9 and T-OHSteA monitored by fluorescence (cross) correlation spectroscopy FCS (FCCS). (A) Autocorrelation function (ACF) of 100 nM ATTO647N-Cas9 showing its interaction with 100 nM ATTO488-sgRNA and 19 µM T-OHSteA (corresponding to N/P 24). The ATTO647N ACF is shown as a reference for a freely diffusing fluorophore. Note that the orange curve is largely overlapping the blue curve. (*) indicates the fluorescent species which is detected (red channel). (B) ACF of 100 nM ATTO488-sgRNA showing its interaction with 100 nM ATTO647N-Cas9 and 19 µM T-OHSteA (corresponding to N/P 24). The ATTO488 ACF is shown as a reference for a freely diffusing fluorophore. The slower decay of the ACFs represented by the shift towards higher time lag τ, indicates a slower diffusion and an increase in the hydrodynamic size due to the complex formation. (*) indicates the fluorescent species which is detected (green channel). (C) Relative cross-correlation (obtained by the division of the CCF amplitude by the ACF amplitude of the ATTO647N-Cas9) between 100 nM ATTO647N-Cas9 and 100 nM ATTO488-sgRNA in the presence (red) or absence (orange) of 19 µM T-OHSteA (corresponding to N/P 24). A mixture of ATTO647N and ATTO488 served as a reference showing the absence of any cross-correlation between the freely diffusing fluorophores (pink curve). The lines represent the obtained fit for the data points represented as dots. (*) indicates the fluorescent species which are detected (red and green channel).

Knock out of an endogenous gene

The delivery system based on lipo-OAA T-OHSteA, the Cas9 protein and sgGFP was optimized to facilitate the knock out of a GFP gene construct in two artificial reporter cell lines (Figure 37 and Figure 39). To verify that this delivery system can mediate knock out of an endogenous gene, a sgRNA targeting the folate receptor 1 gene (sgFolR1) was loaded into the Cas9-protein and complexed with the carrier system (Figure 41). Lipo-nanoparticles were formed with T-OHSteA and either Cas9/sgFolR1 or Cas9/cgRNA with no specific target in the genome. Folate receptor 1 (FolR1) negative Neuro2a cells and FolR1 positive HeLa cells were incubated with HBG or the RNP containing delivery systems at 25 nM, 50 nM and 75 nM (Figure 41A). The FolR1 status upon incubation was assessed by flow cytometry after treatment of cells with an allophycocyanin (APC)-conjugated antibody (FolR1-AB). FolR1 negative Neuro2a cells, which do not express the FolR1, served as a negative control and could not be stained with the FolR1-AB upon treatment with HBG. As a second negative control for unspecific background fluorescence, FolR1 positive HeLa cells were treated with HBG and subsequently incubated with a control antibody (Ctrl-AB). As a positive control, HeLa cells were treated with HBG and stained with Fol1R-AB. At all concentrations, the FolR1 status was clearly positive. Upon incubation of HeLa cells with Cas9/cgRNA, no FolR1 knock out could be detected. In contrast, HeLa cells treated with Cas9/sgRNA showed partial knock out of the endogenous receptor. The FolR1 knock out efficiency of HeLa cells treated with Cas9/sgRNA were quantified (Figure 41B). At all concentrations, FolR1 knock out levels of around 30 % could be detected.

The knock out of the FolR1 gene was additionally confirmed on the genomic level (Figure 41C). After 48 h treatment of HeLa cells with the carrier systems containing 75 nM RNP and T-OHSteA at N/P 24, cells were single cell diluted into 96-well plates to generate monoclonal selected cell lines. After continued cultivation, the genomic DNA of the cell populations was harvested, the FolR1 sequences amplified and analyzed by sequencing. Figure 41C indicates the insertions and deletions (INDELS) introduced due to cell repair mechanisms.
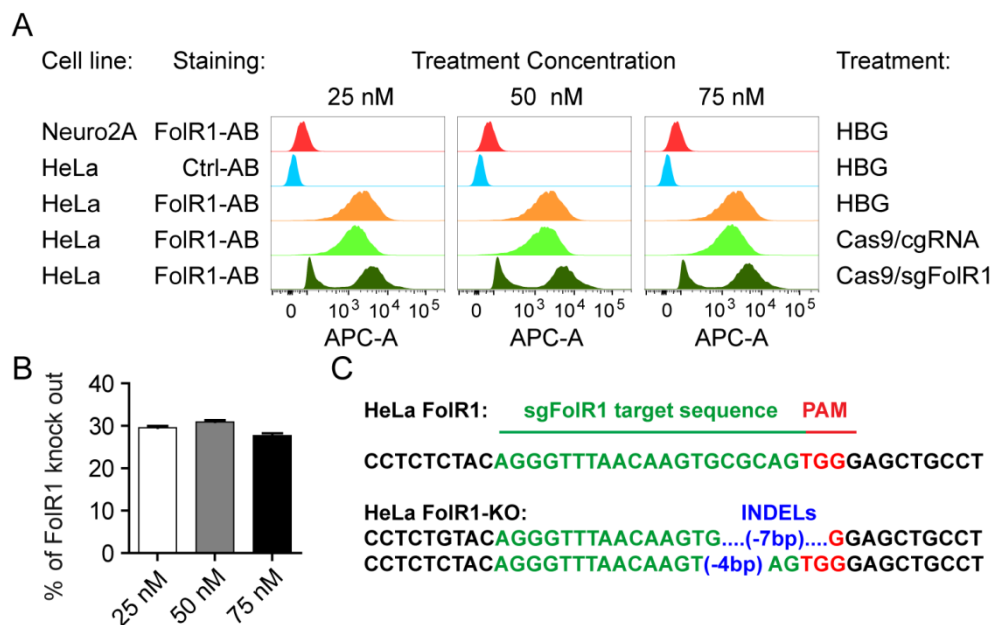
Figure 41: Knock out of the endogenous folate receptor 1 (FolR1). (A) Histograms showing the FolR1 expression of Neuro2a (FolR1 negative cell line) and HeLa (FolR1 positive cell line) cells after 48 h treatment with HBG buffer, Cas9/cgRNA with no specific target in the genome or Cas9/sgFolR1 targeting the endogenous folate receptor 1 gene. Cells were treated with three different RNP concentrations (25, 50, 75 nM RNP) complexed with T-OHSteA at N/P 24. Read out was performed by flow cytometry 7 d after the treatment. For the detection of the folate receptor status, cells were treated with an allophycocyanin (APC)-conjugated antibody against the folate receptor. As a negative control, an (APC)-conjugated anti control antibody with no specific target was used. (B) Quantification of the FolR1 knock out efficiency in %. Cells were normalized to HBG treated cells. Data are presented as mean ± SD ($n = 3$). (C) Sequencing of monoclonal FolR1 knock out cells. Green sequences indicate the sgRNA target sequence in the FolR1 gene next to the protospacer adjacent motive (PAM) sequence in red. Insertions and deletions (INDELS) caused by the DNA repair mechanisms after the Cas9 induced double strand break are highlighted in blue.

3.5   Conclusion

In this study, a novel delivery platform for the delivery of Cas9 protein/sgRNA RNP complexes was developed. Different lipo-oligomers were used to incorporate the Cas9 protein and different sgRNAs into cationic lipo-OAA nanoparticles. Lipo-OAAs were varied in terms of their fatty acid domains. Structures containing the saturated stearic acid were screened side-by-side to mono- or bis-unsaturated as well as amide-functionalized and hydroxylated lipid moieties. The T-shape lipo-OAA T-OHSteA was identified as the best-performing structure, and the hydroxylation of the contained fatty acid changed the properties and relevant parameters dramatically; the cationic lipo-OAA complexes with Cas9/sgRNA were smaller and more defined, exhibited higher cellular uptake and higher membrane lytic potential. T-OHSteA facilitated efficient intracellular delivery of the RNP complex and GFP gene knock out efficiencies up to 40 % on Neuro2a eGFP-Luc and up to 89 % on HeLa GFP-Tub cells, respectively. Additionally, knock out of the endogenous FolR1 gene coding for the folate receptor 1 could be demonstrated in HeLa cells. Overall, the reported lipo-nanoparticles hold great potential for genome editing applications and will be further optimized to target genes for therapeutic applications *in vivo.*

3.6   Acknowledgements

3.7 Supporting information figures and tables

Table 3: Summary of synthesized oligoamino amide sequences with different topologies.

ID	Type	Sequence	Abbreviation	Reference
PEI-Suc	Polymer	PEI-Suc 10 %	-	Zintchenko et al.[245]
689	*3-arm*	C-H-(Stp-H)$_3$-K-[H-(Stp-H)$_3$-C]$_2$	Stp-H-C	Kos et al.[162]
849	*3-arm*	C-Y$_3$-H-(Stp-H)$_3$-K-[H-(Stp-H)$_3$-Y$_3$-C]$_2$	Stp-H-Y3-C	Levacic et al.[259]
784	*4-arm*	K-K-[H-K-(H-Sph-K)$_3$-H-C)$_2$]$_2$	Sph-H-C	Beckert et al.[158]
577	*4-arm*	A-K-(H-K-(H-Gtt-H-Gtt-H-Gtt-H-C)$_2$)$_2$	Gtt-H-C	Lächelt et al.[197]
552	*Comb*	C-[K-(Stp)-H]$_8$-C	C-Stp-H	Scholz et al.[159]
454	*T-shape*	C-Y$_3$-Stp$_2$-K(K-OleA$_2$)-Stp$_2$-Y$_3$-C	T-OleA	Troiber et al.[166]
1104	*T-shape*	C-Y$_3$-Stp$_2$-K(K-NonOcA$_2$)-Stp$_2$-Y$_3$-C	T-NonOcA	Reinhard et al.[164]
1105	*T-shape*	C-Y$_3$-Stp$_2$-K(K-OHSteA$_2$)-Stp$_2$-Y$_3$-C	T-OHSteA	"
1165	*T-shape*	C-Y$_3$-Stp$_2$-K(K-LinA$_2$)-Stp$_2$-Y$_3$-C	T-LinA	"
1072	*T-shape*	C-Y$_3$-Stp$_2$-K(K-SteA$_2$)-Stp$_2$-Y$_3$-C	T-SteA	"

α-amino acids are indicated in one-letter code. Stp, succinyl-tetraethylene pentamine; Sph, succinyl-pentaethylene hexamine; Gtt, glutaryl-triethylene tetramine; OleA, oleic acid; NonOcA,8-nonanamidooctanoic acid; OHSteA, mono-hydroxylated stearic acid; LinA, linoleic acid; SteA, stearic acid.

Figure 42: Synthesis, purification and functionality assay of the Cas9/sgRNA ribonucleoprotein components. (A) Representative analysis of purified recombinant Cas9 protein on a Coomassie Brilliant Blue stained 10 % SDS-PAGE gel. M: Page Ruler, prestained protein ladder, marker band sizes are indicated in kDa. (B) Representative analysis of *in vitro* transcribed and purified sgRNA on a Gel Red stained 10% DNA-PAGE gel. M: 50 bp DNA ladder, marker band sizes are indicated in base pairs (BP). (C) *In vitro* cleavage assay to check the functionality of the RNP complex. Representative analysis of the initially linearized plasmid containing the sgRNA target side (LP) followed by a second cleavage due to incubation with precomplexed RNP visualized on a 1.5 % agarose gel containing Gel Red. DNA cleavage products of the second digest after incubation with sgRNA precomplexed with commercially available NEB Cas9 (NB) or after incubation with sgRNA precomplexed with in-house purified Cas9 (IH).

Figure 43: Confocal laser scanning microscopy (CLSM) images of Cas9-ATTO647N/sgRNA-ATTO488 lipo-nanoparticles uptake. Neuro2a eGFP-Luc cells were incubated with 75 nM RNP lipo-nanoparticles (containing 20 % labeled RNP components) mixed at N/P 24. Images were recorded after 4 h incubation and fixation with 4 % paraformaldehyde. First column: fluorescence of phalloidin-rhodamine stained actin filaments; second column: nuclear staining with DAPI; third column: fluorescence of ATTO488-labeled sgRNA; fourth column: fluorescence of ATTO647N-Cas9; fifth column: merge of all three channels. Subset of the data is shown in Figure 38.
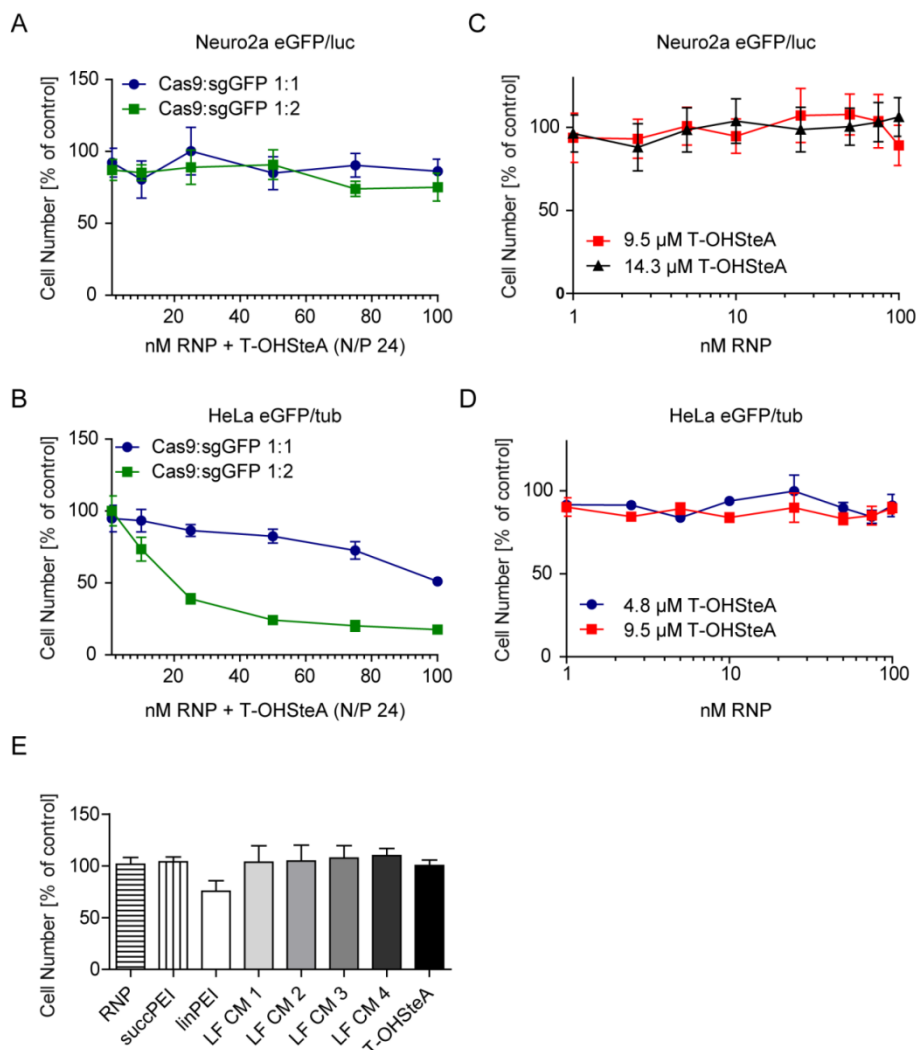
Figure 44: Effect of RNP T-OHSteA treatments on cell number. (A,B) Dose-titration experiment in Neuro2a eGFP-Luc (A) or HeLa-GFP-Tub (B) cells treated with 1-100 nM Cas9/sgRNA RNP complex at a 1:1 (blue) or 1:2 (green) ratio formulated with T-OHSteA at N/P 24. (C) N/P variation in Neuro2a eGFP-Luc cells by keeping T-OHSteA concentration constant (red curve: 9.5 µM; black curve: 14.3 µM) and varying the amount of RNP complex (in nM) at a 1:1 ratio. (D) N/P variation experiment in HeLa GFP-Tub cells by keeping T-OHSteA concentrations constant (blue curve: 4.8 µM; red curve: 9.5 µM) and varying amount of RNP complex at a 1:1 ratio. (E) Comparison of RNP T-OHSteA formulations with established transfection reagents in terms of cell number. RNP complex without carrier served as negative control and were determined as 100 %. Established transfection reagents included succinylated polyethylenimine (PEI-Suc) at a w/w ratio of 4, linear polyethylenimine (linPEI) at w/w 0.8 of polymer to sgRNA. Lipofectamine CRISPRMAX (LF CM) was tested at three different concentrations and with two different mixing procedures. LF CM 1 (6 nM RNP) and 2 (15 nM RNP) and 3 (75 nM RNP) were prepared as recommended by the manufacturer. LF CM 4 (75 nM RNP) as well as T-OHSteA (75 nM RNP) were mixed according to the protocol for formulation of RNP lipo-OAA formulations. All data points indicate % cell numbers 3-4 d after a 48 h treatment in presence of 10 % FBS. The % of cell number was normalized to HBG buffer treated cells. Data are presented as mean ± SD ($n = 3$).

FCS Results

Table 4: The values obtained from the FCS measurements of ATTO488-sgRNA, applying a 2-Component diffusion fit with a triplet fraction, where A_1 and A_2 are the (size-weighted) relative amplitudes of free and RNP complex bound ATTO488-sgRNA. D_1 and D_2 refer to the respective diffusion coefficients of A_1 and A_2, respectively.

	A_1	A_2	D_1 (μm^2/s)	D_2 ($\mu m2$/s)	Triplet/μs (fraction)
ATTO488	1.00	-	373	-	-
ATTO488-sgRNA	1.00	-	56.0	-	38.4 (0.33)
ATTO488-sgRNA +T-OHSteA	0.071	0.929	56.0	4.04	14.1 (0.04)
ATTO488-sgRNA +ATTO647N-Cas9	0.525	0.475	56.0	1.67	30.4 (0.30)
ATTO488-sgRNA +ATTO647N-Cas9 +T-OHSteA	0.407	0.593	56.0	2.32	22.3 (0.27)

Table 5: The values obtained from the FCS measurements of ATTO647N-Cas9, applying a 2-Component diffusion fit with a triplet fraction, where A_1 and A_2 are the (size-weighted) relative amplitudes of free and RNP complex bound ATTO647N-Cas9. D_1 and D_2 refer to the respective diffusion coefficients of A_1 and A_2, respectively.

	A_1	A_2	D_1 (μm^2/s)	D_2 ($\mu m2$/s)	Triplet/μs (fraction)
ATTO488	1.00	-	373	-	-
ATTO488-sgRNA	1.00	-	56.0	-	38.4 (0.33)
ATTO488-sgRNA +T-OHSteA	0.071	0.929	56.0	4.04	14.1 (0.04)
ATTO488-sgRNA +ATTO647N-Cas9	0.525	0.475	56.0	1.67	30.4 (0.30)
ATTO488-sgRNA +ATTO647N-Cas9 +T-OHSteA	0.407	0.593	56.0	2.32	22.3 (0.27)

4   Summary

The fast-growing field of molecular therapeutics represents an innovative way to target diseases on an early molecular level. These compounds, designed to target certain specific molecular structures, comprise several classes of macromolecules with a vast variety of physicochemical and biological characteristics. Safe and efficient delivery of sufficient drug amounts to the specific target site builds a major hurdle for the approval of nanopharmaceuticals. Potent carrier systems must be multifunctional and overcome several barriers to achieve successful drug delivery, including packaging of the cargo, intracellular delivery, endosomal escape as well as cargo release at the target site. Sequence-defined oligo(ethylenamino) amides (OAAs) generated by solid-phase synthesis and based on natural α-amino acids, artificial oligoamino acids and different additional functional units like hydrophobic modifications were recently established as a delivery system for charged nucleic acids, proteins and other therapeutics. They combine the advantages of aminoethylene based polymers with the chemical precision and versatility of peptides. In two different projects, these highly defined molecules were utilized for the development of novel delivery strategies for two completely different and promising molecular therapeutics.

Phosphorodiamidate morpholino oligomers (PMOs), a class of artificial, uncharged ASOs with favorable stability, nuclease-resistance, low immunogenicity and toxicity represent the first cargo of interest. This type of antisense oligonucleotides is able to restore functional gene expression by modification of pre-mRNA splicing to modulate cellular processes. After an initial library screen, potent artificial aminoethylene-lipopeptides were identified for the synthesis of PMO conjugates via copper-free click chemistry. To evaluate efficient site-specific delivery of the cargo, the splice-switching activity in HeLa pLuc/705 cells containing a luciferase reporter gene with an aberrant splicing pattern were used as a test system. In this reporter cell line, successful PMO delivery, resulted in increased luciferase activity, depending on successful splice-switching. Systematic variations of the lead structure by substitution of contained fatty acids revealed that the degree of unsaturation had a critical impact on the splice-switching activity. PMO lipopeptide conjugates containing linolenic acid with three double bonds exhibited the highest splicing correction and significantly increased

functional protein expression in several reporter cell lines containing the pLuc/705 construct. Not only the conjugate type, but also formulation with an excess of lipopeptide increased splice-switching activity *in vitro* as well as *in vivo* after intratumoral injection. Structural and mechanistic studies revealed that the lipopeptide-PMO conjugates associated into nanocomplexes in a concentration dependent manner, remarkably enhanced the uptake kinetic and splicing correction activity. Furthermore, it could be shown that the type of contained fatty acid played an essential role in membrane interaction and pH-dependent lytic activity, promoting better endosomal release of the PMO-LP conjugates. In a final approach, two formulations with the most potent PMO-LP containing linolenic acid were tested in H2K-mdx52 dystrophic skeletal myotubes, to assess the therapeutic potential of the new PMO carrier system in a more clinical relevant model. Already low nanomolar PMO-LP concentrations mediated significant splice-switching of dystrophin pre-mRNA, especially in formulations containing threefold excess of LP. Lipopeptide-PMOs are therefore considered as a promising platform for therapeutic splice-switching with favorable activity/toxicity profile.

The second cargo, a highly specific and programmable endonuclease called Cas9 bound to a single guide RNA resulting in a negatively charged ribonucleoprotein complex, was used to modify gene expression at DNA level. After successful production and purification of both functional components, an initial library screening with different oligo(ethylenamino) amides of different topologies was conducted. In this project, a lipid containing T-shape oligomer (lipo-OAA) with complex stabilizing moieties was identified as the most potent candidate. Further structural mechanistic studies revealed that the type of contained fatty acid had a critical impact on the knock out efficiency, since one hydroxy group in the fatty acid dramatically changed the properties and performance of the resulting Cas9/sgRNA lipo-OAA complexes. A lipo-OAA containing hydroxy-stearic acid was superior compared to analogs with saturated or unsaturated fatty acids without hydroxylation in terms of particle formation, cellular uptake, lytic potential at acidic pH, which suggests enhanced endosomal release and finally knock out efficiency. The investigation of this highly efficient and dynamic delivery platform is considered to have a high potential for the development of precise gene modifying therapeutics to treat diseases at their roots.

5   Appendix

5.1   Abbreviations

ASO	Antisense oligonucleotide
cgRNA	control guide RNA
CRISPR	Clustered, regularly interspaced, short palindromic repeats
Cas	CRISPR-associated
DIPEA	*N,N*-Diisopropylethylamine
DMEM	Dulbecco's modified Eagle's medium
FCS	Fetal calf serum
FolR1	Folate receptor 1
HBG	Hepes-buffered glucose
HEPES	*N*-(2-hydroxethyl) piperazine-N'-(2-ethansulfonic acid)
LP	Lipopeptide
PEI	Polyethylenimine
MTT	3-(4,5-dimethylthiazol-2-yl)-2,5-diphenyltetrazolium bromide
N/P	(Protonatable) nitrogen to phosphates ratio
NHS	*N*-Hydroxysuccinimide
OAA	Oligo(ethylenamino) amides
PDI	Polydispersity index
PMO	Phosphorodiamidate morpholino oligomers
RLU	Relative light units
RNP	Ribonucleoprotein
RT	Room temperature
SEC	Size-exclusion chromatography
sgRNA	single guide RNA
SPAAC	Strain-promoted alkyne-azide cycloaddition
SSO	Splice-switching oligonucleotide
Stp	Succinyl-tetraethylene pentamine

5.2 Analytical Data

5.2.1 MALDI-TOF mass spectrometry of artificial peptides

1 µL matrix solution containing 10 mg/mL Super-DHB (90/10 m/m mixture of 2,5-dihydroxybenzoic acid and 2-hydroxy-5-methoxybenzoic acid) in 69.93/30/0.07 (v/v/v) H_2O/acetonitrile/trifluoroacetic acid was spotted on an MTP AnchorChip (Bruker Daltonics, Germany). After the matrix crystallized, 1 µL of sample solution (10 mg/mL in water) was added to the matrix spot. Samples were analyzed using an Autoflex II mass spectrometer (Bruker Daltonics, Germany). All spectra were recorded in positive ion mode.

Table 6. Summary of peptide mass data.

ID	Description	Molecular formula	$[M+H]^+$ calc.	$[M+H]^+$ found
454	T-OleA	$C_{156}H_{254}N_{32}O_{27}S_2$	3074.0	3064.0
991	LP CholA	$C_{164}H_{259}N_{31}O_{26}$	3079.0	3074.2
1072	T-SteA	$C_{156}H_{258}N_{32}O_{27}S_2$	3078.0	3070.0
1104	T-NonOcA	$C_{154}H_{252}N_{34}O_{29}S_2$	3108.0	3103.0
1105	T-OHSteA	$C_{156}H_{252}N_{32}O_{29}S_2$	3110.0	3103.0
1106	LP CholA	$C_{170}H_{269}N_{35}O_{27}$	3234.1	3233.0
1165	T-LinA	$C_{156}H_{250}N_{32}O_{27}S_2$	3069.0	3067.0
1169	LP OleA	$C_{158}H_{257}N_{35}O_{27}$	3078.0	3076.1
1171	LP LinA	$C_{158}H_{253}N_{35}O_{27}$	3074.0	3074.1
1172	LP SteA	$C_{158}H_{261}N_{35}O_{27}$	3082.0	3083.2
1195	LP LenA	$C_{158}H_{249}N_{35}O_{27}$	3069.9	3170.5
1204	LP GonA	$C_{162}H_{265}N_{35}O_{27}$	3134.0	3131.2
1205	LP AraA	$C_{162}H_{253}N_{35}O_{27}$	3122.0	3120.1
1206	LP EPA	$C_{162}H_{249}N_{35}O_{27}$	3117.9	3116.4
1207	LP DHA	$C_{166}H_{253}N_{35}O_{27}$	3170.0	3169.2
1228	Pip6a-azide	$C_{142}H_{254}N_{60}O_{26}$	3216.0	3214.9
1239	LP(RRRR) CholA	$C_{170}H_{265}N_{47}O_{27}$	3399.2	3394.0
1240	LP(RRXRR) CholA	$C_{182}H_{287}N_{49}O_{29}$	3625.5	3619.1
1241	LP(RKRK) CholA	$C_{170}H_{265}N_{39}O_{27}$	3287.1	3283.1
1242	LP(RHRH) CholA	$C_{170}H_{245}N_{43}O_{27}$	3323.0	3317.9

5.2.2   MALDI-TOF mass spectrometry of PMO derivatives

MALDI-TOF MS of PMO-NH$_2$
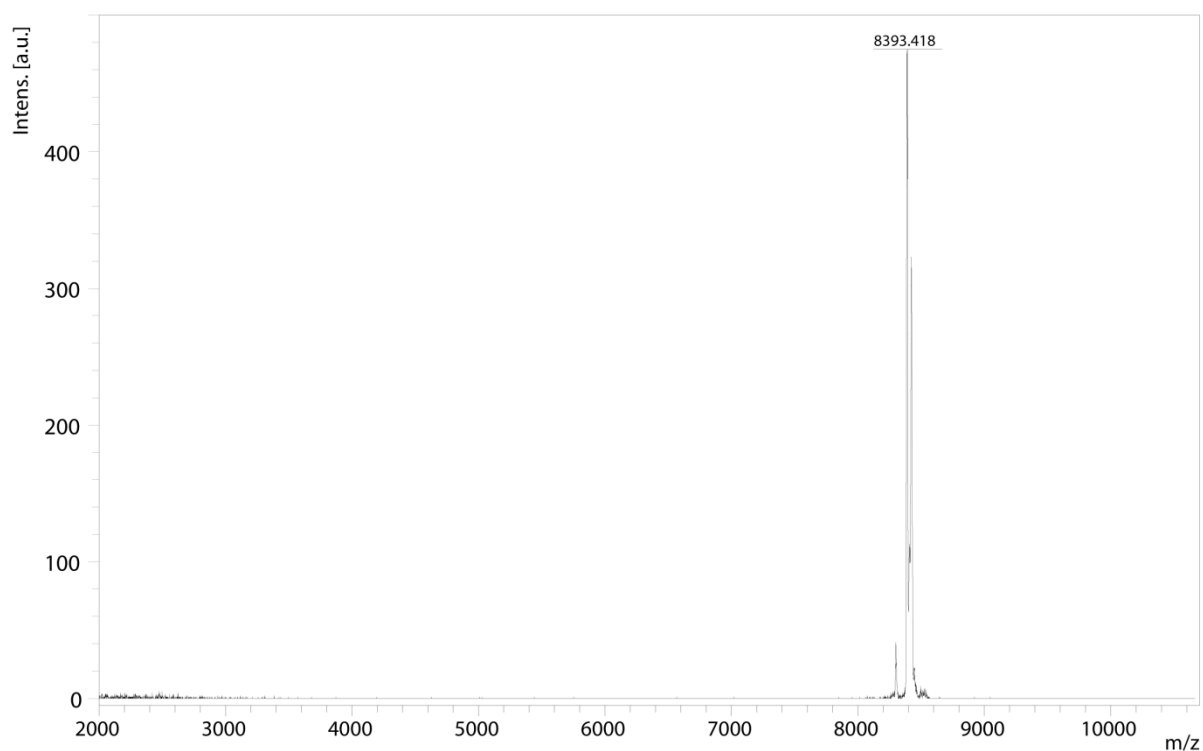
MALDI-TOF MS of PMO-DBCO
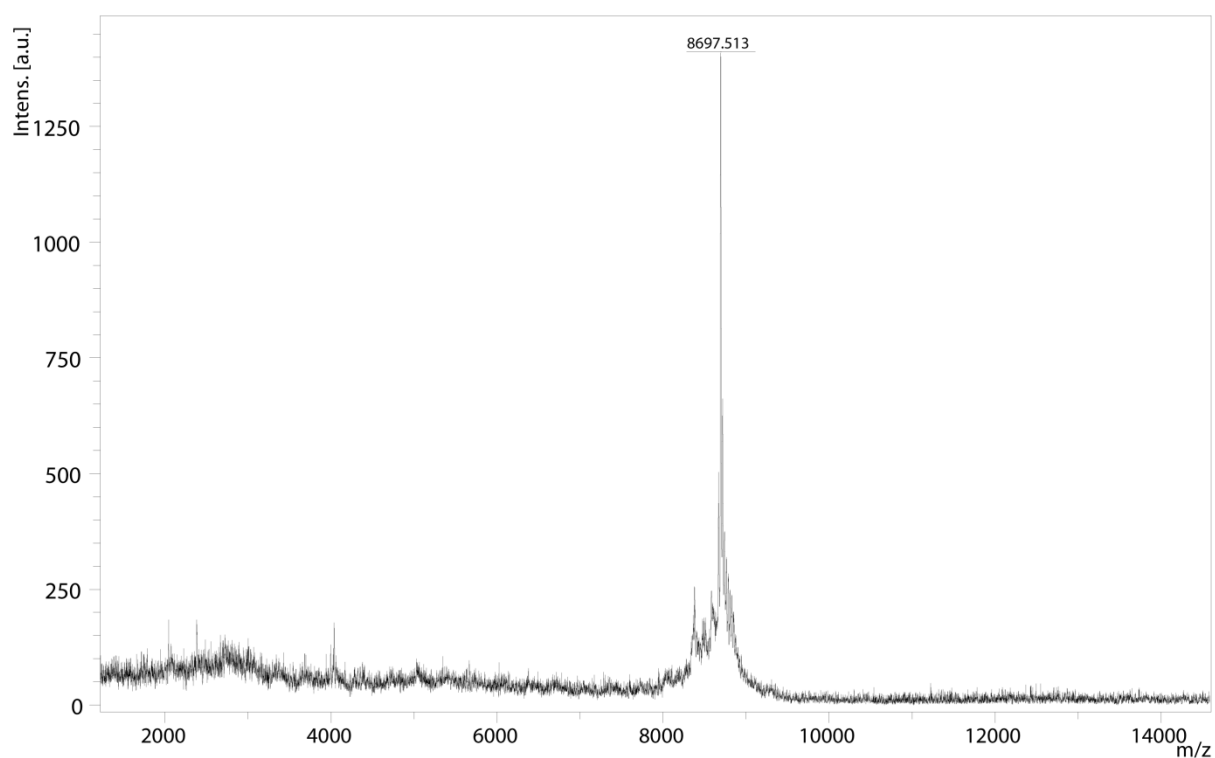
MALDI-TOF MS of PMO-LP CholA

(formulation with excess of free LP CholA)
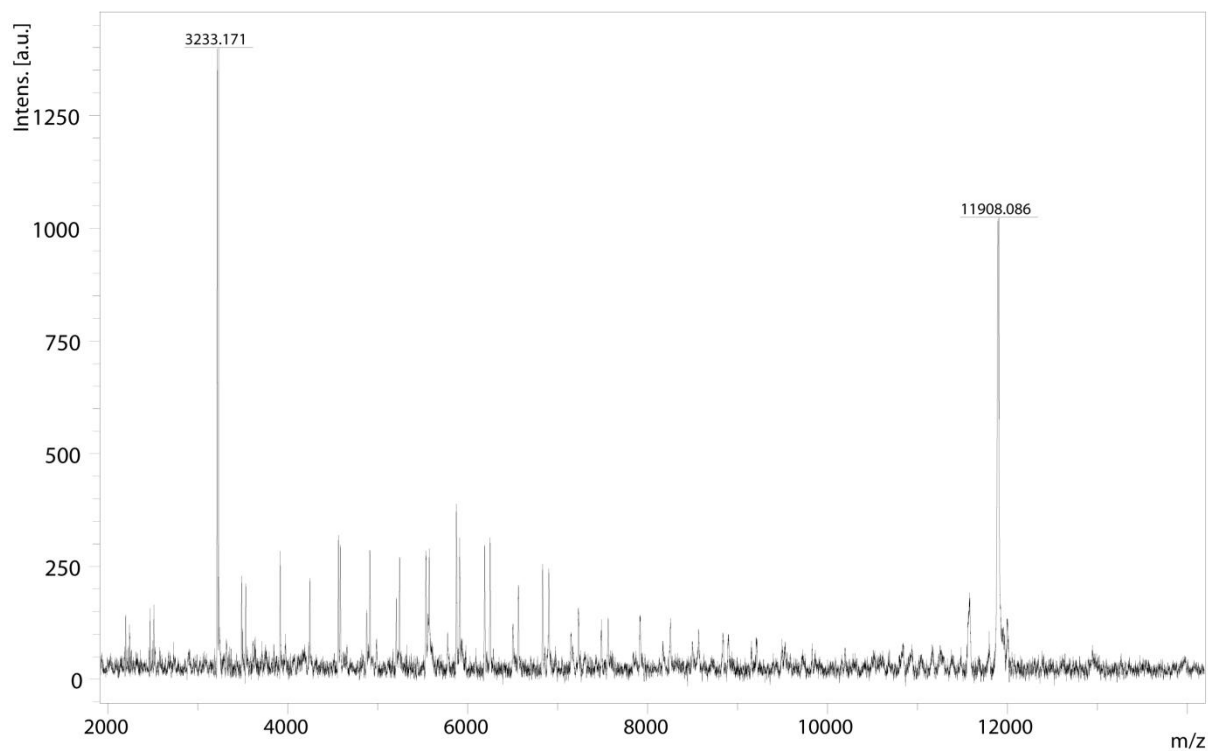
MALDI-TOF MS of PMO-LP CholA

(HPLC purified conjugate)
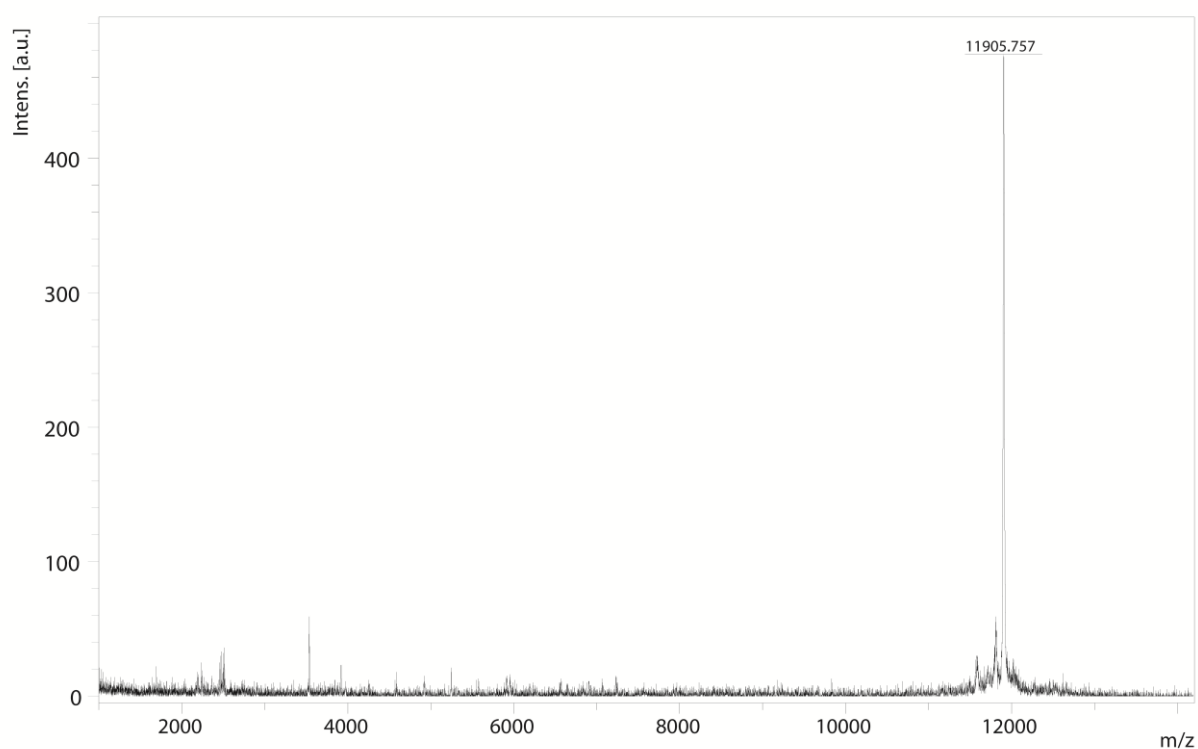
6   References

1.   Lander, E. S.; Linton, L. M.; Birren, B.; Nusbaum, C.; Zody, M. C.; Baldwin, J.; Devon, K.; Dewar, K.; Doyle, M.; FitzHugh, W.; Funke, R.; Gage, D.; Harris, K.; Heaford, A.; Howland, J.; Kann, L.; Lehoczky, J.; LeVine, R.; McEwan, P.; McKernan, K.; Meldrim, J.; Mesirov, J. P.; Miranda, C.; Morris, W.; Naylor, J.; Raymond, C.; Rosetti, M.; Santos, R.; Sheridan, A.; Sougnez, C.; Stange-Thomann, Y.; Stojanovic, N.; Subramanian, A.; Wyman, D.; Rogers, J.; Sulston, J.; Ainscough, R.; Beck, S.; Bentley, D.; Burton, J.; Clee, C.; Carter, N.; Coulson, A.; Deadman, R.; Deloukas, P.; Dunham, A.; Dunham, I.; Durbin, R.; French, L.; Grafham, D.; Gregory, S.; Hubbard, T.; Humphray, S.; Hunt, A.; Jones, M.; Lloyd, C.; McMurray, A.; Matthews, L.; Mercer, S.; Milne, S.; Mullikin, J. C.; Mungall, A.; Plumb, R.; Ross, M.; Shownkeen, R.; Sims, S.; Waterston, R. H.; Wilson, R. K.; Hillier, L. W.; McPherson, J. D.; Marra, M. A.; Mardis, E. R.; Fulton, L. A.; Chinwalla, A. T.; Pepin, K. H.; Gish, W. R.; Chissoe, S. L.; Wendl, M. C.; Delehaunty, K. D.; Miner, T. L.; Delehaunty, A.; Kramer, J. B.; Cook, L. L.; Fulton, R. S.; Johnson, D. L.; Minx, P. J.; Clifton, S. W.; Hawkins, T.; Branscomb, E.; Predki, P.; Richardson, P.; Wenning, S.; Slezak, T.; Doggett, N.; Cheng, J. F.; Olsen, A.; Lucas, S.; Elkin, C.; Uberbacher, E.; Frazier, M.; Gibbs, R. A.; Muzny, D. M.; Scherer, S. E.; Bouck, J. B.; Sodergren, E. J.; Worley, K. C.; Rives, C. M.; Gorrell, J. H.; Metzker, M. L.; Naylor, S. L.; Kucherlapati, R. S.; Nelson, D. L.; Weinstock, G. M.; Sakaki, Y.; Fujiyama, A.; Hattori, M.; Yada, T.; Toyoda, A.; Itoh, T.; Kawagoe, C.; Watanabe, H.; Totoki, Y.; Taylor, T.; Weissenbach, J.; Heilig, R.; Saurin, W.; Artiguenave, F.; Brottier, P.; Bruls, T.; Pelletier, E.; Robert, C.; Wincker, P.; Smith, D. R.; Doucette-Stamm, L.; Rubenfield, M.; Weinstock, K.; Lee, H. M.; Dubois, J.; Rosenthal, A.; Platzer, M.; Nyakatura, G.; Taudien, S.; Rump, A.; Yang, H.; Yu, J.; Wang, J.; Huang, G.; Gu, J.; Hood, L.; Rowen, L.; Madan, A.; Qin, S.; Davis, R. W.; Federspiel, N. A.; Abola, A. P.; Proctor, M. J.; Myers, R. M.; Schmutz, J.; Dickson, M.; Grimwood, J.; Cox, D. R.; Olson, M. V.; Kaul, R.; Raymond, C.; Shimizu, N.; Kawasaki, K.; Minoshima, S.; Evans, G. A.; Athanasiou, M.; Schultz, R.; Roe, B. A.; Chen, F.; Pan, H.; Ramser, J.; Lehrach, H.; Reinhardt, R.; McCombie, W. R.; de la Bastide, M.; Dedhia, N.; Blocker, H.; Hornischer, K.; Nordsiek, G.; Agarwala, R.; Aravind, L.; Bailey, J. A.; Bateman, A.; Batzoglou, S.; Birney, E.; Bork, P.; Brown, D. G.; Burge, C. B.; Cerutti, L.; Chen, H. C.; Church, D.; Clamp, M.; Copley, R. R.; Doerks, T.; Eddy, S. R.; Eichler, E. E.; Furey, T. S.; Galagan, J.; Gilbert, J. G.; Harmon, C.; Hayashizaki, Y.; Haussler, D.; Hermjakob, H.; Hokamp, K.; Jang, W.; Johnson, L. S.; Jones, T. A.; Kasif, S.; Kaspryzk, A.; Kennedy, S.; Kent, W. J.; Kitts, P.; Koonin, E. V.; Korf, I.; Kulp, D.; Lancet, D.; Lowe, T. M.; McLysaght, A.; Mikkelsen, T.; Moran, J. V.; Mulder, N.; Pollara, V. J.; Ponting, C. P.; Schuler, G.; Schultz, J.; Slater, G.; Smit, A. F.; Stupka, E.; Szustakowki, J.; Thierry-Mieg, D.; Thierry-Mieg, J.; Wagner, L.; Wallis, J.; Wheeler, R.; Williams, A.; Wolf, Y. I.; Wolfe, K. H.; Yang, S. P.; Yeh, R. F.; Collins, F.; Guyer, M. S.; Peterson, J.; Felsenfeld, A.; Wetterstrand, K. A.; Patrinos, A.; Morgan, M. J.; de Jong, P.; Catanese, J. J.; Osoegawa, K.; Shizuya, H.; Choi, S.; Chen, Y. J.; Szustakowki, J.; International Human Genome Sequencing, C., Initial sequencing and analysis of the human genome. *Nature* **2001,** *409* (6822), 860-921.

2.   Beadle, G. W.; Tatum, E. L., Genetic Control of Biochemical Reactions in Neurospora. *Proceedings of the National Academy of Sciences of the United States of America* **1941,** *27* (11), 499-506.

3.   Licatalosi, D. D.; Darnell, R. B., RNA processing and its regulation: global insights into biological networks. *Nature Reviews Genetics* **2010,** *11* (1), 75-87.

4.   Gilbert, W., Why genes in pieces? *Nature* **1978,** *271* (5645), 501-501.

5.   Scherrer, K.; Latham, H.; Darnell, J. E., DEMONSTRATION OF AN UNSTABLE RNA AND OF A PRECURSOR TO RIBOSOMAL RNA IN HELA CELLS. **1963,** *49* (2), 240-248.

6.   Soeiro, R., THE TURNOVER OF NUCLEAR DNA-LIKE RNA IN HELA CELLS. **1968,** *39* (1), 112-118.

7.   Hocine, S.; Singer, R. H.; Grunwald, D., RNA Processing and Export. **2010,** *2* (12), a000752-a000752.

8.   Moore, M. J.; Proudfoot, N. J., Pre-mRNA Processing Reaches Back toTranscription and Ahead to Translation. **2009,** *136* (4), 688-700.

9.   Shuman, S., Structure, mechanism, and evolution of the mRNA capping apparatus. *Prog Nucleic Acid Res Mol Biol* **2001,** *66*, 1-40.

10.   Hsu, C. L.; Stevens, A., Yeast cells lacking 5'-->3' exoribonuclease 1 contain mRNA species that are poly(A) deficient and partially lack the 5' cap structure. **1993,** *13* (8), 4826-4835.

11.   Drummond, D. R.; Armstrong, J.; Colman, A., The effect of capping and polyadenylation on the stability, movement and translation of synthetic messenger RNAs in Xenopus oocytes. **1985,** *13* (20), 7375-7394.

12.   Fica, S. M.; Tuttle, N.; Novak, T.; Li, N.-S.; Lu, J.; Koodathingal, P.; Dai, Q.; Staley, J. P.; Piccirilli, J. A., RNA catalyses nuclear pre-mRNA splicing. **2013**.

13.   Milne, J. L. S.; Borgnia, M. J.; Bartesaghi, A.; Tran, E. E. H.; Earl, L. A.; Schauder, D. M.; Lengyel, J.; Pierson, J.; Patwardhan, A.; Subramaniam, S., Cryo-electron microscopy - a primer for the non-microscopist. *FEBS Journal* **2013,** *280* (1), 28-45.

14.   Shi, Y., Mechanistic insights into precursor messenger RNA splicing by the spliceosome. *Nature Reviews Molecular Cell Biology* **2017,** *18* (11), 655-670.

15.   Matera, A. G.; Wang, Z., A day in the life of the spliceosome. *Nature Reviews Molecular Cell Biology* **2014,** *15* (2), 108-121.

16.   Wang, Y.; Liu, J.; Huang, B.; Xu, Y.-M.; Li, J.; Huang, L.-F.; Lin, J.; Zhang, J.; Min, Q.-H.; Yang, W.-M.; Wang, X.-Z., Mechanism of alternative splicing and its regulation. *Biomedical Reports* **2015,** *3* (2), 152-158.

17.   Black, D. L., Mechanisms of Alternative Pre-Messenger RNA Splicing. *Annual Review of Biochemistry* **2003,** *72* (1), 291-336.

18.   Barash, Y.; Calarco, J. A.; Gao, W.; Pan, Q.; Wang, X.; Shai, O.; Blencowe, B. J.; Frey, B. J., Deciphering the splicing code. *Nature* **2010,** *465* (7294), 53-59.

19.   Griffith, M.; Griffith, O. L.; Mwenifumbo, J.; Goya, R.; Morrissy, A. S.; Morin, R. D.; Corbett, R.; Tang, M. J.; Hou, Y. C.; Pugh, T. J.; Robertson, G.; Chittaranjan, S.; Ally, A.; Asano, J. K.; Chan, S. Y.; Li, H. I.; McDonald, H.; Teague, K.; Zhao, Y.; Zeng, T.; Delaney, A.; Hirst, M.; Morin, G. B.; Jones, S. J.; Tai, I. T.; Marra, M. A., Alternative expression analysis by RNA sequencing. *Nat Methods* **2010,** *7* (10), 843-7.

20.   Nilsen, T. W.; Graveley, B. R., Expansion of the eukaryotic proteome by alternative splicing. **2010,** *463* (7280), 457-463.

21.   Lin, C.-L. G.; Bristol, L. A.; Jin, L.; Dykes-Hoberg, M.; Crawford, T.; Clawson, L.; Rothstein, J. D., Aberrant RNA Processing in a Neurodegenerative Disease: the Cause for Absent EAAT2, a Glutamate Transporter, in Amyotrophic Lateral Sclerosis. *Neuron* **1998,** *20* (3), 589-602.

22.   Zhang, J.; Manley, J. L., Misregulation of Pre-mRNA Alternative Splicing in Cancer. *Cancer Discovery* **2013,** *3* (11), 1228-1237.

23.   Wang, G.-S.; Cooper, T. A., Splicing in disease: disruption of the splicing code and the decoding machinery. *Nature Reviews Genetics* **2007,** *8* (10), 749-761.

24.   Caceres, J. F.; Kornblihtt, A. R., Alternative splicing: multiple control mechanisms and involvement in human disease. *Trends Genet* **2002,** *18* (4), 186-93.

25.   Vorechovsky, I., Aberrant 3' splice sites in human disease genes: mutation pattern, nucleotide structure and comparison of computational tools that predict their utilization. **2006,** *34* (16), 4630-4641.

26.   Fukumaki, Y.; Ghosh, P. K.; Benz, E. J., Jr.; Reddy, V. B.; Lebowitz, P.; Forget, B. G.; Weissman, S. M., Abnormally spliced messenger RNA in erythroid cells from patients with beta+ thalassemia and monkey cells expressing a cloned beta+-thalassemic gene. *Cell* **1982,** *28* (3), 585-93.

27.   Sierakowska, H.; Sambade, M. J.; Agrawal, S.; Kole, R., Repair of thalassemic human -globin mRNA in mammalian cells by antisense oligonucleotides. **1996,** *93* (23), 12840-12844.

28.   Faustino, N. A., Pre-mRNA splicing and human disease. *Genes & Development* **2003,** *17* (4), 419-437.

29.   Cheishvili, D.; Maayan, C.; Smith, Y.; Ast, G.; Razin, A., IKAP/hELP1 deficiency in the cerebrum of familial dysautonomia patients results in down regulation of genes involved in oligodendrocyte differentiation and in myelination. **2007,** *16* (17), 2097-2104.

30.   Eriksson, M.; Brown, W. T.; Gordon, L. B.; Glynn, M. W.; Singer, J.; Scott, L.; Erdos, M. R.; Robbins, C. M.; Moses, T. Y.; Berglund, P.; Dutra, A.; Pak, E.; Durkin, S.; Csoka, A. B.; Boehnke, M.; Glover, T. W.; Collins, F. S., Recurrent de novo point mutations in lamin A cause Hutchinson–Gilford progeria syndrome. *Nature* **2003,** *423* (6937), 293-298.

31.   Gallo, J. M.; Noble, W.; Martin, T. R., RNA and protein-dependent mechanisms in tauopathies: consequences for therapeutic strategies. **2007,** *64* (13), 1701-1714.

32.   Schuyer, M.; Burg, M. E. L. V. D.; Henzen-Logmans, S. C.; Fieret, J. H.; Klijn, J. G. M.; Look, M. P.; Foekens, J. A.; Stoter, G.; Berns, E. M. J. J., Reduced expression of BAX is associated with poor prognosis in patients with epithelial ovarian cancer: a multifactorial analysis of TP53, p21, BAX and BCL-2. **2001,** *85* (9), 1359-1367.

33.   Shkreta, L.; Bell, B.; Revil, T.; Venables, J. P.; Prinos, P.; Elela, S. A.; Chabot, B., Cancer-Associated Perturbations in Alternative Pre-messenger RNA Splicing. *Cancer Treat Res* **2013,** *158*, 41-94.

34.   Kwabi-Addo, B.; Ropiquet, F.; Giri, D.; Ittmann, M., Alternative splicing of fibroblast growth factor receptors in human prostate cancer. *Prostate* **2001,** *46* (2), 163-72.

35.   Aigner, A.; Juhl, H.; Malerczyk, C.; Tkybusch, A.; Benz, C. C.; Czubayko, F., Expression of a truncated 100 kDa HER2 splice variant acts as an endogenous inhibitor of tumour cell proliferation. **2001,** *20* (17), 2101-2111.

36.   Mercatante, D. R.; Sazani, P.; Kole, R., Modification of alternative splicing by antisense oligonucleotides as a potential chemotherapy for cancer and other diseases. *Curr Cancer Drug Targets* **2001,** *1* (3), 211-30.

37.   Duncan, E.; Brown, M.; Shore, E. M., The revolution in human monogenic disease mapping. *Genes* **2014,** *5* (3), 792-803.

38.   Wittrup, A.; Lieberman, J., Knocking down disease: a progress report on siRNA therapeutics. *Nat Rev Genet* **2015,** *16* (9), 543-52.

39.   Di Fusco, D.; Dinallo, V.; Marafini, I.; Figliuzzi, M. M.; Romano, B.; Monteleone, G., Antisense Oligonucleotide: Basic Concepts and Therapeutic Application in Inflammatory Bowel Disease. *Frontiers in Pharmacology* **2019,** *10*.

40.   Rinaldi, C.; Wood, M. J. A., Antisense oligonucleotides: the next frontier for treatment of neurological disorders. *Nature Reviews Neurology* **2018,** *14* (1), 9-21.

41.   Havens, M. A.; Hastings, M. L., Splice-switching antisense oligonucleotides as therapeutic drugs. *Nucleic acids research* **2016,** *44* (14), 6549-6563.

42.   Stephenson, M. L.; Zamecnik, P. C., Inhibition of Rous sarcoma viral RNA translation by a specific oligodeoxyribonucleotide. *Proceedings of the National Academy of Sciences* **1978,** *75* (1), 285-288.

43.   Re, R., The application of antisense technology to medicine. *Ochsner J* **2000,** *2* (4), 233-6.

44.   Summerton, J., Morpholino antisense oligomers: the case for an RNase H-independent structural type. **1999,** *1489* (1), 141-158.

45.   Wu, H.; Lima, W. F.; Zhang, H.; Fan, A.; Sun, H.; Crooke, S. T., Determination of the Role of the Human RNase H1 in the Pharmacology of DNA-like Antisense Drugs. **2004,** *279* (17), 17181-17189.

46.   Manoharan, M., 2′-Carbohydrate modifications in antisense oligonucleotide therapy: importance of conformation, configuration and conjugation. **1999,** *1489* (1), 117-130.

47.   Hinrich, A. J.; Jodelka, F. M.; Chang, J. L.; Brutman, D.; Bruno, A. M.; Briggs, C. A.; James, B. D.; Stutzmann, G. E.; Bennett, D. A.; Miller, S. A.; Rigo, F.; Marr, R. A.; Hastings, M. L., Therapeutic correction of ApoER2 splicing in Alzheimer's disease mice using antisense oligonucleotides. **2016**.

48.   Ottesen, E. W., ISS-N1 makes the First FDA-approved Drug for Spinal Muscular Atrophy. *Translational neuroscience* **2017,** *8*, 1-6.

49.   McDonald, C. M.; Wong, B.; Flanigan, K. M.; Wilson, R.; de Kimpe, S.; Lourbakos, A.; Lin, Z.; Campion, G.; group, D. V. s., Placebo-controlled Phase 2 Trial of Drisapersen for Duchenne Muscular Dystrophy. *Ann Clin Transl Neurol* **2018,** *5* (8), 913-926.

50.   Goemans, N.; Mercuri, E.; Belousova, E.; Komaki, H.; Dubrovsky, A.; McDonald, C. M.; Kraus, J. E.; Lourbakos, A.; Lin, Z.; Campion, G.; Wang, S. X.; Campbell, C.; group, D. I. s., A randomized placebo-controlled phase 3 trial of an antisense oligonucleotide, drisapersen, in Duchenne muscular dystrophy. *Neuromuscul Disord* **2018,** *28* (1), 4-15.

51.   Evers, M. M.; Tran, H. D.; Zalachoras, I.; Meijer, O. C.; den Dunnen, J. T.; van Ommen, G. J.; Aartsma-Rus, A.; van Roon-Mom, W. M., Preventing formation of toxic N-terminal huntingtin fragments through antisense oligonucleotide-mediated protein modification. *Nucleic Acid Ther* **2014,** *24* (1), 4-12.

52.   Disterer, P.; Al-Shawi, R.; Ellmerich, S.; Waddington, S. N.; Owen, J. S.; Simons, J. P.; Khoo, B., Exon Skipping of Hepatic APOB Pre-mRNA With Splice-switching Oligonucleotides Reduces LDL Cholesterol In Vivo. **2013,** *21* (3), 602-609.

53.   Bauman, J. A.; Li, S. D.; Yang, A.; Huang, L.; Kole, R., Anti-tumor activity of splice-switching oligonucleotides. **2010,** *38* (22), 8348-8356.

54.   Grunweller, A.; Hartmann, R. K., Locked nucleic acid oligonucleotides: the next generation of antisense agents? *BioDrugs* **2007,** *21* (4), 235-43.

55.   Nielsen, P. E.; Egholm, M.; Berg, R. H.; Buchardt, O., Peptide nucleic acids (PNAs): potential antisense and anti-gene agents. *Anticancer Drug Des* **1993,** *8* (1), 53-63.

56.   Summerton, J.; Weller, D., Morpholino antisense oligomers: design, preparation, and properties. *Antisense Nucleic Acid Drug Dev* **1997,** *7* (3), 187-95.

57.   Summerton, J. E., Invention and Early History of Morpholinos: From Pipe Dream to Practical Products. *Methods Mol Biol* **2017,** *1565*, 1-15.

58.   Shimizu-Motohashi, Y.; Komaki, H.; Motohashi, N.; Takeda, S.; Yokota, T.; Aoki, Y., Restoring Dystrophin Expression in Duchenne Muscular Dystrophy: Current Status of Therapeutic Approaches. *J Pers Med* **2019,** *9* (1).

59.   Levin, A. A., Treating Disease at the RNA Level with Oligonucleotides. *New England Journal of Medicine* **2019,** *380* (1), 57-70.

60.   Lim, K. R.; Maruyama, R.; Yokota, T., Eteplirsen in the treatment of Duchenne muscular dystrophy. *Drug Design, Development and Therapy* **2017,** *Volume11*, 533-545.

61.   Mendell, J. R.; Goemans, N.; Lowes, L. P.; Alfano, L. N.; Berry, K.; Shao, J.; Kaye, E. M.; Mercuri, E., Longitudinal effect of eteplirsen versus historical control on ambulation in Duchenne muscular dystrophy. *Annals of Neurology* **2016,** *79* (2), 257-271.

62.   Jinek, M.; Chylinski, K.; Fonfara, I.; Hauer, M.; Doudna, J. A.; Charpentier, E., A programmable dual-RNA-guided DNA endonuclease in adaptive bacterial immunity. *Science* **2012,** *337* (6096), 816-21.

63.   Mali, P.; Yang, L.; Esvelt, K. M.; Aach, J.; Guell, M.; Dicarlo, J. E.; Norville, J. E.; Church, G. M., RNA-Guided Human Genome Engineering via Cas9. *Science* **2013,** *339* (6121), 823-826.

64.   Shah, S. A.; Erdmann, S.; Mojica, F. J. M.; Garrett, R. A., Protospacer recognition motifs. *RNA Biology* **2013,** *10* (5), 891-899.

65.   Jinek, M.; Jiang, F.; Taylor, D. W.; Sternberg, S. H.; Kaya, E.; Ma, E.; Anders, C.; Hauer, M.; Zhou, K.; Lin, S.; Kaplan, M.; Iavarone, A. T.; Charpentier, E.; Nogales, E.; Doudna, J. A., Structures of Cas9 endonucleases reveal RNA-mediated conformational activation. *Science* **2014,** *343* (6176), 1247997.

66.   Doudna, J. A.; Charpentier, E., Genome editing. The new frontier of genome engineering with CRISPR-Cas9. *Science* **2014,** *346* (6213), 1258096.

67.   San Filippo, J.; Sung, P.; Klein, H., Mechanism of Eukaryotic Homologous Recombination. *Annual Review of Biochemistry* **2008,** *77* (1), 229-257.

68.   Chu, V. T.; Weber, T.; Wefers, B.; Wurst, W.; Sander, S.; Rajewsky, K.; Kühn, R., Increasing the efficiency of homology-directed repair for CRISPR-Cas9-induced precise gene editing in mammalian cells. *Nature Biotechnology* **2015,** *33* (5), 543-548.

69.   Schumann, K.; Lin, S.; Boyer, E.; Simeonov, D. R.; Subramaniam, M.; Gate, R. E.; Haliburton, G. E.; Ye, C. J.; Bluestone, J. A.; Doudna, J. A.; Marson, A., Generation of knock-in primary human T cells using Cas9 ribonucleoproteins. *Proceedings of the National Academy of Sciences* **2015,** *112* (33), 10437-10442.

70.   Cong, L.; Ran, F. A.; Cox, D.; Lin, S.; Barretto, R.; Habib, N.; Hsu, P. D.; Wu, X.; Jiang, W.; Marraffini, L. A.; Zhang, F., Multiplex Genome Engineering Using CRISPR/Cas Systems. *Science* **2013,** *339* (6121), 819-823.

71.   Gaj, T.; Gersbach, C. A.; Barbas, C. F., ZFN, TALEN, and CRISPR/Cas-based methods for genome engineering. *Trends in Biotechnology* **2013,** *31* (7), 397-405.

72.   Nelson, C. E.; Hakim, C. H.; Ousterout, D. G.; Thakore, P. I.; Moreb, E. A.; Castellanos Rivera, R. M.; Madhavan, S.; Pan, X.; Ran, F. A.; Yan, W. X.; Asokan, A.; Zhang, F.; Duan, D.; Gersbach, C. A., In vivo genome editing improves muscle function in a mouse model of Duchenne muscular dystrophy. *Science* **2016,** *351* (6271), 403-7.

73.   Tabebordbar, M.; Zhu, K.; Cheng, J. K. W.; Chew, W. L.; Widrick, J. J.; Yan, W. X.; Maesner, C.; Wu, E. Y.; Xiao, R.; Ran, F. A.; Cong, L.; Zhang, F.;

Vandenberghe, L. H.; Church, G. M.; Wagers, A. J., In vivo gene editing in dystrophic mouse muscle and muscle stem cells. *Science* **2016,** *351* (6271), 407-411.

74. Rodriguez-Rodriguez, D.; Ramirez-Solis, R.; Garza-Elizondo, M.; Garza-Rodriguez, M.; Barrera-Saldana, H., Genome editing: A perspective on the application of CRISPR/Cas9 to study human diseases (Review). *International Journal of Molecular Medicine* **2019**.

75. Fellmann, C.; Gowen, B. G.; Lin, P.-C.; Doudna, J. A.; Corn, J. E., Cornerstones of CRISPR–Cas in drug discovery and therapy. *Nature Reviews Drug Discovery* **2017,** *16* (2), 89-100.

76. Scott, A., How CRISPR is transforming drug discovery. *Nature* **2018,** *555* (7695), S10-S11.

77. Adli, M., The CRISPR tool kit for genome editing and beyond. *Nature Communications* **2018,** *9* (1).

78. Zhang, F., Development of CRISPR-Cas systems for genome editing and beyond. *Quarterly Reviews of Biophysics* **2019,** *52*.

79. Zhan, T.; Rindtorff, N.; Betge, J.; Ebert, M. P.; Boutros, M., CRISPR/Cas9 for cancer research and therapy. *Seminars in Cancer Biology* **2019,** *55*, 106-119.

80. Goncalves, C.; Akhter, S.; Pichon, C.; Midoux, P., Intracellular Availability of pDNA and mRNA after Transfection: A Comparative Study among Polyplexes, Lipoplexes, and Lipopolyplexes. *Mol Pharm* **2016,** *13* (9), 3153-63.

81. Scholz, C.; Wagner, E., Therapeutic plasmid DNA versus siRNA delivery: common and different tasks for synthetic carriers. *J Control Release* **2012,** *161* (2), 554-65.

82. Thomas, C. E.; Ehrhardt, A.; Kay, M. A., Progress and problems with the use of viral vectors for gene therapy. *Nature Reviews Genetics* **2003,** *4* (5), 346-358.

83. Kotterman, M. A.; Chalberg, T. W.; Schaffer, D. V., Viral Vectors for Gene Therapy: Translational and Clinical Outlook. *Annual Review of Biomedical Engineering* **2015,** *17* (1), 63-89.

84. Belting, M.; Wittrup, A., Developments in macromolecular drug delivery. *Methods Mol Biol* **2009,** *480*, 1-10.

85. Blanco, E.; Shen, H.; Ferrari, M., Principles of nanoparticle design for overcoming biological barriers to drug delivery. *Nature Biotechnology* **2015,** *33* (9), 941-951.

86. Lynch, I.; Salvati, A.; Dawson, K. A., Protein-nanoparticle interactions: What does the cell see? **2009,** *4* (9), 546-547.

87. Walkey, C. D.; Chan, W. C. W., Understanding and controlling the interaction of nanomaterials with proteins in a physiological environment. *Chem. Soc. Rev.* **2012,** *41* (7), 2780-2799.

88. Conner, S. D.; Schmid, S. L., Regulated portals of entry into the cell. *Nature* **2003,** *422* (6927), 37-44.

89. Behzadi, S.; Serpooshan, V.; Tao, W.; Hamaly, M. A.; Alkawareek, M. Y.; Dreaden, E. C.; Brown, D.; Alkilany, A. M.; Farokhzad, O. C.; Mahmoudi, M., Cellular uptake of nanoparticles: journey inside the cell. *Chemical Society Reviews* **2017,** *46* (14), 4218-4244.

90. Fröhlich, E., The role of surface charge in cellular uptake and cytotoxicity of medical nanoparticles. *International Journal of Nanomedicine* **2012**, 5577.

91. Lin, J.; Zhang, H.; Chen, Z.; Zheng, Y., Penetration of Lipid Membranes by Gold Nanoparticles: Insights into Cellular Uptake, Cytotoxicity, and Their Relationship. **2010,** *4* (9), 5421-5429.

92.   Nangia, S.; Sureshkumar, R., Effects of Nanoparticle Charge and Shape Anisotropy on Translocation through Cell Membranes. *Langmuir* **2012,** *28* (51), 17666-17671.

93.   Zhu, M.; Nie, G.; Meng, H.; Xia, T.; Nel, A.; Zhao, Y., Physicochemical Properties Determine Nanomaterial Cellular Uptake, Transport, and Fate. *Accounts of Chemical Research* **2013,** *46* (3), 622-631.

94.   Reinhard, S.; Wagner, E., Sequence-Defined Cationic Lipo-Oligomers Containing Unsaturated Fatty Acids for Transfection. *Methods Mol Biol* **2019,** *1943*, 1-25.

95.   Smith, S. A.; Selby, L. I.; Johnston, A. P. R.; Such, G. K., The Endosomal Escape of Nanoparticles: Toward More Efficient Cellular Delivery. *Bioconjugate Chemistry* **2019,** *30* (2), 263-272.

96.   Scott, C. C.; Vacca, F.; Gruenberg, J., Endosome maturation, transport and functions. *Seminars in Cell & Developmental Biology* **2014,** *31*, 2-10.

97.   Bus, T.; Traeger, A.; Schubert, U. S., The great escape: how cationic polyplexes overcome the endosomal barrier. *Journal of Materials Chemistry B* **2018,** *6* (43), 6904-6918.

98.   Behr, J.-P., The Proton Sponge: a Trick to Enter Cells the Viruses Did Not Exploit. *CHIMIA International Journal for Chemistry* **1997,** *51* (1-2), 34-36.

99.   Boussif, O.; Lezoualc'H, F.; Zanta, M. A.; Mergny, M. D.; Scherman, D.; Demeneix, B.; Behr, J. P., A versatile vector for gene and oligonucleotide transfer into cells in culture and in vivo: polyethylenimine. *Proceedings of the National Academy of Sciences* **1995,** *92* (16), 7297-7301.

100.   Ray, M.; Tang, R.; Jiang, Z.; Rotello, V. M., Quantitative Tracking of Protein Trafficking to the Nucleus Using Cytosolic Protein Delivery by Nanoparticle-Stabilized Nanocapsules. *Bioconjugate Chemistry* **2015,** *26* (6), 1004-1007.

101.   Liu, X.; Zhang, P.; He, D.; Rödl, W.; Preiß, T.; Rädler, J. O.; Wagner, E.; Lächelt, U., pH-Reversible Cationic RNase A Conjugates for Enhanced Cellular Delivery and Tumor Cell Killing. **2016,** *17* (1), 173-182.

102.   Wyman, T. B.; Nicol, F.; Zelphati, O.; Scaria, P. V.; Plank, C.; Szoka, F. C., Design, Synthesis, and Characterization of a Cationic Peptide That Binds to Nucleic Acids and Permeabilizes Bilayers †. **1997,** *36* (10), 3008-3017.

103.   Betts, C.; Saleh, A. F.; Arzumanov, A. A.; Hammond, S. M.; Godfrey, C.; Coursindel, T.; Gait, M. J.; Wood, M. J., Pip6-PMO, A New Generation of Peptide-oligonucleotide Conjugates With Improved Cardiac Exon Skipping Activity for DMD Treatment. *Mol Ther Nucleic Acids* **2012,** *1*, e38.

104.   Pardridge, W. M.; Boado, R. J., Enhanced cellular uptake of biotinylated antisense oligonucleotide or peptide mediated by avidin, a cationic protein. **1991,** *288* (1-2), 30-32.

105.   Felgner, P. L.; Gadek, T. R.; Holm, M.; Roman, R.; Chan, H. W.; Wenz, M.; Northrop, J. P.; Ringold, G. M.; Danielsen, M., Lipofection: a highly efficient, lipid-mediated DNA-transfection procedure. *Proceedings of the National Academy of Sciences* **1987,** *84* (21), 7413-7417.

106.   Zhang, P.; He, D.; Klein, P. M.; Liu, X.; Röder, R.; Döblinger, M.; Wagner, E., Enhanced Intracellular Protein Transduction by Sequence Defined Tetra-Oleoyl Oligoaminoamides Targeted for Cancer Therapy. *Advanced Functional Materials* **2015,** *25* (42), 6627-6636.

107.   Bangham, A. D.; Standish, M. M.; Watkins, J. C., Diffusion of univalent ions across the lamellae of swollen phospholipids. *Journal of Molecular Biology* **1965,** *13* (1), 238-IN27.

108. Woodle, M. C., Sterically stabilized liposome therapeutics. **1995,** *16* (2-3), 249-265.

109. Bulbake, U.; Doppalapudi, S.; Kommineni, N.; Khan, W., Liposomal Formulations in Clinical Use: An Updated Review. *Pharmaceutics* **2017,** *9* (4), 12.

110. Fawell, S.; Seery, J.; Daikh, Y.; Moore, C.; Chen, L. L.; Pepinsky, B.; Barsoum, J., Tat-mediated delivery of heterologous proteins into cells. **1994,** *91* (2), 664-668.

111. Zuris, J. A.; Thompson, D. B.; Shu, Y.; Guilinger, J. P.; Bessen, J. L.; Hu, J. H.; Maeder, M. L.; Joung, J. K.; Chen, Z.-Y.; Liu, D. R., Cationic lipid-mediated delivery of proteins enables efficient protein-based genome editing in vitro and in vivo. *Nature Biotechnology* **2015,** *33* (1), 73-80.

112. Alter, J.; Lou, F.; Rabinowitz, A.; Yin, H.; Rosenfeld, J.; Wilton, S. D.; Partridge, T. A.; Lu, Q. L., Systemic delivery of morpholino oligonucleotide restores dystrophin expression bodywide and improves dystrophic pathology. *Nat Med* **2006,** *12* (2), 175-7.

113. Klein, P. M.; Reinhard, S.; Lee, D. J.; Müller, K.; Ponader, D.; Hartmann, L.; Wagner, E., Precise redox-sensitive cleavage sites for improved bioactivity of siRNA lipopolyplexes. *Nanoscale* **2016,** *8* (42), 18098-18104.

114. Shen, X.; Corey, D. R., Chemistry, mechanism and clinical status of antisense oligonucleotides and duplex RNAs. *Nucleic Acids Research* **2018,** *46* (4), 1584-1600.

115. Cirak, S.; Arechavala-Gomeza, V.; Guglieri, M.; Feng, L.; Torelli, S.; Anthony, K.; Abbs, S.; Garralda, M. E.; Bourke, J.; Wells, D. J.; Dickson, G.; Wood, M. J.; Wilton, S. D.; Straub, V.; Kole, R.; Shrewsbury, S. B.; Sewry, C.; Morgan, J. E.; Bushby, K.; Muntoni, F., Exon skipping and dystrophin restoration in patients with Duchenne muscular dystrophy after systemic phosphorodiamidate morpholino oligomer treatment: an open-label, phase 2, dose-escalation study. *The Lancet* **2011,** *378* (9791), 595-605.

116. McMahon, B. M.; Mays, D.; Lipsky, J.; Stewart, J. A.; Fauq, A.; Richelson, E., Pharmacokinetics and tissue distribution of a peptide nucleic acid after intravenous administration. *Antisense Nucleic Acid Drug Dev* **2002,** *12* (2), 65-70.

117. Amantana, A.; Moulton, H. M.; Cate, M. L.; Reddy, M. T.; Whitehead, T.; Hassinger, J. N.; Youngblood, D. S.; Iversen, P. L., Pharmacokinetics, biodistribution, stability and toxicity of a cell-penetrating peptide-morpholino oligomer conjugate. *Bioconjug Chem* **2007,** *18* (4), 1325-31.

118. Abes, S.; Moulton, H. M.; Clair, P.; Prevot, P.; Youngblood, D. S.; Wu, R. P.; Iversen, P. L.; Lebleu, B., Vectorization of morpholino oligomers by the (R-Ahx-R)4 peptide allows efficient splicing correction in the absence of endosomolytic agents. *J Control Release* **2006,** *116* (3), 304-13.

119. Lebleu, B.; Moulton, H. M.; Abes, R.; Ivanova, G. D.; Abes, S.; Stein, D. A.; Iversen, P. L.; Arzumanov, A. A.; Gait, M. J., Cell penetrating peptide conjugates of steric block oligonucleotides. *Adv Drug Deliv Rev* **2008,** *60* (4-5), 517-29.

120. Moulton, H. M.; Nelson, M. H.; Hatlevig, S. A.; Reddy, M. T.; Iversen, P. L., Cellular Uptake of Antisense Morpholino Oligomers Conjugated to Arginine-Rich Peptides. *Bioconjugate Chemistry* **2004,** *15* (2), 290-299.

121. Nielsen, P. E.; Shiraishi, T., Peptide nucleic acid (PNA) cell penetrating peptide (CPP) conjugates as carriers for cellular delivery of antisense oligomers. **2011,** *2* (3), 90-99.

122. Morcos, P. A.; Li, Y.; Jiang, S., Vivo-Morpholinos: A non-peptide transporter delivers Morpholinos into a wide array of mouse tissues. *BioTechniques* **2008,** *45* (6), 613-623.

123. Warren, T. K.; Shurtleff, A. C.; Bavari, S., Advanced morpholino oligomers: a novel approach to antiviral therapy. *Antiviral Res* **2012,** *94* (1), 80-8.

124.   Shen, G.; Fang, H.; Song, Y.; Bielska, A. A.; Wang, Z.; Taylor, J.-S. A., Phospholipid Conjugate for Intracellular Delivery of Peptide Nucleic Acids. **2009,** *20* (9), 1729-1736.

125.   Nastruzzi, C.; Cortesi, R.; Esposito, E.; Gambari, R.; Borgatti, M.; Bianchi, N.; Feriotto, G.; Mischiati, C., Liposomes as carriers for DNA–PNA hybrids. **2000,** *68* (2), 237-249.

126.   Betts, C. A.; McClorey, G.; Healicon, R.; Hammond, S. M.; Manzano, R.; Muses, S.; Ball, V.; Godfrey, C.; Merritt, T. M.; van Westering, T.; O'Donovan, L.; Wells, K. E.; Gait, M. J.; Wells, D. J.; Tyler, D.; Wood, M. J., Cmah-dystrophin deficient mdx mice display an accelerated cardiac phenotype that is improved following peptide-PMO exon skipping treatment. *Hum Mol Genet* **2019,** *28* (3), 396-406.

127.   Betts, C. A.; Saleh, A. F.; Carr, C. A.; Hammond, S. M.; Coenen-Stass, A. M.; Godfrey, C.; McClorey, G.; Varela, M. A.; Roberts, T. C.; Clarke, K.; Gait, M. J.; Wood, M. J., Prevention of exercised induced cardiomyopathy following Pip-PMO treatment in dystrophic mdx mice. *Sci Rep* **2015,** *5*, 8986.

128.   Hammond, S. M.; Hazell, G.; Shabanpoor, F.; Saleh, A. F.; Bowerman, M.; Sleigh, J. N.; Meijboom, K. E.; Zhou, H.; Muntoni, F.; Talbot, K.; Gait, M. J.; Wood, M. J., Systemic peptide-mediated oligonucleotide therapy improves long-term survival in spinal muscular atrophy. *Proceedings of the National Academy of Sciences of the United States of America* **2016,** *113* (39), 10962-7.

129.   Vivès, E.; Brodin, P.; Lebleu, B., A Truncated HIV-1 Tat Protein Basic Domain Rapidly Translocates through the Plasma Membrane and Accumulates in the Cell Nucleus. *Journal of Biological Chemistry* **1997,** *272* (25), 16010-16017.

130.   Mishra, A.; Lai, G. H.; Schmidt, N. W.; Sun, V. Z.; Rodriguez, A. R.; Tong, R.; Tang, L.; Cheng, J.; Deming, T. J.; Kamei, D. T.; Wong, G. C. L., Translocation of HIV TAT peptide and analogues induced by multiplexed membrane and cytoskeletal interactions. *Proceedings of the National Academy of Sciences* **2011,** *108* (41), 16883.

131.   Lättig-Tünnemann, G.; Prinz, M.; Hoffmann, D.; Behlke, J.; Palm-Apergi, C.; Morano, I.; Herce, H. D.; Cardoso, M. C., Backbone rigidity and static presentation of guanidinium groups increases cellular uptake of arginine-rich cell-penetrating peptides. *Nature Communications* **2011,** *2*, 453.

132.   Ezzat, K.; Aoki, Y.; Koo, T.; McClorey, G.; Benner, L.; Coenen-Stass, A.; O'Donovan, L.; Lehto, T.; Garcia-Guerra, A.; Nordin, J.; Saleh, A. F.; Behlke, M.; Morris, J.; Goyenvalle, A.; Dugovic, B.; Leumann, C.; Gordon, S.; Gait, M. J.; El−Andaloussi, S.; Wood, M. J. A., Self-Assembly into Nanoparticles Is Essential for Receptor Mediated Uptake of Therapeutic Antisense Oligonucleotides. *Nano Letters* **2015,** *15* (7), 4364-4373.

133.   Brooks, H.; Lebleu, B.; Vivès, E., Tat peptide-mediated cellular delivery: back to basics. *Advanced Drug Delivery Reviews* **2005,** *57* (4), 559-577.

134.   Herce, H. D.; Garcia, A. E.; Cardoso, M. C., Fundamental Molecular Mechanism for the Cellular Uptake of Guanidinium-Rich Molecules. *Journal of the American Chemical Society* **2014,** *136* (50), 17459-17467.

135.   Boisguerin, P.; Deshayes, S.; Gait, M. J.; O'Donovan, L.; Godfrey, C.; Betts, C. A.; Wood, M. J.; Lebleu, B., Delivery of therapeutic oligonucleotides with cell penetrating peptides. *Adv Drug Deliv Rev* **2015,** *87*, 52-67.

136.   Bauman, J.; Jearawiriyapaisarn, N.; Kole, R., Therapeutic potential of splice-switching oligonucleotides. *Oligonucleotides* **2009,** *19* (1), 1-13.

137.   Wang, H.; Yang, H.; Shivalila, C. S.; Dawlaty, M. M.; Cheng, A. W.; Zhang, F.; Jaenisch, R., One-Step Generation of Mice Carrying Mutations in Multiple Genes by CRISPR/Cas-Mediated Genome Engineering. *Cell* **2013,** *153* (4), 910-918.

138.   Horii, T.; Arai, Y.; Yamazaki, M.; Morita, S.; Kimura, M.; Itoh, M.; Abe, Y.; Hatada, I., Validation of microinjection methods for generating knockout mice by CRISPR/Cas-mediated genome engineering. **2014,** *4*.

139.   Matano, M.; Date, S.; Shimokawa, M.; Takano, A.; Fujii, M.; Ohta, Y.; Watanabe, T.; Kanai, T.; Sato, T., Modeling colorectal cancer using CRISPR-Cas9–mediated engineering of human intestinal organoids. *Nature Medicine* **2015,** *21* (3), 256-262.

140.   Kim, S.; Kim, D.; Cho, S. W.; Kim, J.; Kim, J. S., Highly efficient RNA-guided genome editing in human cells via delivery of purified Cas9 ribonucleoproteins. *Genome Research* **2014,** *24* (6), 1012-1019.

141.   Yin, H.; Xue, W.; Chen, S.; Bogorad, R. L.; Benedetti, E.; Grompe, M.; Koteliansky, V.; Sharp, P. A.; Jacks, T.; Anderson, D. G., Genome editing with Cas9 in adult mice corrects a disease mutation and phenotype. *Nature Biotechnology* **2014,** *32* (6), 551-553.

142.   Long, C.; Amoasii, L.; Mireault, A. A.; McAnally, J. R.; Li, H.; Sanchez-Ortiz, E.; Bhattacharyya, S.; Shelton, J. M.; Bassel-Duby, R.; Olson, E. N., Postnatal genome editing partially restores dystrophin expression in a mouse model of muscular dystrophy. *Science* **2016,** *351* (6271), 400-403.

143.   Voets, O.; Tielen, F.; Elstak, E.; Benschop, J.; Grimbergen, M.; Stallen, J.; Janssen, R.; Van Marle, A.; Essrich, C., Highly efficient gene inactivation by adenoviral CRISPR/Cas9 in human primary cells. *PLOS ONE* **2017,** *12* (8), e0182974.

144.   Kabadi, A. M.; Ousterout, D. G.; Hilton, I. B.; Gersbach, C. A., Multiplex CRISPR/Cas9-based genome engineering from a single lentiviral vector. *Nucleic Acids Research* **2014,** *42* (19), e147-e147.

145.   Ramakrishna, S.; Kwaku Dad, A. B.; Beloor, J.; Gopalappa, R.; Lee, S. K.; Kim, H., Gene disruption by cell-penetrating peptide-mediated delivery of Cas9 protein and guide RNA. *Genome Research* **2014,** *24* (6), 1020-1027.

146.   Mout, R.; Ray, M.; Yesilbag Tonga, G.; Lee, Y.-W.; Tay, T.; Sasaki, K.; Rotello, V. M., Direct Cytosolic Delivery of CRISPR/Cas9-Ribonucleoprotein for Efficient Gene Editing. *ACS Nano* **2017,** *11* (3), 2452-2458.

147.   Lee, K.; Conboy, M.; Park, H. M.; Jiang, F.; Kim, H. J.; Dewitt, M. A.; Mackley, V. A.; Chang, K.; Rao, A.; Skinner, C.; Shobha, T.; Mehdipour, M.; Liu, H.; Huang, W.-C.; Lan, F.; Bray, N. L.; Li, S.; Corn, J. E.; Kataoka, K.; Doudna, J. A.; Conboy, I.; Murthy, N., Nanoparticle delivery of Cas9 ribonucleoprotein and donor DNA in vivo induces homology-directed DNA repair. *Nature Biomedical Engineering* **2017,** *1* (11), 889-901.

148.   Cullis, P. R.; Hope, M. J., Lipid Nanoparticle Systems for Enabling Gene Therapies. *Mol Ther* **2017,** *25* (7), 1467-1475.

149.   Wang, M.; Zuris, J. A.; Meng, F.; Rees, H.; Sun, S.; Deng, P.; Han, Y.; Gao, X.; Pouli, D.; Wu, Q.; Georgakoudi, I.; Liu, D. R.; Xu, Q., Efficient delivery of genome-editing proteins using bioreducible lipid nanoparticles. *Proceedings of the National Academy of Sciences* **2016,** *113* (11), 2868-2873.

150.   Cho, E. Y.; Ryu, J.-Y.; Lee, H. A. R.; Hong, S. H.; Park, H. S.; Hong, K. S.; Park, S.-G.; Kim, H. P.; Yoon, T.-J., Lecithin nano-liposomal particle as a CRISPR/Cas9 complex delivery system for treating type 2 diabetes. *Journal of Nanobiotechnology* **2019,** *17* (1).

151. Liu, C.; Wan, T.; Wang, H.; Zhang, S.; Ping, Y.; Cheng, Y., A boronic acid–rich dendrimer with robust and unprecedented efficiency for cytosolic protein delivery and CRISPR-Cas9 gene editing. *Science Advances* **2019,** *5* (6), eaaw8922.

152. Schaffert, D.; Troiber, C.; Salcher, E. E.; Fröhlich, T.; Martin, I.; Badgujar, N.; Dohmen, C.; Edinger, D.; Kläger, R.; Maiwald, G.; Farkasova, K.; Seeber, S.; Jahn-Hofmann, K.; Hadwiger, P.; Wagner, E., Solid-Phase Synthesis of Sequence-Defined T-, i-, and U-Shape Polymers for pDNA and siRNA Delivery. *Angewandte Chemie International Edition* **2011,** *50* (38), 8986-8989.

153. He, D.; Müller, K.; Krhac Levacic, A.; Kos, P.; Lächelt, U.; Wagner, E., Combinatorial Optimization of Sequence-Defined Oligo(ethanamino)amides for Folate Receptor-Targeted pDNA and siRNA Delivery. *Bioconjug Chem* **2016,** *27* (3), 647-59.

154. Truebenbach, I.; Kern, S.; Loy, D. M.; Höhn, M.; Gorges, J.; Kazmaier, U.; Wagner, E., Combination Chemotherapy of L1210 Tumors in Mice with Pretubulysin and Methotrexate Lipo-Oligomer Nanoparticles. *Molecular Pharmaceutics* **2019,** *16* (6), 2405-2417.

155. Steinborn, B.; Truebenbach, I.; Morys, S.; Lächelt, U.; Wagner, E.; Zhang, W., Epidermal growth factor receptor targeted methotrexate and small interfering RNA co-delivery. *The Journal of Gene Medicine* **2018,** *20* (7-8), e3041.

156. Dohmen, C.; Edinger, D.; Fröhlich, T.; Schreiner, L.; Lächelt, U.; Troiber, C.; Rädler, J.; Hadwiger, P.; Vornlocher, H.-P.; Wagner, E., Nanosized Multifunctional Polyplexes for Receptor-Mediated SiRNA Delivery. **2012,** *6* (6), 5198-5208.

157. Salcher, E. E.; Kos, P.; Fröhlich, T.; Badgujar, N.; Scheible, M.; Wagner, E., Sequence-defined four-arm oligo(ethanamino)amides for pDNA and siRNA delivery: Impact of building blocks on efficacy. *J Control Release* **2012,** *164* (3), 380-6.

158. Beckert, L.; Kostka, L.; Kessel, E.; Krhac Levacic, A.; Kostkova, H.; Etrych, T.; Lächelt, U.; Wagner, E., Acid-labile pHPMA modification of four-arm oligoaminoamide pDNA polyplexes balances shielding and gene transfer activity in vitro and in vivo. *Eur J Pharm Biopharm* **2016,** *105*, 85-96.

159. Scholz, C.; Kos, P.; Wagner, E., Comb-Like Oligoaminoethane Carriers: Change in Topology Improves pDNA Delivery. *Bioconjugate Chemistry* **2014,** *25* (2), 251-261.

160. Schaffert, D.; Badgujar, N.; Wagner, E., Novel Fmoc-Polyamino Acids for Solid-Phase Synthesis of Defined Polyamidoamines. *Organic Letters* **2011,** *13* (7), 1586-1589.

161. Fröhlich, T.; Edinger, D.; Klager, R.; Troiber, C.; Salcher, E.; Badgujar, N.; Martin, I.; Schaffert, D.; Cengizeroglu, A.; Hadwiger, P.; Vornlocher, H. P.; Wagner, E., Structure-activity relationships of siRNA carriers based on sequence-defined oligo (ethane amino) amides. *J Control Release* **2012,** *160* (3), 532-41.

162. Kos, P.; Lächelt, U.; Herrmann, A.; Mickler, F. M.; Döblinger, M.; He, D.; Krhac Levacic, A.; Morys, S.; Brauchle, C.; Wagner, E., Histidine-rich stabilized polyplexes for cMet-directed tumor-targeted gene transfer. *Nanoscale* **2015,** *7* (12), 5350-62.

163. Shin, M. L.; Hansch, G.; Mayer, M. M., Effect of agents that produce membrane disorder on lysis of erythrocytes by complement. *Proceedings of the National Academy of Sciences* **1981,** *78* (4), 2522-2525.

164. Reinhard, S.; Zhang, W.; Wagner, E., Optimized Solid-Phase-Assisted Synthesis of Oleic Acid Containing siRNA Nanocarriers. *ChemMedChem* **2017,** *12* (17), 1464-1470.

165. Kuhn, J.; Klein, P. M.; Al Danaf, N.; Nordin, J. Z.; Reinhard, S.; Loy, D. M.; Höhn, M.; El Andaloussi, S.; Lamb, D. C.; Wagner, E.; Aoki, Y.; Lehto, T.; Lächelt, U.,

Supramolecular Assembly of Aminoethylene-Lipopeptide PMO Conjugates into RNA Splice-Switching Nanomicelles. *Advanced Functional Materials* **2019**, 1906432.

166. Troiber, C.; Edinger, D.; Kos, P.; Schreiner, L.; Kläger, R.; Herrmann, A.; Wagner, E., Stabilizing effect of tyrosine trimers on pDNA and siRNA polyplexes. *Biomaterials* **2013,** *34* (5), 1624-1633.

167. Klein, P. M.; Kern, S.; Lee, D. J.; Schmaus, J.; Höhn, M.; Gorges, J.; Kazmaier, U.; Wagner, E., Folate receptor-directed orthogonal click-functionalization of siRNA lipopolyplexes for tumor cell killing in vivo. *Biomaterials* **2018,** *178*, 630-642.

168. Luo, J.; Höhn, M.; Reinhard, S.; Loy, D. M.; Klein, P. M.; Wagner, E., IL4-Receptor-Targeted Dual Antitumoral Apoptotic Peptide—siRNA Conjugate Lipoplexes. *Advanced Functional Materials* **2019,** *29* (25), 1900697.

169. Kole, R.; Krainer, A. R.; Altman, S., RNA therapeutics: beyond RNA interference and antisense oligonucleotides. *Nat Rev Drug Discov* **2012,** *11* (2), 125-40.

170. Dunckley, M. G.; Manoharan, M.; Villiet, P.; Eperon, I. C.; Dickson, G., Modification of splicing in the dystrophin gene in cultured Mdx muscle cells by antisense oligoribonucleotides. *Hum Mol Genet* **1998,** *7* (7), 1083-90.

171. Muntoni, F.; Wood, M. J., Targeting RNA to treat neuromuscular disease. *Nat Rev Drug Discov* **2011,** *10* (8), 621-37.

172. Lu, Q. L.; Mann, C. J.; Lou, F.; Bou-Gharios, G.; Morris, G. E.; Xue, S. A.; Fletcher, S.; Partridge, T. A.; Wilton, S. D., Functional amounts of dystrophin produced by skipping the mutated exon in the mdx dystrophic mouse. *Nat Med* **2003,** *9* (8), 1009-14.

173. Burghes, A. H. M.; McGovern, V. L.; Porensky, P. N.; Mitrpant, C.; Wilton, S. D.; Bevan, A. K.; Kaspar, B. K.; Foust, K. D., A single administration of morpholino antisense oligomer rescues spinal muscular atrophy in mouse. *Human Molecular Genetics* **2011,** *21* (7), 1625-1638.

174. Dominski, Z.; Kole, R., Restoration of correct splicing in thalassemic pre-mRNA by antisense oligonucleotides. *Proceedings of the National Academy of Sciences of the United States of America* **1993,** *90* (18), 8673-7.

175. Svasti, S.; Suwanmanee, T.; Fucharoen, S.; Moulton, H. M.; Nelson, M. H.; Maeda, N.; Smithies, O.; Kole, R., RNA repair restores hemoglobin expression in IVS2-654 thalassemic mice. *Proceedings of the National Academy of Sciences of the United States of America* **2009,** *106* (4), 1205-10.

176. Graziewicz, M. A.; Tarrant, T. K.; Buckley, B.; Roberts, J.; Fulton, L.; Hansen, H.; Orum, H.; Kole, R.; Sazani, P., An endogenous TNF-alpha antagonist induced by splice-switching oligonucleotides reduces inflammation in hepatitis and arthritis mouse models. *Mol Ther* **2008,** *16* (7), 1316-22.

177. Gérard, X.; Perrault, I.; Munnich, A.; Kaplan, J.; Rozet, J.-M., Intravitreal Injection of Splice-switching Oligonucleotides to Manipulate Splicing in Retinal Cells. *Molecular Therapy - Nucleic Acids* **2015,** *4*.

178. Garanto, A.; Chung, D. C.; Duijkers, L.; Corral-Serrano, J. C.; Messchaert, M.; Xiao, R.; Bennett, J.; Vandenberghe, L. H.; Collin, R. W., In vitro and in vivo rescue of aberrant splicing in CEP290-associated LCA by antisense oligonucleotide delivery. *Hum Mol Genet* **2016,** *25* (12), 2552-2563.

179. Zammarchi, F.; de Stanchina, E.; Bournazou, E.; Supakorndej, T.; Martires, K.; Riedel, E.; Corben, A. D.; Bromberg, J. F.; Cartegni, L., Antitumorigenic potential of STAT3 alternative splicing modulation. *Proceedings of the National Academy of Sciences of the United States of America* **2011,** *108* (43), 17779-84.

180. Mercatante, D. R.; Bortner, C. D.; Cidlowski, J. A.; Kole, R., Modification of Alternative Splicing of Bcl-x Pre-mRNA in Prostate and Breast Cancer Cells:

ANALYSIS OF APOPTOSIS AND CELL DEATH. *Journal of Biological Chemistry* **2001,** *276* (19), 16411-16417.

181. Lächelt, U.; Wagner, E., Nucleic Acid Therapeutics Using Polyplexes: A Journey of 50 Years (and Beyond). *Chem Rev* **2015,** *115* (19), 11043-78.

182. Godfrey, C.; Desviat, L. R.; Smedsrød, B.; Piétri-Rouxel, F.; Denti, M. A.; Disterer, P.; Lorain, S.; Nogales-Gadea, G.; Sardone, V.; Anwar, R.; El Andaloussi, S.; Lehto, T.; Khoo, B.; Brolin, C.; van Roon-Mom, W. M. C.; Goyenvalle, A.; Aartsma-Rus, A.; Arechavala-Gomeza, V., Delivery is key: lessons learnt from developing splice-switching antisense therapies. *EMBO Molecular Medicine* **2017,** *9* (5), 545-557.

183. Moulton, H. M.; Hase, M. C.; Smith, K. M.; Iversen, P. L., HIV Tat peptide enhances cellular delivery of antisense morpholino oligomers. *Antisense Nucleic Acid Drug Dev* **2003,** *13* (1), 31-43.

184. Wu, R. P.; Youngblood, D. S.; Hassinger, J. N.; Lovejoy, C. E.; Nelson, M. H.; Iversen, P. L.; Moulton, H. M., Cell-penetrating peptides as transporters for morpholino oligomers: effects of amino acid composition on intracellular delivery and cytotoxicity. *Nucleic acids research* **2007,** *35* (15), 5182-5191.

185. Wolfe, J. M.; Fadzen, C. M.; Choo, Z.-N.; Holden, R. L.; Yao, M.; Hanson, G. J.; Pentelute, B. L., Machine Learning To Predict Cell-Penetrating Peptides for Antisense Delivery. *ACS Central Science* **2018,** *4* (4), 512-520.

186. Wolfe, J. M.; Fadzen, C. M.; Holden, R. L.; Yao, M.; Hanson, G. J.; Pentelute, B. L., Perfluoroaryl Bicyclic Cell-Penetrating Peptides for Delivery of Antisense Oligonucleotides. *Angewandte Chemie International Edition* **2018,** *57* (17), 4756-4759.

187. Blain, A. M.; Greally, E.; McClorey, G.; Manzano, R.; Betts, C. A.; Godfrey, C.; O'Donovan, L.; Coursindel, T.; Gait, M. J.; Wood, M. J.; MacGowan, G. A.; Straub, V. W., Peptide-conjugated phosphodiamidate oligomer-mediated exon skipping has benefits for cardiac function in mdx and Cmah-/-mdx mouse models of Duchenne muscular dystrophy. *PLoS One* **2018,** *13* (6), e0198897.

188. Boussif, O.; Lezoualc; h, F.; Zanta, M. A.; Mergny, M. D.; Scherman, D.; Demeneix, B.; Behr, J. P., A versatile vector for gene and oligonucleotide transfer into cells in culture and in vivo: polyethylenimine. *Proceedings of the National Academy of Sciences* **1995,** *92* (16), 7297.

189. Pun, S. H.; Bellocq, N. C.; Liu, A.; Jensen, G.; Machemer, T.; Quijano, E.; Schluep, T.; Wen, S.; Engler, H.; Heidel, J.; Davis, M. E., Cyclodextrin-Modified Polyethylenimine Polymers for Gene Delivery. *Bioconjugate Chemistry* **2004,** *15* (4), 831-840.

190. Wang, X.-L.; Jensen, R.; Lu, Z.-R., A novel environment-sensitive biodegradable polydisulfide with protonatable pendants for nucleic acid delivery. *Journal of Controlled Release* **2007,** *120* (3), 250-258.

191. Russ, V.; Günther, M.; Halama, A.; Ogris, M.; Wagner, E., Oligoethylenimine-grafted polypropylenimine dendrimers as degradable and biocompatible synthetic vectors for gene delivery. *Journal of Controlled Release* **2008,** *132* (2), 131-140.

192. Miyata, K.; Oba, M.; Nakanishi, M.; Fukushima, S.; Yamasaki, Y.; Koyama, H.; Nishiyama, N.; Kataoka, K., Polyplexes from Poly(aspartamide) Bearing 1,2-Diaminoethane Side Chains Induce pH-Selective, Endosomal Membrane Destabilization with Amplified Transfection and Negligible Cytotoxicity. *Journal of the American Chemical Society* **2008,** *130* (48), 16287-16294.

193. Lin, C.; Blaauboer, C.-J.; Timoneda, M. M.; Lok, M. C.; van Steenbergen, M.; Hennink, W. E.; Zhong, Z.; Feijen, J.; Engbersen, J. F. J., Bioreducible poly(amido

amine)s with oligoamine side chains: Synthesis, characterization, and structural effects on gene delivery. *Journal of Controlled Release* **2008,** *126* (2), 166-174.

194. Wei, H.; Pahang, J. A.; Pun, S. H., Optimization of Brush-Like Cationic Copolymers for Nonviral Gene Delivery. *Biomacromolecules* **2013,** *14* (1), 275-284.

195. Uchida, H.; Miyata, K.; Oba, M.; Ishii, T.; Suma, T.; Itaka, K.; Nishiyama, N.; Kataoka, K., Odd–Even Effect of Repeating Aminoethylene Units in the Side Chain of N-Substituted Polyaspartamides on Gene Transfection Profiles. *Journal of the American Chemical Society* **2011,** *133* (39), 15524-15532.

196. Uchida, H.; Itaka, K.; Nomoto, T.; Ishii, T.; Suma, T.; Ikegami, M.; Miyata, K.; Oba, M.; Nishiyama, N.; Kataoka, K., Modulated Protonation of Side Chain Aminoethylene Repeats in N-Substituted Polyaspartamides Promotes mRNA Transfection. *Journal of the American Chemical Society* **2014,** *136* (35), 12396-12405.

197. Lächelt, U.; Kos, P.; Mickler, F. M.; Herrmann, A.; Salcher, E. E.; Rödl, W.; Badgujar, N.; Brauchle, C.; Wagner, E., Fine-tuning of proton sponges by precise diaminoethanes and histidines in pDNA polyplexes. *Nanomedicine* **2014,** *10* (1), 35-44.

198. Jarzębińska, A.; Pasewald, T.; Lambrecht, J.; Mykhaylyk, O.; Kümmerling, L.; Beck, P.; Hasenpusch, G.; Rudolph, C.; Plank, C.; Dohmen, C., A Single Methylene Group in Oligoalkylamine-Based Cationic Polymers and Lipids Promotes Enhanced mRNA Delivery. *Angewandte Chemie International Edition* **2016,** *55* (33), 9591-9595.

199. Vermeulen, L. M. P.; De Smedt, S. C.; Remaut, K.; Braeckmans, K., The proton sponge hypothesis: Fable or fact? *European Journal of Pharmaceutics and Biopharmaceutics* **2018,** *129*, 184-190.

200. Schaffert, D.; Badgujar, N.; Wagner, E., Novel Fmoc-polyamino acids for solid-phase synthesis of defined polyamidoamines. *Org Lett* **2011,** *13* (7), 1586-9.

201. Schaffert, D.; Troiber, C.; Salcher, E. E.; Frohlich, T.; Martin, I.; Badgujar, N.; Dohmen, C.; Edinger, D.; Klager, R.; Maiwald, G.; Farkasova, K.; Seeber, S.; Jahn-Hofmann, K.; Hadwiger, P.; Wagner, E., Solid-phase synthesis of sequence-defined T-, i-, and U-shape polymers for pDNA and siRNA delivery. *Angew Chem Int Ed Engl* **2011,** *50* (38), 8986-9.

202. Agard, N. J.; Prescher, J. A.; Bertozzi, C. R., A Strain-Promoted [3 + 2] Azide−Alkyne Cycloaddition for Covalent Modification of Biomolecules in Living Systems. *Journal of the American Chemical Society* **2004,** *126* (46), 15046-15047.

203. Kang, S. H.; Cho, M. J.; Kole, R., Up-regulation of luciferase gene expression with antisense oligonucleotides: implications and applications in functional assay development. *Biochemistry* **1998,** *37* (18), 6235-9.

204. Scholz, C.; Kos, P.; Wagner, E., Comb-like oligoaminoethane carriers: change in topology improves pDNA delivery. *Bioconjug Chem* **2014,** *25* (2), 251-61.

205. Troiber, C.; Edinger, D.; Kos, P.; Schreiner, L.; Klager, R.; Herrmann, A.; Wagner, E., Stabilizing effect of tyrosine trimers on pDNA and siRNA polyplexes. *Biomaterials* **2013,** *34* (5), 1624-33.

206. Creusat, G.; Zuber, G., Self-Assembling Polyethylenimine Derivatives Mediate Efficient siRNA Delivery in Mammalian Cells. *ChemBioChem* **2008,** *9* (17), 2787-2789.

207. Creusat, G.; Rinaldi, A.-S.; Weiss, E.; Elbaghdadi, R.; Remy, J.-S.; Mulherkar, R.; Zuber, G., Proton Sponge Trick for pH-Sensitive Disassembly of Polyethylenimine-Based siRNA Delivery Systems. *Bioconjugate Chemistry* **2010,** *21* (5), 994-1002.

208. Ewe, A.; Przybylski, S.; Burkhardt, J.; Janke, A.; Appelhans, D.; Aigner, A., A novel tyrosine-modified low molecular weight polyethylenimine (P10Y) for efficient siRNA delivery in vitro and in vivo. *Journal of Controlled Release* **2016,** *230*, 13-25.

209. Rocha, C. S.; Lundin, K. E.; Behlke, M. A.; Zain, R.; El Andaloussi, S.; Smith, C. I., Four Novel Splice-Switch Reporter Cell Lines: Distinct Impact of Oligonucleotide Chemistry and Delivery Vector on Biological Activity. *Nucleic Acid Ther* **2016,** *26* (6), 381-391.

210. Saher, O.; Rocha, C. S. J.; Zaghloul, E. M.; Wiklander, O. P. B.; Zamolo, S.; Heitz, M.; Ezzat, K.; Gupta, D.; Reymond, J. L.; Zain, R.; Hollfelder, F.; Darbre, T.; Lundin, K. E.; El Andaloussi, S.; Smith, C. I. E., Novel peptide-dendrimer/lipid/oligonucleotide ternary complexes for efficient cellular uptake and improved splice-switching activity. *Eur J Pharm Biopharm* **2018,** *132*, 29-40.

211. Summerton, J. E., Endo-Porter: a novel reagent for safe, effective delivery of substances into cells. *Ann N Y Acad Sci* **2005,** *1058*, 62-75.

212. Magde, D.; Elson, E.; Webb, W. W., Thermodynamic Fluctuations in a Reacting System---Measurement by Fluorescence Correlation Spectroscopy. *Physical Review Letters* **1972,** *29* (11), 705-708.

213. Elson, E. L.; Magde, D., Fluorescence correlation spectroscopy. I. Conceptual basis and theory. *Biopolymers* **1974,** *13* (1), 1-27.

214. Ivanchenko, S.; Lamb, D. C. In *Fluorescence Correlation Spectroscopy: Principles and Developments*, Supramolecular Structure and Function 10, Dordrecht, 2011//; Brnjas-Kraljević, J.; Pifat-Mrzljak, G., Eds. Springer Netherlands: Dordrecht, 2011; pp 1-30.

215. Plank, C.; Oberhauser, B.; Mechtler, K.; Koch, C.; Wagner, E., The influence of endosome-disruptive peptides on gene transfer using synthetic virus-like gene transfer systems. *Journal of Biological Chemistry* **1994,** *269* (17), 12918-12924.

216. Vermeulen, L. M. P.; Brans, T.; Samal, S. K.; Dubruel, P.; Demeester, J.; De Smedt, S. C.; Remaut, K.; Braeckmans, K., Endosomal Size and Membrane Leakiness Influence Proton Sponge-Based Rupture of Endosomal Vesicles. *ACS Nano* **2018,** *12* (3), 2332-2345.

217. Miyatake, S.; Mizobe, Y.; Tsoumpra, M. K.; Lim, K. R. Q.; Hara, Y.; Shabanpoor, F.; Yokota, T.; Takeda, S. i.; Aoki, Y., Scavenger Receptor Class A1 Mediates Uptake of Morpholino Antisense Oligonucleotide into Dystrophic Skeletal Muscle. *Molecular Therapy - Nucleic Acids* **2019,** *14*, 520-535.

218. Araki, E.; Nakamura, K.; Nakao, K.; Kameya, S.; Kobayashi, O.; Nonaka, I.; Kobayashi, T.; Katsuki, M., Targeted Disruption of Exon 52 in the Mouse Dystrophin Gene Induced Muscle Degeneration Similar to That Observed in Duchenne Muscular Dystrophy. *Biochemical and Biophysical Research Communications* **1997,** *238* (2), 492-497.

219. Aoki, Y.; Yokota, T.; Nagata, T.; Nakamura, A.; Tanihata, J.; Saito, T.; Duguez, S. M. R.; Nagaraju, K.; Hoffman, E. P.; Partridge, T.; Takeda, S. i., Bodywide skipping of exons 45-55 in dystrophic mdx52 mice by systemic antisense delivery. *Proceedings of the National Academy of Sciences of the United States of America* **2012,** *109* (34), 13763-13768.

220. Leader, B.; Baca, Q. J.; Golan, D. E., Protein therapeutics: a summary and pharmacological classification. *Nature Reviews Drug Discovery* **2008,** *7* (1), 21-39.

221. Goeddel, D. V.; Kleid, D. G.; Bolivar, F.; Heyneker, H. L.; Yansura, D. G.; Crea, R.; Hirose, T.; Kraszewski, A.; Itakura, K.; Riggs, A. D., Expression in Escherichia coli of chemically synthesized genes for human insulin. *Proceedings of the National Academy of Sciences* **1979,** *76* (1), 106-110.

222. Usmani, S. S.; Bedi, G.; Samuel, J. S.; Singh, S.; Kalra, S.; Kumar, P.; Ahuja, A. A.; Sharma, M.; Gautam, A.; Raghava, G. P. S., THPdb: Database of FDA-approved peptide and protein therapeutics. *PLOS ONE* **2017,** *12* (7), e0181748.

223. Horvath, P.; Barrangou, R., CRISPR/Cas, the immune system of bacteria and archaea. *Science* **2010,** *327* (5962), 167-70.

224. Jiang, W.; Bikard, D.; Cox, D.; Zhang, F.; Marraffini, L. A., RNA-guided editing of bacterial genomes using CRISPR-Cas systems. *Nature Biotechnology* **2013,** *31* (3), 233-239.

225. Li, J.-F.; Norville, J. E.; Aach, J.; McCormack, M.; Zhang, D.; Bush, J.; Church, G. M.; Sheen, J., Multiplex and homologous recombination–mediated genome editing in Arabidopsis and Nicotiana benthamiana using guide RNA and Cas9. *Nature Biotechnology* **2013,** *31* (8), 688-691.

226. Friedland, A. E.; Tzur, Y. B.; Esvelt, K. M.; Colaiácovo, M. P.; Church, G. M.; Calarco, J. A., Heritable genome editing in C. elegans via a CRISPR-Cas9 system. *Nature Methods* **2013,** *10* (8), 741-743.

227. Cho, S. W.; Kim, S.; Kim, J. M.; Kim, J. S., Targeted genome engineering in human cells with the Cas9 RNA-guided endonuclease. *Nat Biotechnol* **2013,** *31* (3), 230-2.

228. Lino, C. A.; Harper, J. C.; Carney, J. P.; Timlin, J. A., Delivering CRISPR: a review of the challenges and approaches. *Drug Delivery* **2018,** *25* (1), 1234-1257.

229. Lächelt, U.; Wagner, E., Nucleic Acid Therapeutics Using Polyplexes: A Journey of 50 Years (and Beyond). *Chemical Reviews* **2015,** *115* (19), 11043-11078.

230. Zhang, P.; He, D.; Klein, P. M.; Liu, X.; Röder, R.; Döblinger, M.; Wagner, E., Enhanced Intracellular Protein Transduction by Sequence Defined Tetra-Oleoyl Oligoaminoamides Targeted for Cancer Therapy. **2015,** *25* (42), 6627-6636.

231. Fu, A.; Tang, R.; Hardie, J.; Farkas, M. E.; Rotello, V. M., Promises and Pitfalls of Intracellular Delivery of Proteins. **2014,** *25* (9), 1602-1608.

232. Sun, W.; Ji, W.; Hall, J. M.; Hu, Q.; Wang, C.; Beisel, C. L.; Gu, Z., Self-assembled DNA nanoclews for the efficient delivery of CRISPR-Cas9 for genome editing. *Angew Chem Int Ed Engl* **2015,** *54* (41), 12029-33.

233. Chen, G.; Ma, B.; Wang, Y.; Gong, S., A Universal GSH-Responsive Nanoplatform for the Delivery of DNA, mRNA, and Cas9/sgRNA Ribonucleoprotein. *ACS Applied Materials & Interfaces* **2018,** *10* (22), 18515-18523.

234. Yue, H.; Zhou, X.; Cheng, M.; Xing, D., Graphene oxide-mediated Cas9/sgRNA delivery for efficient genome editing. *Nanoscale* **2018,** *10* (3), 1063-1071.

235. Liu, C.; Wan, T.; Wang, H.; Zhang, S.; Ping, Y.; Cheng, Y., A boronic acid-rich dendrimer with robust and unprecedented efficiency for cytosolic protein delivery and CRISPR-Cas9 gene editing. *Sci Adv* **2019,** *5* (6), eaaw8922.

236. Schaffert, D.; Badgujar, N.; Wagner, E., Novel Fmoc-Polyamino Acids for Solid-Phase Synthesis of Defined Polyamidoamines. **2011,** *13* (7), 1586-1589.

237. Boussif, O.; Lezoualc'h, F.; Zanta, M. A.; Mergny, M. D.; Scherman, D.; Demeneix, B.; Behr, J. P., A versatile vector for gene and oligonucleotide transfer into cells in culture and in vivo: polyethylenimine. *Proceedings of the National Academy of Sciences of the United States of America* **1995,** *92* (16), 7297-301.

238. Fröhlich, T.; Edinger, D.; Kläger, R.; Troiber, C.; Salcher, E.; Badgujar, N.; Martin, I.; Schaffert, D.; Cengizeroglu, A.; Hadwiger, P.; Vornlocher, H.-P.; Wagner, E., Structure–activity relationships of siRNA carriers based on sequence-defined oligo (ethane amino) amides. *Journal of Controlled Release* **2012,** *160* (3), 532-541.

239. Ramakrishna, S.; Kwaku Dad, A.-B.; Beloor, J.; Gopalappa, R.; Lee, S.-K.; Kim, H., Gene disruption by cell-penetrating peptide-mediated delivery of Cas9 protein and guide RNA. *Genome Research* **2014,** *24* (6), 1020-1027.

240. Larson, M. H.; Gilbert, L. A.; Wang, X.; Lim, W. A.; Weissman, J. S.; Qi, L. S., CRISPR interference (CRISPRi) for sequence-specific control of gene expression. *Nature protocols* **2013,** *8* (11), 2180-96.

241. Qi, L. S.; Larson, M. H.; Gilbert, L. A.; Doudna, J. A.; Weissman, J. S.; Arkin, A. P.; Lim, W. A., Repurposing CRISPR as an RNA-guided platform for sequence-specific control of gene expression. *Cell* **2013,** *152* (5), 1173-83.

242. Smoluchowski, M. V., Drei Vortrage uber Diffusion, Brownsche Bewegung und Koagulation von Kolloidteilchen. *Zeitschrift fur Physik* **1916,** *17*, 557-585.

243. Hendrix, J.; Baumgartel, V.; Schrimpf, W.; Ivanchenko, S.; Digman, M. A.; Gratton, E.; Krausslich, H. G.; Müller, B.; Lamb, D. C., Live-cell observation of cytosolic HIV-1 assembly onset reveals RNA-interacting Gag oligomers. *The Journal of cell biology* **2015,** *210* (4), 629-46.

244. Schrimpf, W.; Barth, A.; Hendrix, J.; Lamb, D. C., PAM: A Framework for Integrated Analysis of Imaging, Single-Molecule, and Ensemble Fluorescence Data. *Biophysical journal* **2018,** *114* (7), 1518-1528.

245. Zintchenko, A.; Philipp, A.; Dehshahri, A.; Wagner, E., Simple Modifications of Branched PEI Lead to Highly Efficient siRNA Carriers with Low Toxicity. **2008,** *19* (7), 1448-1455.

246. Akinc, A.; Zumbuehl, A.; Goldberg, M.; Leshchiner, E. S.; Busini, V.; Hossain, N.; Bacallado, S. A.; Nguyen, D. N.; Fuller, J.; Alvarez, R.; Borodovsky, A.; Borland, T.; Constien, R.; De Fougerolles, A.; Dorkin, J. R.; Narayanannair Jayaprakash, K.; Jayaraman, M.; John, M.; Koteliansky, V.; Manoharan, M.; Nechev, L.; Qin, J.; Racie, T.; Raitcheva, D.; Rajeev, K. G.; Sah, D. W. Y.; Soutschek, J.; Toudjarska, I.; Vornlocher, H.-P.; Zimmermann, T. S.; Langer, R.; Anderson, D. G., A combinatorial library of lipid-like materials for delivery of RNAi therapeutics. *Nature Biotechnology* **2008,** *26* (5), 561-569.

247. Semple, S. C.; Akinc, A.; Chen, J.; Sandhu, A. P.; Mui, B. L.; Cho, C. K.; Sah, D. W. Y.; Stebbing, D.; Crosley, E. J.; Yaworski, E.; Hafez, I. M.; Dorkin, J. R.; Qin, J.; Lam, K.; Rajeev, K. G.; Wong, K. F.; Jeffs, L. B.; Nechev, L.; Eisenhardt, M. L.; Jayaraman, M.; Kazem, M.; Maier, M. A.; Srinivasulu, M.; Weinstein, M. J.; Chen, Q.; Alvarez, R.; Barros, S. A.; De, S.; Klimuk, S. K.; Borland, T.; Kosovrasti, V.; Cantley, W. L.; Tam, Y. K.; Manoharan, M.; Ciufolini, M. A.; Tracy, M. A.; De Fougerolles, A.; Maclachlan, I.; Cullis, P. R.; Madden, T. D.; Hope, M. J., Rational design of cationic lipids for siRNA delivery. *Nature Biotechnology* **2010,** *28* (2), 172-176.

248. Albanese, A.; Tang, P. S.; Chan, W. C., The effect of nanoparticle size, shape, and surface chemistry on biological systems. *Annu Rev Biomed Eng* **2012,** *14*, 1-16.

249. Lundqvist, M.; Stigler, J.; Elia, G.; Lynch, I.; Cedervall, T.; Dawson, K. A., Nanoparticle size and surface properties determine the protein corona with possible implications for biological impacts. *Proceedings of the National Academy of Sciences of the United States of America* **2008,** *105* (38), 14265-70.

250. Huhn, D.; Kantner, K.; Geidel, C.; Brandholt, S.; De Cock, I.; Soenen, S. J.; Rivera Gil, P.; Montenegro, J. M.; Braeckmans, K.; Mullen, K.; Nienhaus, G. U.; Klapper, M.; Parak, W. J., Polymer-coated nanoparticles interacting with proteins and cells: focusing on the sign of the net charge. *ACS Nano* **2013,** *7* (4), 3253-63.

251. Varkouhi, A. K.; Scholte, M.; Storm, G.; Haisma, H. J., Endosomal escape pathways for delivery of biologicals. *J Control Release* **2011,** *151* (3), 220-8.

252. Lonn, P.; Kacsinta, A. D.; Cui, X. S.; Hamil, A. S.; Kaulich, M.; Gogoi, K.; Dowdy, S. F., Enhancing Endosomal Escape for Intracellular Delivery of Macromolecular Biologic Therapeutics. *Sci Rep* **2016,** *6*, 32301.

253. Le Gall, T.; Loizeau, D.; Picquet, E.; Carmoy, N.; Yaouanc, J. J.; Burel-Deschamps, L.; Delepine, P.; Giamarchi, P.; Jaffres, P. A.; Lehn, P.; Montier, T., A novel cationic lipophosphoramide with diunsaturated lipid chains: synthesis, physicochemical properties, and transfection activities. *Journal of medicinal chemistry* **2010,** *53* (4), 1496-508.

254. Malamas, A. S.; Gujrati, M.; Kummitha, C. M.; Xu, R.; Lu, Z. R., Design and evaluation of new pH-sensitive amphiphilic cationic lipids for siRNA delivery. *J Control Release* **2013,** *171* (3), 296-307.

255. Zou, S. M.; Erbacher, P.; Remy, J. S.; Behr, J. P., Systemic linear polyethylenimine (L-PEI)-mediated gene delivery in the mouse. *J Gene Med* **2000,** *2* (2), 128-34.

256. Ivanchenko, S., Lamb, D. C.; Brnjas-Kraljević, J.; Pifat-Mrzljak, G., Supramolecular Structure and Function 10. *Springer Netherlands* **2011** p. 1.

257. Schwille, P.; Meyer-Almes, F. J.; Rigler, R., Dual-color fluorescence cross-correlation spectroscopy for multicomponent diffusional analysis in solution. *Biophysical journal* **1997,** *72* (4), 1878-86.

258. Müller, B. K.; Zaychikov, E.; Brauchle, C.; Lamb, D. C., Pulsed interleaved excitation. *Biophysical journal* **2005,** *89* (5), 3508-22.

259. Levacic, A. K.; Morys, S.; Kempter, S.; Lächelt, U.; Wagner, E., Minicircle Versus Plasmid DNA Delivery by Receptor-Targeted Polyplexes. *Hum Gene Ther* **2017,** *28* (10), 862-874.

7   Publications

Original articles

Kuhn, J., Klein, P. M., Al Danaf, N., Nordin, J. Z., Reinhard, S., Loy, D. M., Höhn, M., El Andaloussi, S., Lamb, D. C., Wagner, E., Aoki, Y., Lehto, T., Lächelt, U. (2019) *Supramolecular Assembly of Aminoethylene-Lipopeptide PMO Conjugates into RNA Splice-Switching Nanomicelles*, Adv. Funct. Mater. 2019, 1906432.

Holm, R., Schwiertz, D., Weber, B., Schultze, J., **Kuhn, J.**, Koynov, K., Lächelt, U., Barz, M. (2019) *Multifunctional Cationic PeptoStars as siRNA Carrier: Influence of Architecture and Histidine Modification on Knockdown Potential*. Macromol Biosci. 2019 Aug 20:e1900152.

Zimpel, A., Al Danaf, N., Steinborn, B., **Kuhn, J.**, Höhn, M., Bauer, T., Hirschle, P., Schrimpf, W., Engelke, H., Wagner, E., Barz, M., Lamb, D.C., Lächelt, U., Wuttke, S. (2019) *Coordinative binding of polymers to metal-organic framework nanoparticles for control of interactions at the biointerface*, ACS Nano. 2019 Apr 23;13(4):3884-3895

Truebenbach, I., Gorges, J., **Kuhn, J.**, Kern, S., Baratti, E., Kazmaier, U., Wagner, E., Lächelt, U. (2017) *Sequence-Defined Oligoamide Drug Conjugates of Pretubulysin and Methotrexate for Folate Receptor Targeted Cancer Therapy*, Macromol Biosci. 2017 Oct;17(10). doi: 10.1002/mabi.201600520

Submitted Manuscript

Kuhn, J., Lin, Y., Krhac Levacic, A., Danaf, N. A., Peng, L., Höhn, M., Lamb, D. C., Wagner, E., Lächelt, U. *Delivery of Cas9/sgRNA Ribonucleoprotein Complexes via Hydroxystearyl Oligoamino Amides.* (submitted 2019)

Meeting abstracts and poster presentations

10/19   Oligonucleotide Therapeutics Society (OTS), Munich, Germany

09/18   Annual Meeting German Society of Gene Therapy (DG-GT), Freiburg, Germany, Oral presentation

05/18   Annual meeting of the American Society of Gene and Cell Therapy, Chicago, USA, Poster presentation

04/18   Sino-German Young Researcher Symposium, Munich , Germany, "*Nanopharmaceuticals: Drug Delivery in the Nanoscale*", Poster presentation

05/17   Nanosystems Initiative Munich (NIM) workshop, Munich, Germany, Poster presentation

10/16   Annual Meeting of the German Pharmaceutical Society (DPhG), Munich, Germany

09/16   Nanoscale Matter - Novel Concepts and Functions, Venice, Italy, Poster presentation

8   Acknowledgements

Der schönste Moment am Ende jeder Abenteuerreise ist wenn man sich die Zeit nimmt zurück zu blicken und all den Menschen zu danken, die das hier ermöglicht haben und ohne die es niemals das Selbe gewesen wäre.

Als Erstes möchte ich meinen Dank an Professor Ernst Wagner richten, der all das hier erst möglich gemacht hat. Seine unermüdliche Unterstützung, für jeden einzelnen seiner Doktoranten, sowie seine inspirierende Faszination für die Forschung machen ihn zu einem ganz besonderen Vorbild.

Das wohl größte Dankeschön gilt Dr. Ulrich Lächelt. Es ist mir eine Ehre, dir aus der Sicht deiner ersten Doktorandin zu sagen, dass man sich keinen besseren Supervisor wünschen kann. Immer eine offene Tür und ein offenes Ohr, der Lebensretter in der Labornot und einfach die gute Seele im Labor. Das abendliche tüfteln und planen von Versuchen wird mir schon sehr fehlen.

I also want to thank my collaboration partners Dr. Joel Z. Nordin, Dr. Samir El Andaloussi, Don C. Lamb, Prof. Yoshitsugu Aoki and Dr. Taavi Lehto for the close collaboration across several country borders.

Ein besonderer Dank geht hier natürlich auch an Nader, der mich in die fantastische Welt der Laser eingeführt hat und für mich immer ein kleines Licht parat hatte, sodass ich unbeschadet den Weg durch seinen Laser-Irrgarten gefunden habe.

Special thanks goes to Yi, Ana, Philipp, Sören, Doom, Lun, and Miriam, with whom I have been working closely together. Thank you for spending a lot of your time for several of my experiments and the synthesis of all the oligomers. I appreciate their excellent work.

Natürlich möchte ich mich auch bei unseren Helden im Hintergrund bedanken. Wolfgang, ohne den wahrscheinlich schon einige PCs aus dem Fenster geflogen wären und Ursula, die immer für volle Schubladen und eine entkalkte Kaffeemaschine gesorgt hat. Was gibt es schon schöneres, als ein freundliches Lächeln und einen warmen Kaffee am Morgen.

Ein riesen Dank geht auch an all die motivierten Studenten, die ich in meiner Zeit an der LMU betreuen durfte. Der Dank richtet sich hier vor allem an Bene und Anna, mit deren Hilfe und Ideen sie einen beachtlichen Beitrag zu unseren Projekten geleistet haben.

Und jetzt zu dem wohl liebeswertesten Chaoshaufen auf diesem Planeten. Der AK Wagner ist schon etwas ganz Besonderes und jeder der ein Teil davon sein darf, hat eine kleine Familie dazu gewonnen. Wo fange ich da nur an... Danke an: Sarah und Eva, die unser kleines Büro zu dem lauschigsten Plätzchen im ganzen Labor gemacht haben, in dem es auch so allerhand Gesprächsstoff gab. Sören und Doom, die mit den besten Frisuren etwas mehr Style in den AK gebracht haben. Teo, der mit seinen liebevollen Umarmungen ab und zu auch mal Rippen anknackst. Simoni, mit der jeder Jägermeister nur halb so schlimm schmeckt und die mit Franzi und Elisa den Frauennachwuchs in unserem Labor perfekt macht. Danke auch an Janin, die nach misslungenen Versuchen sofort mit einer motivierenden Packung Toffifee zur Stelle war.

Ganz besonders dankbar bin ich dafür, dass ich Ines im AK Wagner gefunden habe, eine Freundin fürs Leben. Danke für diese unvergessliche gemeinsame Zeit, sowie die Kraft und Überzeugung alles im Leben erreichen zu können.

Unendlicher dank geht auch an die beste Familie der Welt. Danke Mama, für all die schlaflosen Nächte die du meinetwegen hattest, das Mitfiebern vor jeder Prüfung und deine grenzenlose Unterstützung und Liebe. Dank gilt auch meiner großen Schwester Tamara, die wohl beste Zuhörerin auf diesem Planeten, mit den zwei süßesten Kindern. Ich bin sehr froh euch zu haben.

Zuletzt geht mein tiefster Dank an Tim, der es selbst an den schwierigsten Tagen schafft ein Lächeln in mein Gesicht zu zaubern und mit seiner Liebe mein ganzes Leben bereichert. Ich freue mich wahnsinnig auf unsere gemeinsame Zukunft.